UNIVERSITÀ DEGLI STUDI DI ROMA "LA SAPIENZA"

FACULTY OF ENGINEERING

PH.D. PROGRAMME

IN

AEROSPACE ENGINEERING

XXII CYCLE

PRESSURE WAVES OSCILLATION LEVELS: THE INFLUENCE OF SCALE EFFECTS IN SOLID ROCKET MOTORS

AUTHOR

ING. MARCO IANNUCCELLI

SUPERVISOR

PROF. FULVIO STELLA

INDEX

LIST OF FIGURES

LIST OF TABLES

SYMBOLS

T	Temperature	[K]
We	Weber Number	[-]
U, u	Velocity	[m/s]
d, ϕ	Diametre	[μm]
σ	Surface Tensione	[Pa/s]
μ	Viscosity	[Kg/m.s]
D	Duct Diametre	[m]
Y	Rosin-Rammler Function	[-]
t	Time	[s]
St	Stokes Number	[-]
r	Duct Radius	[m]
p	Pressure	[Pa]
C_D	Drag Coefficient	[-]
Re	Reynolds Number	[-]
h, H	Specific Hentalpy	[J/Kg]
$\dot{q}$	Heat Flux	[J/s]
m	Mass	[Kg]
C_p	Thermal Capacity	[J/Kg.K]
$B_{o,q}$	Spalding Number	[-]
Nu	Nusselt Number	[-]
K	Thermal Conductivity	[w/m.K]
Pr	Prandtl Number	[-]
V	Volume	[m^3]

SUBSCRIPTS

fus	fusion
boil	boiling
p	particulate
rel	relative

f	fluid
c	continuous phasese
d	discrete phase
cr	critical
in	initial
fin	final
out	exiting
tot	total
vap	vaporous phase
P-F	from particulate to fluid
Al	aluminum
Al_2O_3	aluminum oxide

ACRONYMS

PWO	pressure waves oscillation
SRM	solid rocket motor
FTP	face thermal protection

ACKNOWLEDGEMENTS

In this occasion I would like to take the opportunity to thank Prof. Fulvio Stella for his constant support, which offered the possibility to improve both on the human and professional sides.
I have to thank the entire Doctoral Board, which offered precious advises regarding the evolution and the development of the research.
A special expression of gratitude is addressed to Doctor Biagio Ancarola, whose constant presence has been always available for both the development of the research, the evolution of the work and my personal development.
A special expression of gratitude is addressed to Doctor Fabio Paglia, for the wide advises offered.
A final expression of gratitude is addressed to Doctor Domenico Simone, who often offered fundamental technical suggestions and moments of careful intellectual consideration.

1 INTRODUCTION

The main objective of the present research is the characterisation of the unsteady internal fluid dynamics occurring in solid rocket motors (SRM). In particular, the attention is focused on the evaluation and the analysis of pressure waves oscillation (PWO) available in such type of motors and the manner through which such waves modify the amplitude and the frequency as the motor characteristic dimensions vary.

Though calculating devices and computer machines have reached very high performance levels, offering remarkable support in the solution of complex numerical problems, the comprehension of fluid dynamic phenomena occurring in solid rocket motors combustion chamber did not advance in a sensible manner and still the most reliable experimental tests are the means through which scientists can evaluate the phenomena, though if such test are very expensive and not fully explanatory. Indeed, still today a reliable theory has not been found to exactly describe and foresee the PWO phenomena. For such reason, in the last 20 years, the PWO problem in combustion chambers has represented a new and important research argument [1].

Furthermore, the need to achieve higher and higher thrust levels has induced SRM designers and engineers towards higher dimensions and scales, requiring considerable technological and engineering investments for the development of modern propellant grains, thermal isolating systems, motor cases, etc. This led to new configurations for which the PWO's generated during the engine functioning represent a non-negligible issue [2].

Since normally such investments are mainly supported at the aim of increasing the performances of already existing and functioning motors, such as the P230 engine, the reference configuration adopted for the investigation of the PWO phenomenon is the one of the above mentioned industrial motor.

The P230 is a solid rocket booster (see **Fig. 1**), twin mounted and employed during the lift-off phase and the subsequent ascent through the atmosphere of the Ariane 5 launch vehicle.

For such types of SRM the propellant is directly loaded inside the combustion chamber and for manufacturing reasons it is typically subdivided in several segments (**Fig. 1a** together with **elements A** in **Fig. 2**).

The propellant grain segments are separated by thermal protection panels referred to as *face thermal protections* (FTP) characterised by a circular ring shape (see the highlighted areas in **Fig. 1a** and the **elements B** in **Fig. 2**).

Fig. 1 – PWO in Ariane 5 solid rocket boosters (P230)

During engine operation the FTP burns while losing mass and getting consumed at a radial speed which is lower than the bonded propellant grain regression rate, therefore generating a ring shaped protrusion partially immersed through the main inner flow (see the highlighted areas in **Fig. 1b** and the **elements C** in **Fig. 2**).

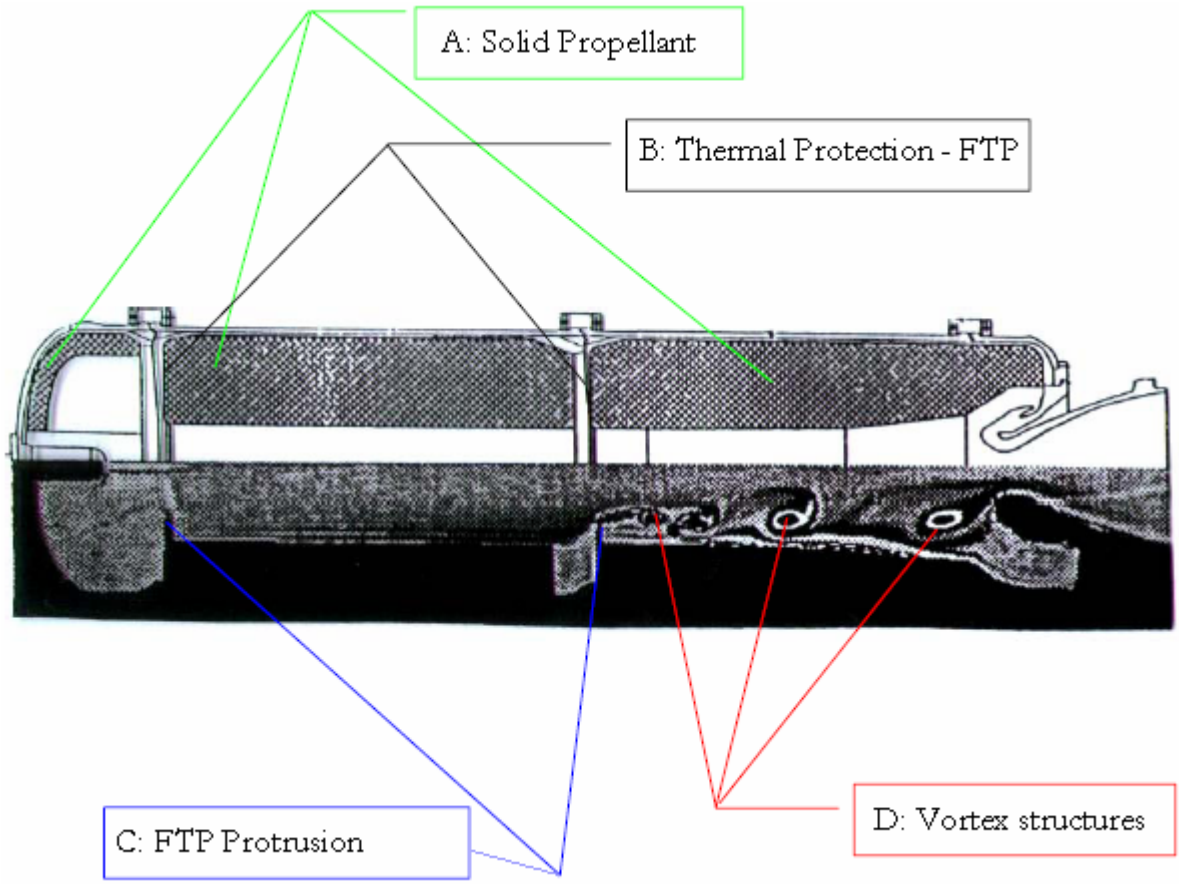

Fig. 2 – SRM internal scheme

The fluid dynamic domain in the vicinity of such obstacles is characterised by the presence of local flows for which, the level of instability generates a periodic vortex release (see the highlighted square box area in **Fig. 1b** and the **elements D** in **Fig. 2**). Such vortexes are the main responsible for the generation of pressure waves oscillation and, as a consequence, for the extra structural loading and thrust oscillation.

Although the phenomena under investigation open a path to an interesting research field, the presence of PWO represents an effective risk for the mission success due to the fact that the generation of structural vibration and thrust oscillation, might induce stability, structural and performance issues for the engine or for the vehicle on which it is mounted.

At the aim of eliminating such vibrations, it is generally required to employ tools and instruments that make the vehicle heavier otherwise it becomes necessary to perform extra tests that would contribute to increase the design costs. This can be seen, during the design and manufacturing phases, in additional engineering endeavours therefore in extra costs.

As a matter of fact the phenomena involved in the internal SRM fluid dynamics is more complex, because a remarkable amount of variables could be introduced and play a significant role. For example one could think about the chemical reactions occurring during gas combustion or about the presence of reacting metallic particles immersed through the flow, generated during the combustion, which could modify the intrinsic dynamics of the flow.

Though if the theoretical development of such factors might look like complex, it should be considered that, also at experimental level, the investigation of the phenomenon for real scale motors could be forbidden by the costs and the difficulty of reproducing the experiment with a certain frequency.

For such reason, the idea of recurring to the employment of reduced scaled motors for the investigation of PWO has already been taken into account by several research institutions and industries (e.g. ONERA, SNPE, AVIO Group, etc). At this aim, adopting such reduced scaled models, numerical simulations have been conducted in order to preliminarily demonstrate the possibility to obtain results reproducing the PWO levels for an equivalent full scale configuration [5]. However, the results obtained have shown to be difficult to interpret. Indeed, the simulations conducted for some scales large scales (1:1 down to 1:2.5) have shown a representative behaviour of the real physics occurring in the motor. On the other hand for lower scales, the PWO phenomena have shown drastic variations in the behaviour, without having clear how such results could be representative for the full scale PWO phenomenon.

It is not clear yet if either a real scale threshold exists, or if the simulation of PWO in reduced scale motors requires to take into account other physical phenomena that for lower dimensions become relevant, deeply modifying the flow field that generates such PWO.

In particular, some preliminary numerical analyses performed by SNPE for scaled demonstrators have shown that the amplitudes and the frequencies of the PWO do not linearly depend on the size of the engine, assuming behaviour completely different, depending on the nature of the flow in the combustion chamber being multi phase or simply gaseous [5].

In such extent, it should be reminded to the reader that typically the SRM thrust level is increased by means of the introduction of an aluminum powder added in the propellant grain matrix, due to the fact that its combustion releases high energy levels. As a consequence during the combustion the aluminum

gets released in the combustion chamber generating a bi-phase or a multi-phase depending on the state (liquid/solid) of each single particle [6].

This behaviour suggested that probably the difference in the PWO levels obtained for different scales can be related to the presence of a discrete phase, and in particular to the characteristic times that each particle requires to travel through the motor and burn [7]. Indeed, independently from the dimension of the engine, the combustion characteristic times of the discrete phase remain the same, while the related residence times very proportionally to the dimensions of the combustion chamber to be crossed.

Thus for high sized motors the discrete phase combustion duration to residence characteristic time ratio can be considered negligible, while for lower sized motors such characteristic times can reach the same order of magnitude. As a consequence the particulate might not have the possibility to completely burn because of an extremely quick ejection from the nozzle, leading to significant physical differences with respect to the case for which the full combustion occurs within the combustion chamber.
Considering the actual state of the art and the limited related knowledge of the phenomena under investigation, at the moment still not fully clear within the scientific community, due to the lack of wide literature and reliable documented experimental tests, the study of the discrete phase combustion would be extremely onerous in terms of engineering and computational efforts.
For such reason, within the present work the attention has been mainly focused on the determination of the *non-reacting discrete phase granulometry* and the numerical evaluation and simulation of the PWO's and the influence on their levels due to the presence of the non-reacting particles.
However, at the aim of offering a support for future research, the dedicated modelling to describe the combustion phenomenon has been investigated, determined and reported in the Annex for the reader.

2 SCOPE OF THE RESEARCH

The present research is addressed to the investigation of the pressure waves oscillation (PWO) inside of solid rocket motors (SRM). In particular, the attention has been focused on the influence of geometrical scale effects of the motor on the PWO's.
Considering the high complexity of the phenomenon and the absence of an effective indication on how such problem should be faced, within this work a first analysis has been conducted to verify the existence that PWO's modify their amplitude and frequency when the characteristic dimensions of the engine vary.
Subsequently it has been verified what occurs in case the particulate is present in the flow and what is the related level of influence on the pressure waves oscillation. It should be noticed that typical industrial propellant grains adopt particulate.
As an engineering necessity, the first aim has been to understand how the particulate dimensions (granulometry) present within the combustion chamber could be determined, then the way and the effects on the internal fluid dynamics and on the PWO's caused by the presence of the non-reacting particulate in a real scale engine.

Summarising, the investigated issues of the present research can be listed in three points:

1) Evaluation of PWO for a single phase configuration;
2) Engine scale effects on the evaluation of PWO for single phase configuration;
3) Investigation of the effects on the PWO levels due to the presence of an additional discrete phase for scaled and real scaled engine configuration.

For such reason the research has been initially articulated modelling the phenomena in a singular manner: the combustion chamber scale effects on the PWO's were first analysed and only afterwards the characteristics of the discrete phase within the combustion chamber flow were studied.
Finally the two phenomena (geometrical scaling and particulate presence) were coupled and their effects on the PWO levels were evaluated.

The investigation conducted on the effects due to the presence of particulate has been subdivided in several parts as follows:

1. The first part of the study, mainly theoretical, has been conducted in order to comprehend and model the behaviour of the discrete phase, which contributes to modify the characteristics of the main flow when the particles get injected in the combustion chamber (cap. 4 e cap. 6);
2. On the other hand, the second part regarded the integration of the developed models within the numerical codes and the related simulation of the PWO for the several scaled configurations under consideration. This part has been mainly performed by means of computer machines and clusters;
3. Finally, within the third part, the results have been analysed and compared.

A further point could be added to such subdivision, related to the particulate combustion modelling. However such case should be considered as preliminary and of scope for future development; the related argumentation has been added in the Annex.

3 STATE OF THE ART

The research related to the PWO phenomena within solid rocket motors is recent.
In Europe the first research programme in such a field has been defined in 1989, named ASSM, supported by the French Space Agency (CNES) and started by ONERA, AVIO and several other research centres and institutions. The programme was focused on the fluid dynamics of Segmented Solid Rocket Motors, such as the ones under industrial interest and employed by Ariane 5.
The main objective was to develop tools to analyse, comprehend, foresee and answer to the issues that might occur during SRM development programmes. Because of the employment of "*segmented technology*" in SRM and the potential acoustic oscillation occurring within the combustion chamber of such motors, previously foreseen and experimentally confirmed within the programme, the main objective of such programme was focused on the study of the internal flow instability for such types of engines.

The first period of activity was spent to identify the parameters influencing the PWO. However the results were not satisfactory due to the difficulty to reproduce the behaviour of both the steady and the unsteady phases of the engine.
The subsequent period was organised foreseeing the definition of an experimental installation. This was realised in a reduced configuration (1:15 scale) and though the results offered excellent understanding of PWO generation and propagation, it was not possible to reveal any correlation with the full-scale configuration case.
Meanwhile, several models were developed in parallel to describe the additional phase (solid or liquid), to be adopted as inert discrete first, and as reacting afterwards. All this was mainly finalised to the forecast of a single issue: the **thrust oscillation**.
The results of such research, which lasted for about ten years, led to the identification of the main issues responsible for the generation of the PWO observed in several types of SRM such as the ones employed onboard the Space Shuttle, Titan and Ariane 5. The final objective of this research was the forecast of the frequencies, the oscillation levels and the estimation of their margins.
One of the most important results obtained within this programme is the comprehension of the "*parietal vortex shedding*" and the "*obstacle vortex shedding*" phenomena, for which the instabilities are directly related to the PWO generation. Particular efforts, that offered only qualitative response, were performed while studying pressure oscillation phenomena for bi-phase flows adopting inert particulate.

As a result it was possible to show that for scale simulations the presence of a dispersed phase shall be taken into account and that some scale effects could be identified. Moreover, such research has shown that the particle dimension represents a sensible parameter that could act and influence on the oscillation levels, not necessarily offering a damping effect.

At the end of this further phase of the research, a new argument was introduced: the aluminum (Al) combustion during engine firing. Such study, complex and still under investigation, led to an important first result stating that the dimension of the particulate within SRM is not uniform, but a function of both the combustion chemistry and the physics of the flow in which the particles are immersed.
Several other researches have led to the confirmation of such qualitative results applying the knowledge acquired during these studies and developing the set-up for the related simulations or tests: ONERA has developed models for porous walls to demonstrate the *parietal vortex shedding* effects within ducts and visualisation techniques for vortex convection. The Von Karman Institute has conducted analogous research to study the effect on vortex shedding due to a segmented engine configuration.
However, though such researches could take advantage of full scale motor models, they always focused the attention on the reasons determining the generation of instability phenomena that could then lead to the generation of PWO; therefore wide importance was given to qualitative data describing the generation of the phenomena under investigation rather than to quantitative data that could instead offer information on their evolution.
A recent activity conducted by SNPE, presented in 2007 [5], has just put into evidence that the PWO levels for a scaled configuration do not always offer the appropriate indication in regards to what occurs to the equivalent full scale configuration. It was therefore numerically noticed a scale effect that kept the doubt alive regarding its effective existence, and the uncertainty to adopt motors with highly reduced scale to foresee the oscillation levels in full scale motors.
The present work, while considering a part of the information, knowledge, errors, etc inherited during previous works, aims at offering a quantitative contribution to the research. Indeed, it is considered that the comprehension of the geometrical engine scale effects in regards to PWO, combined to the effects due to particulate introduction, could offer further information on the existence of other phenomena that have not been adequately considered so far.
An example of such phenomena, developed and adopted in this research, is represented by the generation of a particulate granulometric distribution, theoretically defined within this work, which was never taken into consideration in the frame of numerous other studies reported in literature.

4 THE PHYSICS OF THE PHENOMENA

The SRM internal fluid dynamics represents a very complex scientific argument involving several variables, each of which could offer a significant contribution to the characterisation of the flow.

Within the present work several factors have been introduced and studied, which could significantly influence the phenomena under investigation (PWO). For such reason the PWO phenomenon is first described. Afterwards the physical evolution of the discrete phase is described; this part represents the introduced novelty, for which the effects are to be studied.

4.1 THE PRESSURE WAVES OSCILLATION PHENOMENON

The geometric configuration of the motor under investigation (P230) presents two fundamental features for the PWO generation.
The first feature, caused by the necessity to respect some production and manufacturing constraints, foresees the existence of some protrusions, named *face thermal protections* (FTP), immersed in the main fluid flow, which constitute an obstacle to the flow (Fig. 3).

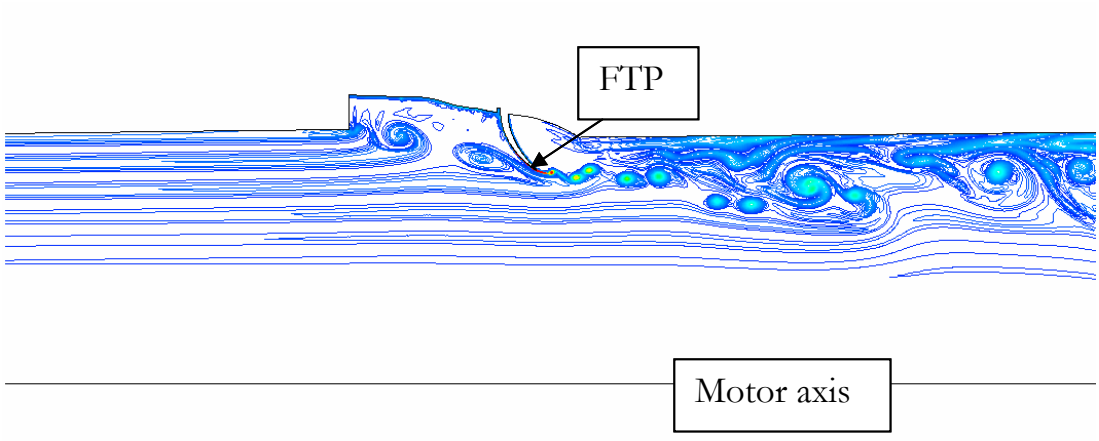

Fig. 3 – Geometrical discontinuities in SRM

Such FTP's get uncovered during engine firing due to the lower regression rate, with respect to the one of the grain in which the FTP's are contained. In such manner, as indicated in Fig. 4, such obstacles tend to emerge in a more considerable manner as functioning time evolves.

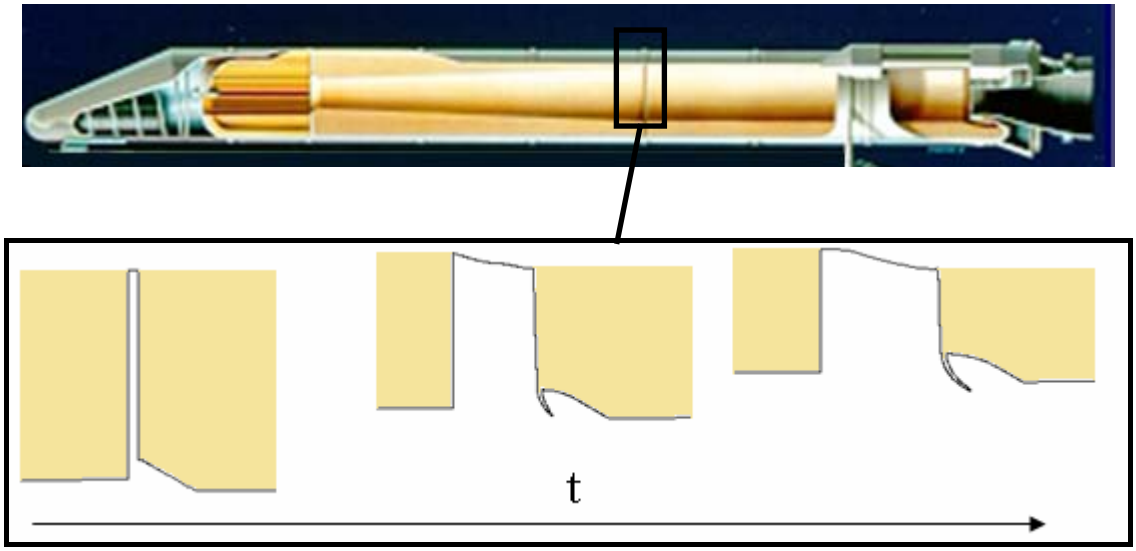

Fig. 4 – Propellant grain regression evolution scheme

A second feature is represented by the nozzle head section which is partially immersed in the engine itself. Considering the study of the vibrations induced, the nozzle head is a particularly important zone because just in its vicinity several acoustic disturbances are generated, which travel through the rest of the engine in the shape of pressure oscillation.

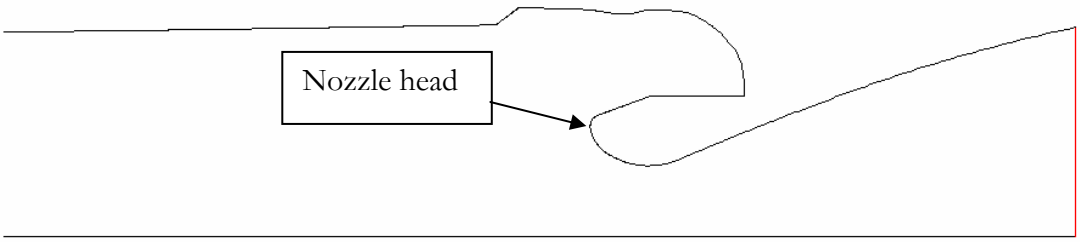

Fig. 5 – Nozzle head

The real process of generation and propagation of disturbance starts in correspondence to the FTP, because of its protrusion towards the inner side of the combustion chamber. Indeed a drastic area variation gets generated and the flow gets constrained in its patch, with a subsequent generation of a shear layer (Fig. 6).

Such layer separates two flow regions with significantly different velocity level; the first region, closer to the engine axis, is characterised by a faster flow, while the second region, closer to the engine wall, is characterised by low speed circulation.

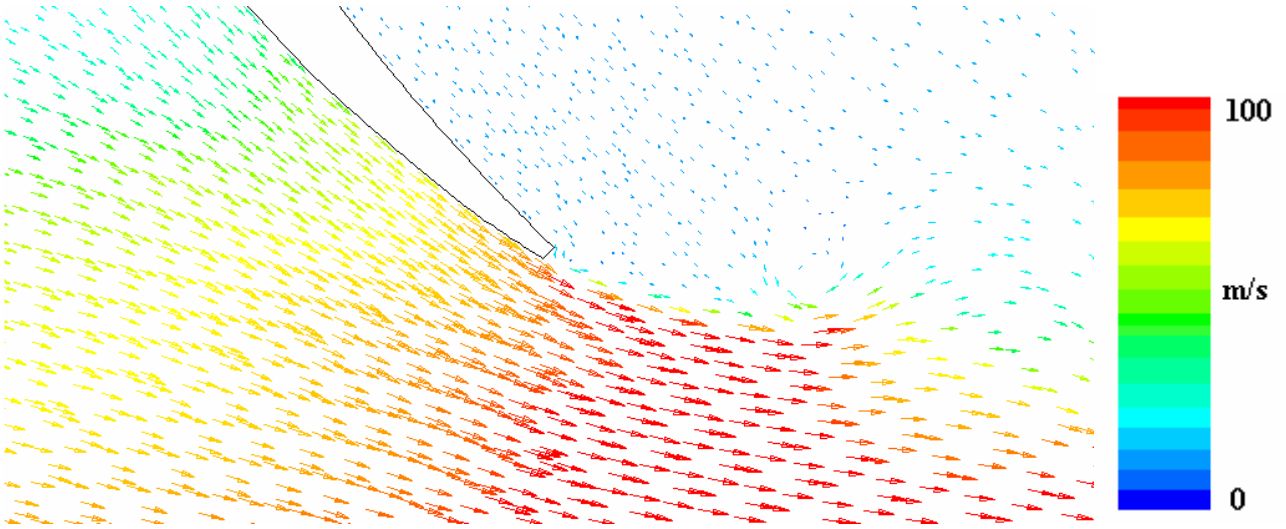

Fig. 6 – Geometrical discontinuity induced differential speed domains

The deep velocity gradient existing through the shear layer makes the flow fairly unstable and small disturbances in the vicinity of the free protrusion could increase such instabilities up to vortex release, which get periodically detached from the FTP, travelling through the combustion chamber (Fig. 7).

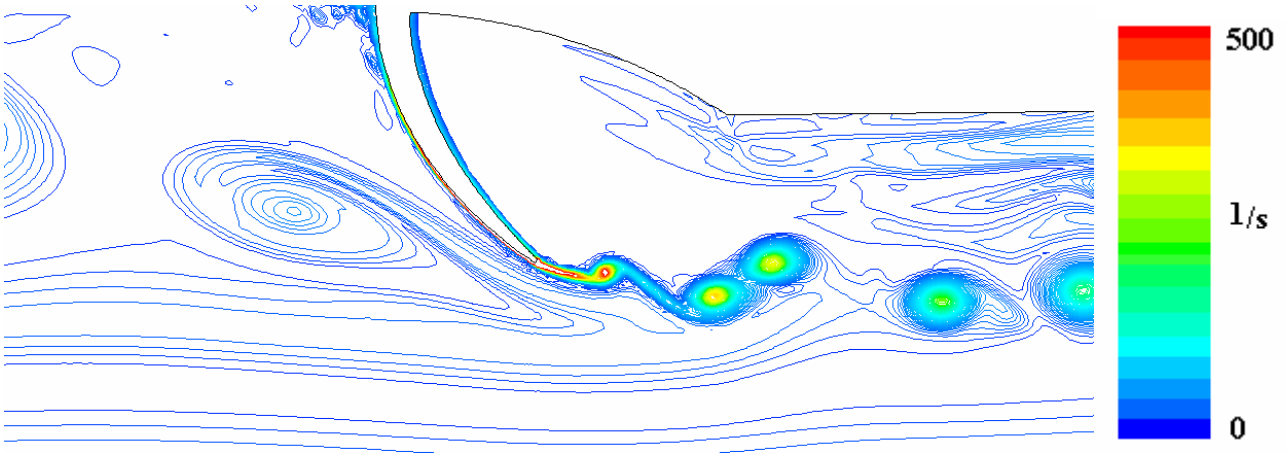

Fig. 7 – Geometrical discontinuity generated vortexes

When the vortex, after travelling through the motor, impact on the nozzle head a dipole source gets generated and the energy passes from the vortex to the acoustic field. Therefore the pressure disturbance, going up again upstream, allows to yield such energy from the acoustic field to the shear layer, which getting excited again, releases a new vortex closing the loop (Fig. 8).

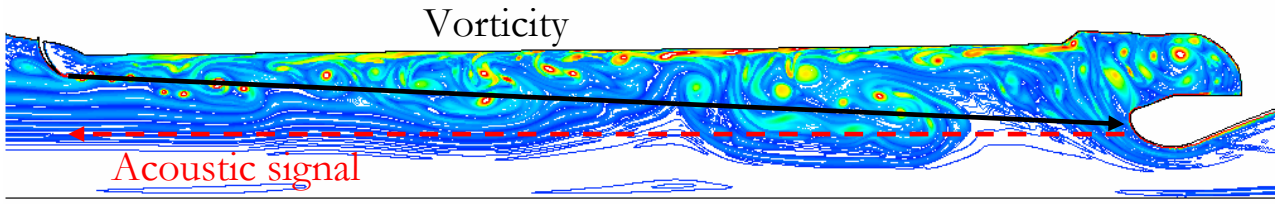

Fig. 8 – Vortexes and acoustic signals propagation direction

The pressure waves oscillation can be self sustained only when generated by an intrinsic the shear layer instability [3].

Therefore, taking into account such observations, it was possible to clearly identify the main steps of the fluid dynamic and acoustic interaction process, as summarised in the following points:

- ✓ Generation of shear layer at the FTP tip;
- ✓ Development, growth and detachment of vortex structures;
- ✓ Vortex impact against a downstream reflecting surface (nozzle head);
- ✓ Fluid dynamic field energy transfer to the acoustic field;
- ✓ Generation of a pressure disturbance going up again upstream towards engine head;
- ✓ Shear layer re-activation;
- ✓ New vortex generation and release with subsequent closure of the loop.

4.2 DISCRETE PHASE PHYSICS

As mentioned in the previous chapter, one of the main and most important investigated aspects in this study is represented by the presence of a multi-phase flow within the engine. The experimental evidence and then the theoretical support have put into evidence how, in this case it is possible to precisely describe a continuous gaseous flow through which a discrete phase is immersed and moves, rather than describing a generic multi-phase flow.
Indeed, as described, the two phases show fairly different characteristics. The first important difference stands in the fact that a phase is considered and treated numerically as a continuous one (the gaseous phase), while the other is treated as a discrete one (the dispersed phase). Moreover, the discrete phase constitutes not only a discontinuous set of inert matter, interacting while exchanging momentum with the main flow, but also as a set of energy sources travelling inside the motor, releasing and therefore distributing heat to the fluid along the path [61].
Due to such behaviour, the particulate combustion process is named "*distributed combustion*".

Inside the engine, during the combustion, several chemical, physical and fluid dynamic phenomena occur. Such phenomena involve the participation of a wide range of characteristic scales. For such reason, the physics is fairly complex and a dedicated modelling is necessary to describe the phenomenon.
In this work the presence of particulate and its influence on the PWO was of interest, also without considering particles combustion. The study of the discrete phase evolution, containing also information on the combustion process, is under development and the theoretical model to be implemented has also been described.

The addition of metallic powders within the propellant grains induces particulate production during the combustion process. Since several propellant types exist holding in particular several metallic powder types, a general behaviour of combustion and particulate evolution could not be described in case a specific propellant to be analysed is not described.
Therefore, the present work has been conducted adopting one of the most employed propellants in the aerospace sector. Such propellant is composed of HTPB (*Hydroxyl Termenated PolyButadiene*), AP (*Ammonium Perclorate*) and Al (*Aluminum*) [9].

The AP grains represent the oxidiser, while the fuel is represented by the Al grains. Although HTPB contributes to offer heat during combustion, its main function is to operate as an adhesive matrix for the AP-Al composed grains. The weight percentages of the single components reported are used for the P230 motor propellant, employed in the Ariane 5 launch vehicle.

HTPB	AP	Al
14%	68%	18%

Tab. 1 – Propellant components mass fractions

Initially the Al powder is contained in the HTPB matrix together with the AP grains as shown in Fig. 9.

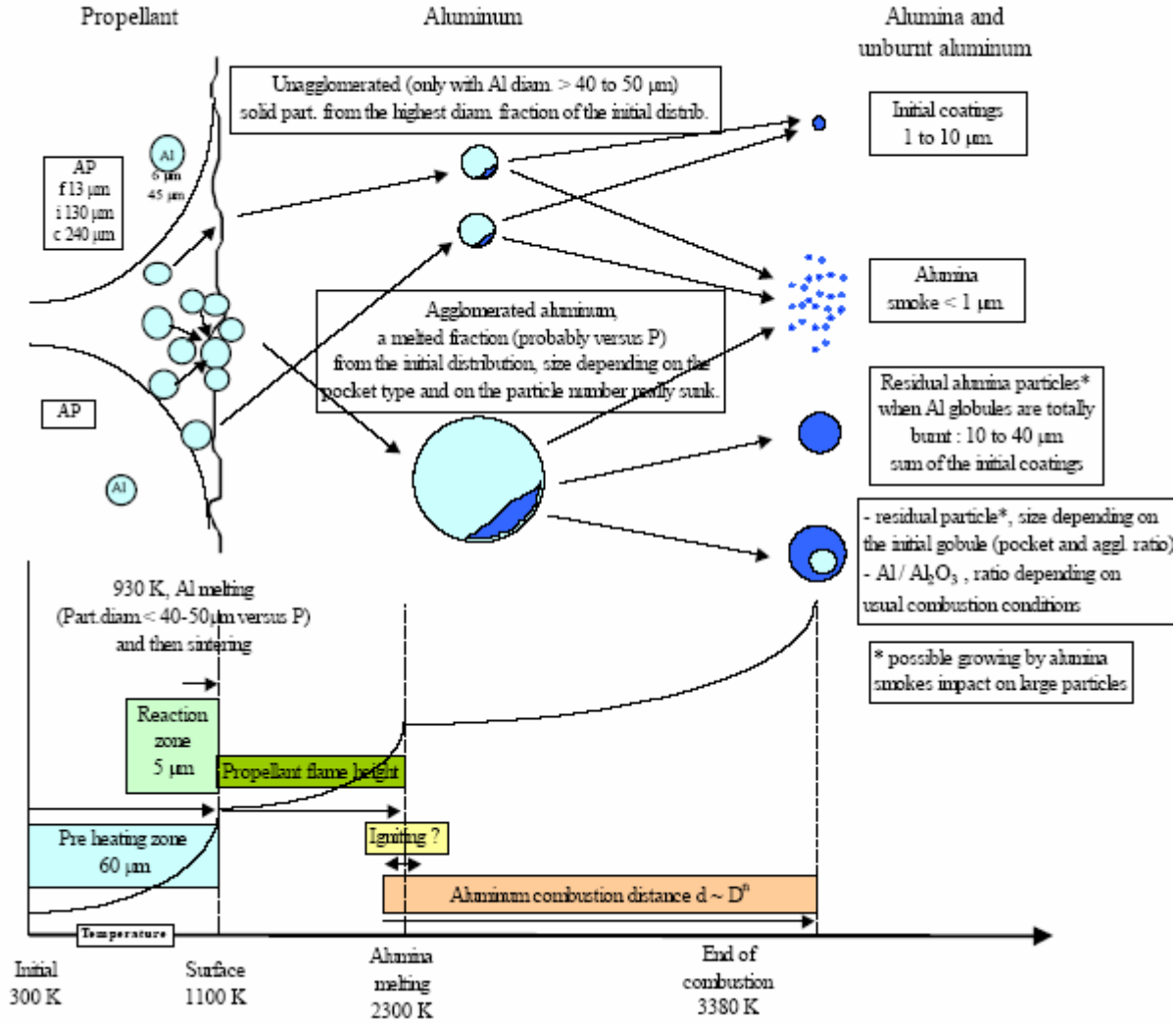

Fig. 9 – Particulate injection phases

During the combustion process, the HTPB matrix vaporises and the most superficial aluminium grains get uncovered. In such manner Al gets in touch with the high temperature fluid in the combustion chamber. Such temperature melts the superficial Al (T_{fus}=933 K [10]) generating a subtle liquid layer on the propellant free surface (Fig. 10).

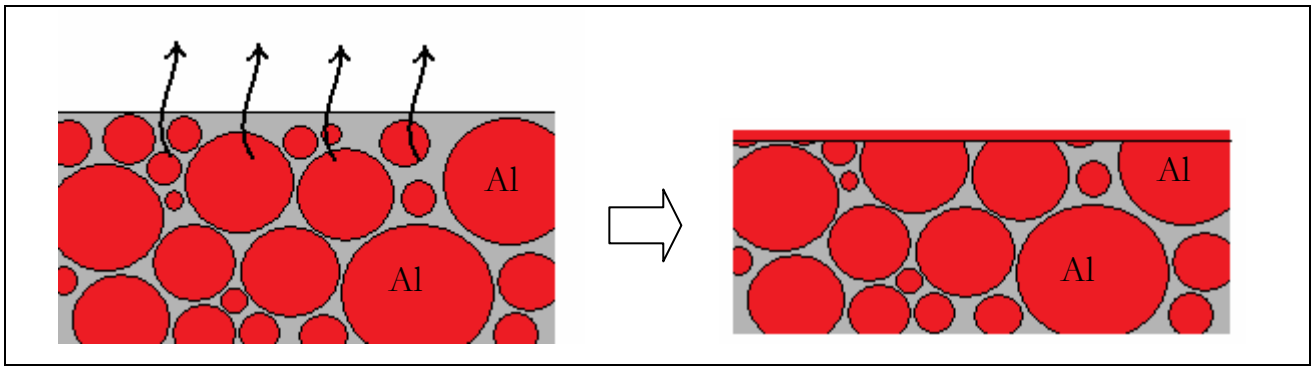

Fig. 10 – Al in the grain melting process

Due to the speed and the turbulent nature of the fluid flowing through the combustion chamber, such liquid aluminum layer gets fragmented into droplets, which get randomly and chaotically dispersed in the chamber (*primary break-up*) and then further shattered by the fluid (*secondary break-up*) (Fig. 11).

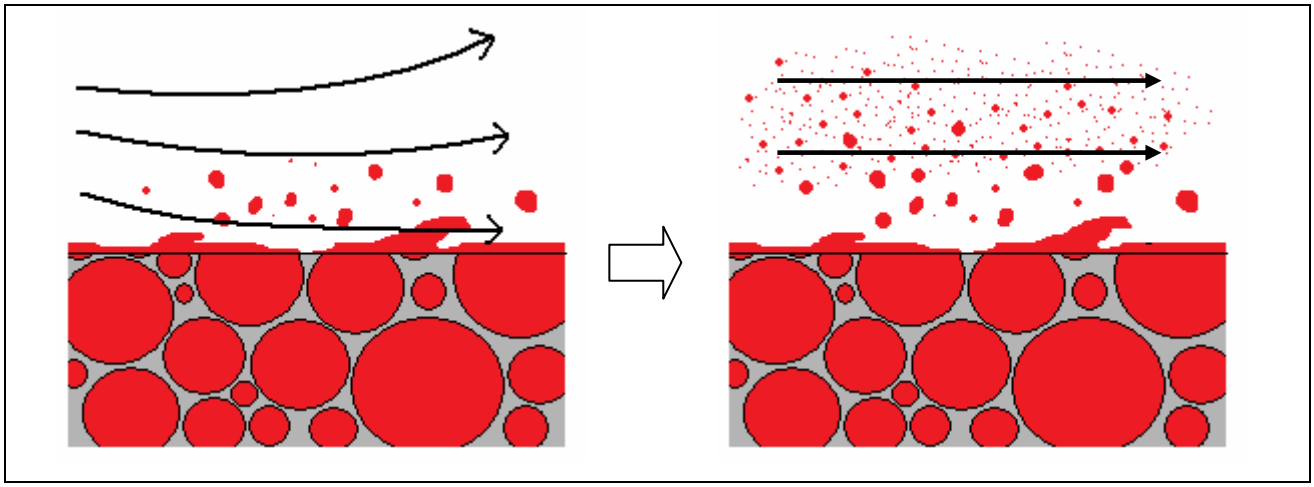

Fig. 11 – Al droplets fragmentation

Within this research the effect of the presence of such particles, supposed inert, is investigated together with their influence on the fluid dynamics and on the pressure waves oscillation (PWO).

In reality, from this point ahead the evolution of the discrete phase is considered as driven also by combustion, which in this work is studied only preliminarily as reported in the Annex; however the effects have not been simulated and are considered of interest for future works.

5 ADOPTED SIMPLIFICATIONS

Although available numerical computer codes can offer a wide range of tools suitable for the evaluation of complex phenomena, it is not always sufficient to employ such tools to describe the entire phenomena under investigation in this work. For example, in some cases when a high level of detail is required, such as in the cased under consideration, it is possible to find numerical behaviours that could not be represented by means of the commercially implemented codes.

In the last part of the present work, for example, several physical phenomena are modelled; such phenomena are theoretically well known at microscopic level (e.g.: Al transformation and combustion, particle transport through the fluid), however the coupling of several macroscopic effects could not be sufficiently described (e.g.: bi-phase reacting flow).

Therefore some assumptions are required, taking into consideration only some physical phenomena that could be considered as the most relevant ones at macroscopic level [48]. For such reason, only some effects generated by the intrinsic preliminarily studied physics were modelled, disregarding some specific phenomena occurring. Indeed, in case one would have to reproduce several characteristics such as a multi-phase flow and its combustion, by solving in detail each single chemical reaction together with each state transition of the particulate, the numerical simulation would have been extremely heavy.

Indeed, considering that an enormous issue of the available numerical codes is related to the computer power limits, the reader can have a feeling that the adopted simplifications become essential, in particular for motors characterised by large dimensions and intrinsic phenomena such as the ones under consideration.

The following two points describe the adopted simplifications:

1. Considering the multi-phase flow, the liquid and solid phases, present within the motor in shape of droplets or combusted grains, have been represented as a single discrete phase composed of particles dispersed within the gaseous phase;
2. The particles injected in the engine are considered to have a spherical shape and their dimensions have been preliminarily modelled as a function of the functioning conditions that time after time the engine can assume. Indeed, in this work the hypothesis is made that the particulate dimensions could depend both on the engine geometry and the internal fluid dynamic characteristics [56].

A third point should be added when the particulate combustion effects will be under consideration: according to the effective particle heat exchange occurring during combustion, the following issues should be modelled:

- Heat exchange between particulate and surrounding fluid;
- Granulometric evolution of the particulate due to combustion.

Already in the past a CFD approach has been considered to study PWO in real scale SRM. Such approach has been further readapted and developed integrating the generated models to the codes for the evaluation of the bi-phase flow.

When describing the physical process, it is possible to show that the presence of an additional phase, to be introduced as a discrete phase, represents an effective novelty to be investigated.
For such reason, in the following chapters the attention has been focused on this novel issue, describing its generation and evaluating its importance during the PWO simulation processes.

6 DISCRETE PHASE MODELLING

When the presence of a particulate is considered of interest of investigation, the first step to be taken regards the granulometry determination. Indeed, as mentioned in the previous chapter, once ejected from the matrix the particulate undergoes a geometric transformation that depends on some characteristics of both the motor and the related internal flow.

Therefore, the approach to the study of the discrete phase within SRM begins just with the determination of such transformation.

The determination of the particulate dimensions distribution within the combustion chamber still represents a problem for which it is difficult to find a solution. Such difficulty is experimentally related to the impossibility to observe and find data within the combustor during its functioning, while theoretically due to the complexity and the multiplicity of phenomena occurring during combustion [50], [54]. Moreover, the coupling of the intrinsic particulate phenomena and the fluid dynamics holds chaotic properties [20], [21], [43], therefore difficult to be represented.

For such reason, in literature it is often found that the description of the particulate combustion in SRM is offered simplifying the problem adopting either a random distribution for the discrete phase [58] otherwise constant initial dimensions [6], while for what concerns the thermal and geometrical evolution (equal for each particle) experimental laws are taken into account [9], [13], [20], [22]. However in such manner the reliability of the results should be influenced by such limitations.

At the aim of evaluating the particulate characteristic dimensions with higher reliability within the combustion chamber, several experiments have been conducted in the past in order to measure the granulometry of the particulate collected at nozzle outlet. Although not offering rigorous information, such collections could be used to have a preliminary estimation of the particulate order of magnitude during its presence within the combustion chamber [23].

As mentioned in advance, the dimension assigned to the particle within this work, is intended as the one assumed by the particle, originally injected in the combustion chamber, after its several break-ups (*primary/secondary break-up*) attained while passing through the chamber. Such break-ups are difficult to estimate and from this point of view, the determination of the final dimensions (hence after secondary break-up), also passing through intermediate break-ups (primary break-up) constitutes a significant problem. However, in this case the problem is faced in a different manner. Hence the intermediate particle conditions during break-up processes have not been considered; indeed only the maximum

dimensions assumed by a liquid droplet in a specific flowing fluid have been determined, disregarding what the particle could experiment in the moments before break-up.
In order to perform such evaluation it is necessary to have knowledge of the physics of particle break-up: it holds an equilibrium as a consequence of the balance between fluid dynamic stresses acting on the particle surface and its superficial tension. When the fluid dynamic stresses win the superficial tension the droplet becomes unstable suffering a break-up into two or more smaller drops [24].
This effect suggests that, independently from the type of break-up under experimentation, for each particle a maximum or critical diameter can be assumed along its path, and its value is a function of the fluid dynamic actions suffered by the particle. A diameter value higher than the critical value would induce the particle to be unstable and therefore break-up [25].
The break-up process is therefore described in this work as a single process, though if in reality it would occur in two steps. The break modelling and the employed methodology to calculate the most probable granulometry present in the motor during functioning is reported in paragraph 6.1.
In this treaty, after analysing the trajectory of each single particle and determining the respective critical diameter, it has been assumed that:

- Each particle destined to break-up (hence having at least for a position along its trajectory a diameter higher than its critical diameter), assumes a smaller diameter, exactly equal to its critical diameter;
- Each particle destined to remain complete (therefore having for each position along its trajectory a diameter which is lower than its critical diameter), keeps its own diameter.

This choice to consider each particle as a treated different from all the others, allows to determine a most probable diameter distribution, instead of considering all the particles with the same dimension. Such model is certainly more representative of the real conditions.
For such scope a methodology has been adopted that could preliminarily reveal the most probable granulometric distributions as function of the engine geometry and ballistics.

6.1 PARTICULATE GRANULOMETRY DETERMINATION

The methodology to determine the initial granulometric distribution assumes an important role within the present study because, when applied to the geometry of full scale and then of reduced scale SRM, it identifies different characteristic dimensions of the particulate, therefore highlighting that when scaling

the engine it is possible that also the particulate receives a certain re-dimensioning, which is not proportional to the scale factor.

Some studies report on the possibility that the particle dimension within a duct depends on the duct dimensions [24], [26]; however the dimensioning procedure is not clear yet.

However, considering that a deeper work on the argument has not been attained yet, within the present research an approach is proposed to determine a probable granulometric distribution as function of the geometry and the fluid dynamic conditions in the combustion chamber.

Such approach is mainly based on the analysis of the critical break conditions of the particles flowing through the fluid. The achievement of such conditions would generate a droplet destabilisation and consequent break-up occurring with different intensity, as function of the surrounding fluid dynamics.

As mentioned before, since the knowledge of such phenomenon is not completely well known, the description of particle break process is still generally performed through the adoption of adimentional numbers and engineering formula based on theory under development, therefore requiring appropriate tuning and correction, to be offered comparing with experimental data.

The most suitable number to be considered for the description of the droplet break-up is the Weber number (*We*), defined as follows [27]:

$$We = \frac{\rho_{gas} u_{rel}^2 \phi_p}{\sigma} \qquad \textbf{eq. 1}$$

Where ρ_{gas} indicates the gas density, u_{rel} the relative speed between the particle and the flow, ϕ_p indicates the particle diameter and σ its superficial tension.

This number describes the relative importance between the fluid dynamic actions tending to break the particle and the superficial tensions, which tend to oppose to such break, contributing to have the particle maintaining its own shape.

When a particle *We* exceeds a certain critical value, the particle breaks generating two or more smaller particles [27].

The value of this edge, called ***critical We***, defined and calculated for each single particle, is not represented by an unambiguous value; it varies depending on the nature of the flow, therefore on the accelerations suffered by the particle and the superficial stresses, according to the geometry and material characteristics of the particle [24], [28], [29], [30].

Since for the study of such critical parameter a consolidated theory does not exist, it was necessary to understand its most representative values as function of the chemical/physical conditions of the flow.

It is possible to comprehend in this manner the reason why in literature several different formulas exist for the determination of the critical *We*, each of which defining the critical Weber conditions in particular conditions functioning (particles in spray, particles in incompressible flow, in co-axial duct, etc.), without having a universal law.

In literature the critical Weber is typically defined as follows [24]:

$$We_{cr} \equiv \frac{\tau d_{\max}}{2\sigma} \qquad \textbf{eq. 2}$$

Where $d_{\max}$ indicates the maximum particle stable diameter, τ defines the stress tending to generate particle break, while σ indicates the superficial tension, which is opposed to the action of τ.

The stress term, τ, can be expressed in terms of particle to fluid kinetic energy difference as follows:

$$\tau = \rho_f u_{rel-\max}^2 \qquad \textbf{eq. 3}$$

Leading to:

$$We_c \equiv \frac{\rho_f u_{rel-\max}^2 d_{\max}}{2\sigma} \qquad \textbf{eq. 4}$$

From this point on the development of the analytical expression of *We* can take several directions, depending on the type of problem to be solved. In case of duct with internal flow, it can be helpful to represent some dimensions, present in the formula, in terms of turbulence, introducing the simplest case of turbulence (isotropic and homogeneous). In this manner the main contribution to the kinetic energy is caused by the fluctuations in the regions of the wavelengths where the *Kolmogorov* energy distribution is valid. In such region, the local turbulence model is determined by the turbulent dissipation rate ε [m^2/s^3].

In terms of ε, the maximum relative velocity is offered by Levich [69]:

$$u_{rel-\max} \approx \left[\varepsilon d_{\max}\left(\rho_p/\rho_f\right)\right]^{1/3}\left(|\Delta\rho|/\rho_0\right)^{1/2} \qquad \textbf{eq. 5}$$

Where ε represents the turbulent dissipation rate, ρ the particulate and the fluid density. This induces to:

$$We_{cr} = \rho_f \varepsilon^{2/3} d_{\max}^{5/3}\left(\rho_p/\rho_f\right)^{2/3}\left(|\Delta\rho|/\rho_0\right)/\sigma \qquad \textbf{eq. 6}$$

Observing this formula, effective only in cases for which the Kolmogorov energy distribution can be assumed, it should be noted that the critical *We* is mainly a function of the discrete to surrounding fluid density ratio ($We = f\left(\frac{\rho_p}{\rho_f}\right)$).

As mentioned in advance, the critical Weber value of varies as function of the geometry and the characteristics of the flow. Starting from eq. 6, this led to develop further formulas. In the present case, given the engine geometry and the nature of the flow, the modifications brought to eq. 6 that develop the ε term and reported in [24] and in [29] conduct to the law describing the behaviour of a particle in a very lower density medium inside ducts:

$$We_{cr} = \left(\frac{\rho_p}{\rho_f}\right)^{\frac{2}{3}}\left(\frac{\left|\rho_p - \rho_f\right|}{\rho_p}\right)\cdot\frac{24}{\pi^2\left(\frac{3\rho_p}{\rho_f}+2\right)} \qquad \textbf{eq. 7}$$

Where again ρ_p and ρ_f indicate respectively the discrete and the continuous phase. In the case under examination, the density ratio assumes a value equal to $\frac{\rho_p}{\rho_f} = \frac{2700Kg/m^3}{4.5Kg/m^3} = 600$ and the related critical Weber value corresponds to about 0.1.

Such law is indeed valid only for particles for which the density is very higher than the surrounding fluid density $\left(\rho_p >> \rho_f\right)$.

Several other engineering formulas deriving from experimental data fitting are reported in literature [28], such as:

Karabelas (1978) $$We_{cr} = 5.9\left(\frac{\rho_c D U_f}{\mu_c}\right)^{-\frac{1}{6}} \qquad \textbf{eq. 8}$$

Hesketh et al (1987) $$We_{cr} = 1.1\left(\frac{\rho_f}{\rho_p}\right)^{\frac{1}{6}} \qquad \textbf{eq. 9}$$

They are also valid for turbulent flows in ducts, which offer dimensions with the same order of magnitude with respect to the ones obtained in eq. 7.

The methodology adopted in this work for the determination of the most probable granulometry takes into account considerations regarding the particle break just presented.

The present methodology is articulated in three main phases:

1) Definition of an initial granulometric distribution representing the presence of each diameter with the same number of particles in a range defined by a minimum and a maximum diameter (an example is reported in Fig. 12);

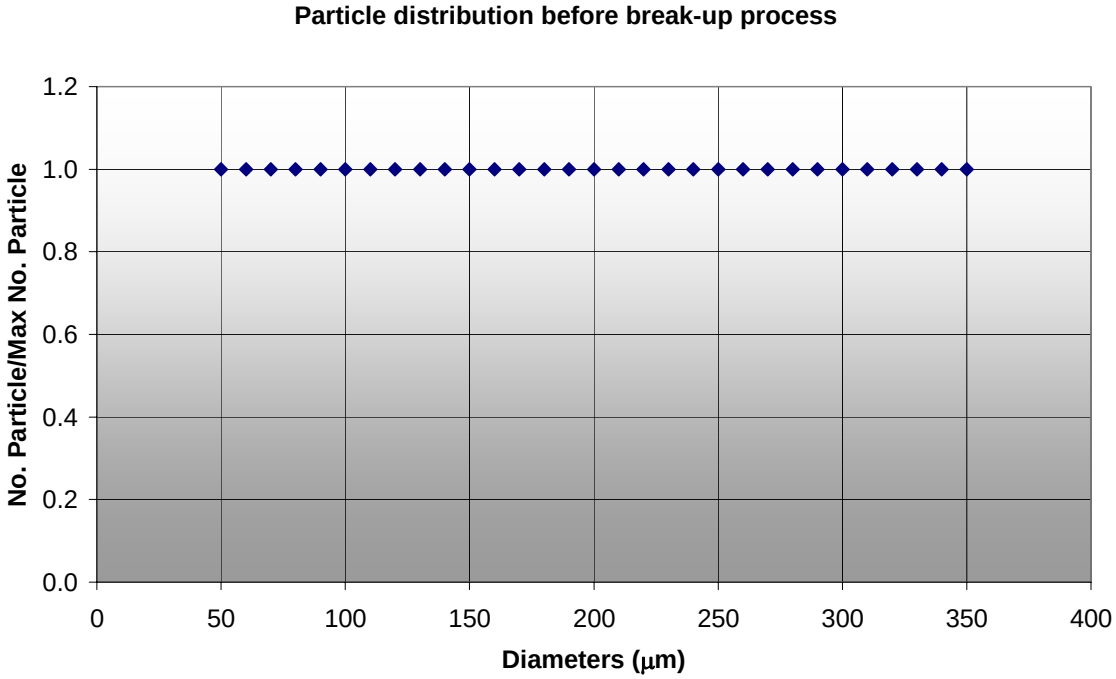

Fig. 12 – Particulate input dimensions

2) CFD simulation of the bi-phase flow with inert particulate, adopting the granulometry as defined in point 1;
3) Maximum theoretical dimension evaluation assumed along the trajectory by each single particle recurring to the critical Weber theory.

The development of this third point occurs in a fairly articulated manner. For such reason several ad-hoc FORTRAN codes were written, which could operate functional transformations on the data offered by the CFD simulation (point 2) considered now as input, and offering back as outputs the wanted granulometries (for example in Fig. 13 is reported an output distribution obtained with the described procedure).

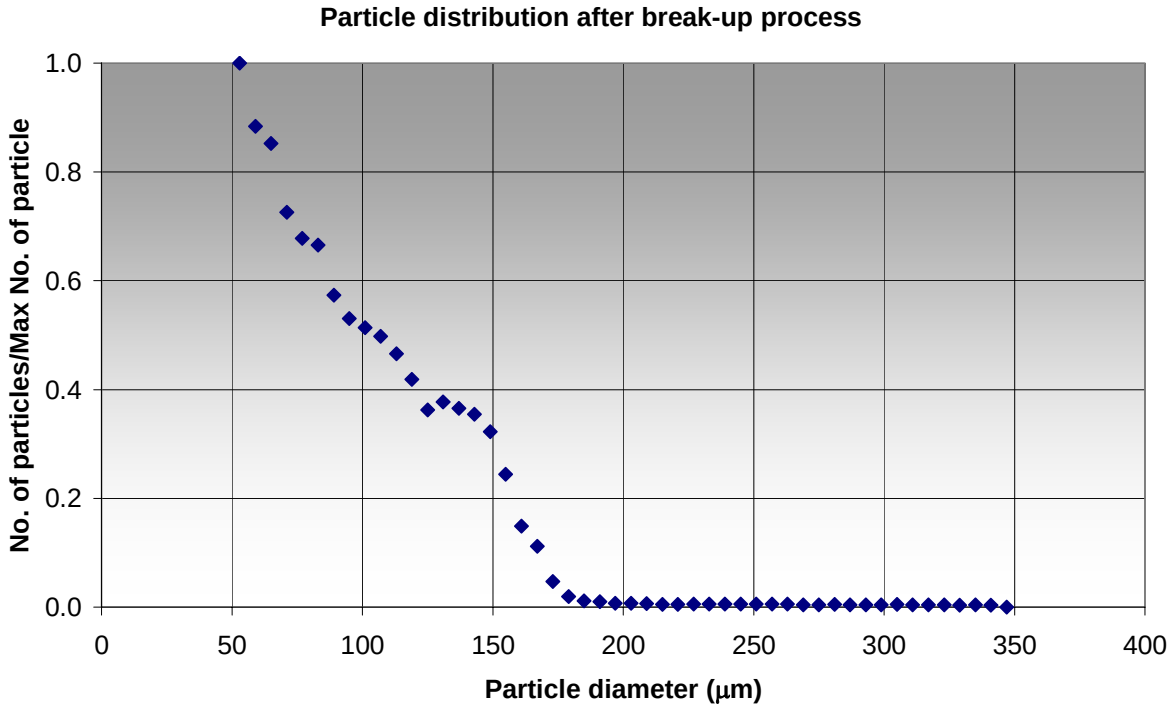

Fig. 13 – Particulate output dimensions

The process described so far is graphically represented in the following block (Fig. 14).

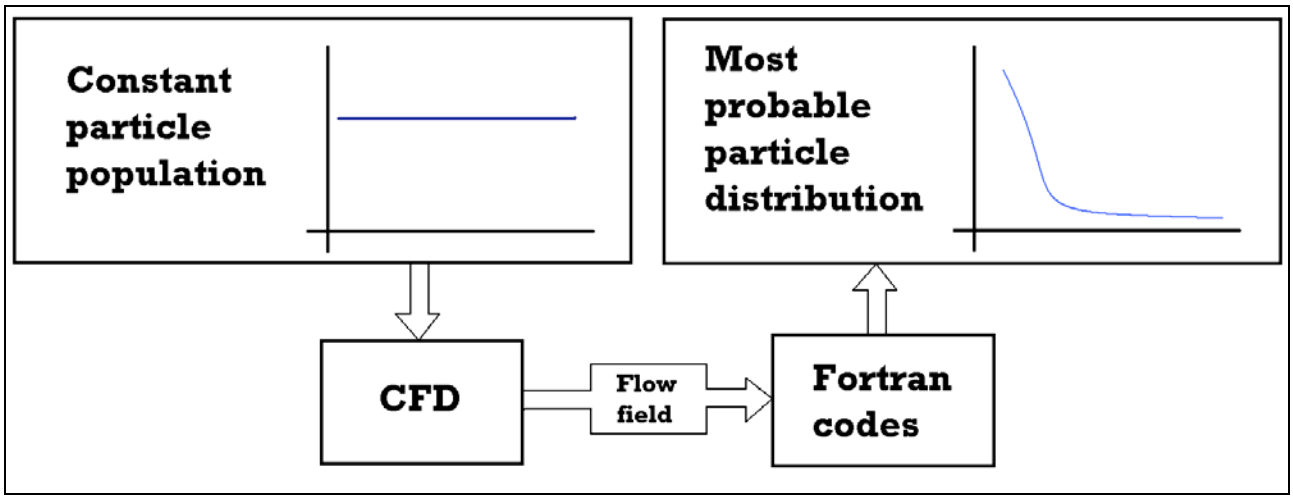

Fig. 14 – Particulate dimension transformation process

The input data for the FORTRAN codes, obtained as result of the CFD defined in point 2, are represented by the magnitudes reported in the following list;

- Residence time (time spent from particle injection in the combustion chamber);
- Particle space coordinates;

- Particle speed components;
- Particle temperature;
- Particle density;
- Particle mass;
- ID number.

Where the last information allows to determine the trajectory of the particles injected along the propellant grain.

Such parameters are contained in a tabular file, such as the one reported in Fig. 15, where each row contains information related to a single particle and the columns identify the parameters expressed in the top of the file.

Each file of this type contains only information related to the particles ejected by a single inlet. Hence for combustion chambers such as the one of the P230, characterised by several separated propellant blocks (i.e. containing more than one inlet) it has been necessary to produce a higher number of files of such type.

```
FILE TYPE:      1
COLUMNS: 13
TITLE:  TRACK HISTORY

 COLUMN         TYPE    VARIABLE                (UNITS)
 ------         ----    --------                ------
      1          2      TIME                    (SECONDS)
      2         10      X-POSITION              (METERS)
      3         10      Y-POSITION              (METERS)
      4         10      Z-POSITION              (METERS)
      5         10      U-VELOCITY              (M/SEC)
      6         10      V-VELOCITY              (M/SEC)
      7         10      W-VELOCITY              (M/SEC)
      8         10      DIAMETER                (METERS)
      9         10      TEMPERATURE             (KELVIN)
     10         10      DENSITY                 (KG/M3)
     11         10      MASS                    (KG)
     12         10      NUMBER
     13         10      COLORBY                  -
-----------------------------------------------

1.71500e-001    1.49342e+001    1.01919e+000    0.00000e+000    2.77355e+001    -1.25708e+000   0.00000e+000    5.61224e-005
1.66500e-001    1.47958e+001    1.02567e+000    0.00000e+000    2.71485e+001    -1.20508e+000   0.00000e+000    5.61224e-005
1.61500e-001    1.46622e+001    1.03169e+000    0.00000e+000    2.57079e+001    -1.17179e+000   0.00000e+000    5.61224e-005
1.56500e-001    1.45316e+001    1.03780e+000    0.00000e+000    2.54499e+001    -1.20053e+000   0.00000e+000    5.61224e-005
1.51500e-001    1.44070e+001    1.04389e+000    0.00000e+000    2.43096e+001    -1.29291e+000   0.00000e+000    5.61224e-005
1.46500e-001    1.42846e+001    1.05081e+000    0.00000e+000    2.40487e+001    -1.50125e+000   0.00000e+000    5.61224e-005
1.41500e-001    1.41654e+001    1.05963e+000    0.00000e+000    2.36183e+001    -1.94077e+000   0.00000e+000    5.61224e-005
1.36500e-001    1.40507e+001    1.07125e+000    0.00000e+000    2.09672e+001    -2.73785e+000   0.00000e+000    5.61224e-005
1.31500e-001    1.39543e+001    1.08822e+000    0.00000e+000    1.75821e+001    -4.05242e+000   0.00000e+000    5.61224e-005
1.26500e-001    1.38932e+001    1.10892e+000    0.00000e+000    3.23684e+000    -2.98301e+000   0.00000e+000    5.61224e-005
1.21500e-001    1.38785e+001    1.12326e+000    0.00000e+000    2.54828e+000    -2.66024e+000   0.00000e+000    5.61224e-005
1.16500e-001    1.38663e+001    1.13593e+000    0.00000e+000    2.29672e+000    -2.44475e+000   0.00000e+000    5.61224e-005
1.11500e-001    1.38552e+001    1.14799e+000    0.00000e+000    2.14268e+000    -2.39631e+000   0.00000e+000    5.61224e-005
```

Fig. 15 – Output file of the CFD block

Moreover, in the same file, for each position occupied by the particle, also the local gaseous flow characteristics were recorded (pressure, temperature, density, etc.).

The input and output sequence used and generated by the attained Fortran codes for the determination of the granulometry is represented in the diagram of Fig. 16 (where "CFD" and "Flow field" represent the same blocks already presented in Fig. 14)

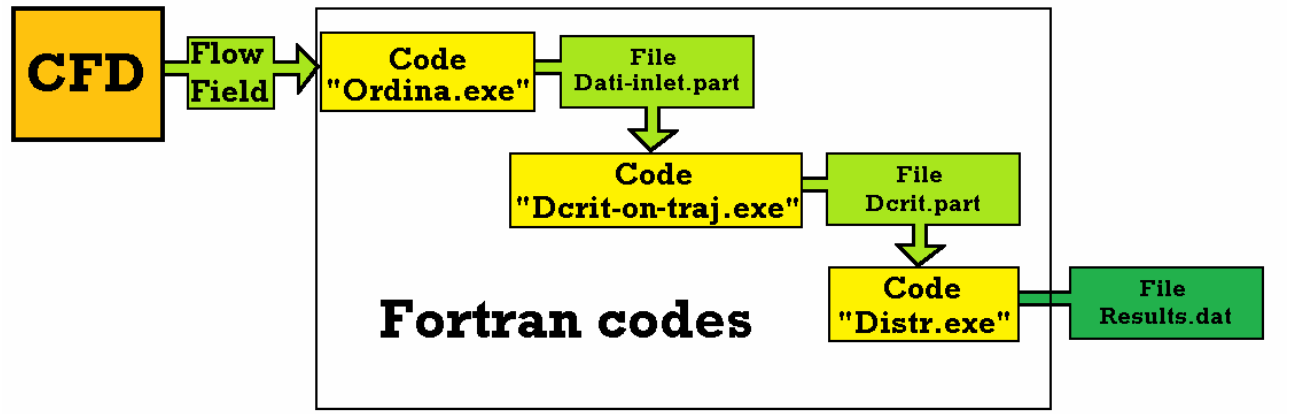

Fig. 16 – FORTRAN codes block for the evaluation of the particulate dimension

It gas been summarised in the following three points:

1. Recognition of the trajectories followed by the particles;

   This is executed via a code defined "*ordina*", which takes as input the several files as indicated in Fig. 15, where information on the flow field is contained ("*Flow field*" block in Fig. 16) and gathers the particles moving along the same stream line in the file "*Dati-inlet.part*". In the steady flow the stream line identifies the trajectory travelled by the particles.

2. Critical diameter evaluation along each trajectory;

   This is executed by the programme named "Dcrit-on-traj", which analyses separately each trajectory (contained in the file "*Dati-inlet.part*" generated by the code "*ordina*") and applying the relations indicated represented by eq. 1 and eq. 7 determines for each trajectory the maximum diameter that each particle on a specific trajectory can maintain, according to the received fluid dynamic actions.

3. Assignment of a specific diameter to each particle;

   Once determined the critical diameter or the maximum one, sustainable by a set of particles along the same trajectory, the code *Dcrit-on-traj* decides to assign this new dimension to the particle in case for which the particle diameter should result higher than the critical diameter (hence unstable). Instead, in case the particle dimension would be lower than the critical diameter, the code would not operate any variations on the particle dimensions.

Once terminated the assignment of each new characteristic diameter for each trajectory, the code writes such value on a file named "*dcrit.part*". A new file is generated containing a number of rows equal to the

umber of trajectories, for which each row indicates the value of the diameter assumed by the particle along such trajectory (Fig. 17).

```
9.433084727320881E-005
9.240054124226509E-005
9.236142926044421E-005
9.070184884696862E-005
8.887630115513519E-005
8.883612857441570E-005
8.707338152008631E-005
8.726618595246090E-005
8.554274260384983E-005
8.387150823259648E-005
8.547376053561329E-005
8.405854478944487E-005
8.242393542171175E-005
8.239232234011488E-005
7.929313558379884E-005
8.076520239206916E-005
8.257385554132497E-005
7.946838676179316E-005
7.796723074974412E-005
7.939535192553984E-005
7.789932536263449E-005
7.933331944079029E-005
7.960497647696150E-005
7.666590918310790E-005
7.663461658451916E-005
7.660477876847659E-005
7.656542192708172E-005
7.795878858363375E-005
7.684380511545096E-005
7.540648693157680E-005
7.401623158220374E-005
```

Fig. 17 – "Dcrit.part" file example

Subsequently a third code named "*Distr*", discretises the entire range of diameters reported in the file dcrit.part in a finite number of intervals and distributes the particles in intervals depending on the value of their diameter. The output of this last code is again contained in a file shown in Fig. 18 named "*results.dat*". Inside of it the first column the average value of the diameters of each single interval is contained, in the second column the number of particles contained in it and in the third column the particulate mass fraction associated to such interval.

2.079999994748505E-005	516	2.431247608035265E-012
2.239999994344544E-005	520	3.060108910806278E-012
2.399999993940583E-005	481	3.481515126065361E-012
2.559999993536622E-005	454	3.988092599793103E-012
2.719999993132660E-005	442	4.657131128634313E-012
2.879999992728699E-005	405	5.065495937267323E-012
3.039999992324738E-005	384	5.648608302997156E-012
3.199999991920777E-005	383	6.571101776400564E-012
3.359999991516815E-005	376	7.467842707333011E-012
3.519999991112855E-005	357	8.152403962890148E-012
3.679999990708893E-005	327	8.532586379733441E-012
3.839999990304933E-005	300	8.894149245133299E-012
3.999999989900971E-005	265	8.880048398468858E-012
4.159999989497010E-005	234	8.820340159383753E-012
4.319999989093049E-005	215	9.075680220937287E-012
4.479999988689087E-005	194	9.133248133791045E-012
4.639999988285127E-005	182	9.519514824700810E-012
4.799999987881165E-005	143	8.280360299831128E-012
4.959999987477204E-005	109	6.964036076782527E-012
5.119999987073243E-005	80	5.621980757417591E-012
5.279999986669281E-005	67	5.163760073133149E-012
5.439999986265321E-005	55	4.636058137102033E-012
5.599999985861359E-005	38	3.494114741906207E-012
5.759999985457399E-005	30	3.001775370232488E-012
5.919999985053437E-005	21	2.281255347219443E-012
6.079999984649475E-005	13	1.529831415395063E-012
6.239999984245515E-005	5	6.360822230324822E-013
6.399999983841553E-005	5	6.862769479269518E-013

Fig. 18 – "Result.dat" file example

The output offered in point 3) in the file named "*Results.dat*" offers a granulometric distribution normally very different from the starting one. This is visible in the explanatory distributions already reported in Fig. 12 and Fig. 13.

It is evident from this comparison that the probability that the bigger particles could be in critical conditions, therefore could get to break is very high and this, during engine functioning, decreases their number, modifying the diameter and repositioning in the graph such particles in the zones characterised by lower diameters.

Certainly for a particle destined to break, the higher the fluid dynamic actions on the surface, the lower the maximum diameter to be assumed.

With reference to Fig. 13, the new distribution obtained through the analysis contained in the file "results.dat", is used as initial granulometry for the multiphase distribution.

Inside the calculus code employed, at the aim of introducing the granulometry as input, it is necessary to reproduce it analytically under the shape of a *Rosin-Rammler* function [40], as indicated in the following equation:

$$Y_d = e^{-\left(\frac{\phi}{\bar{\phi}}\right)^n} \qquad \textbf{eq. 10}$$

However this shape does not simply indicate the probability associated to each diameter □ to be represented by a number N of particles, but as the probability to find, within the whole set of injected particles, diameters higher than ϕ. It indicates an integral of the particle distribution of probability density.

For example, in Fig. 19, the value of the red curve (Rosin-Rammler function) in correspondence of ϕ represents the integral between ϕ and ∞ of the black curve, which pointwise represents the number of particle associated to each diameter represented in abscissa, datum contained in the "results.dat" file.

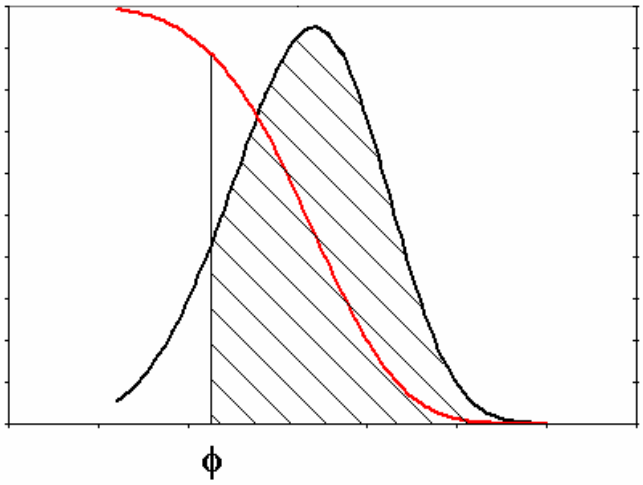

Fig. 19 – Rosin-Rammler function scheme

Therefore, in order to analytically represent the behaviour of the particulate distribution obtained under Rosin-Rammler function shape, it is necessary to obtain the integrating function.

Hence indicating $Y_d = \int_a^x f(t)dt$, it results that its derivative is:

$$\frac{d}{d\phi}(Y_d) = \frac{d}{d\phi}\int_{\phi}^{\phi_{max}} f(t)dt = -\frac{d}{d\phi}\int_{\phi_{max}}^{\phi} f(t)dt \qquad \textbf{eq. 11}$$

Being $\frac{d}{dx}\int_a^x f(t)dt = f(x)$, results:

$$\frac{d}{d\phi}(Y_d) = -\frac{d}{d\phi}\int_{\phi_{max}}^{\phi} f(t)dt = -f(\phi) \qquad \textbf{eq. 12}$$

therefore

$$f(\phi) = -\frac{d}{d\phi}\left(e^{-\left(\frac{\phi}{\bar{\phi}}\right)}\right) = \left(\frac{n}{\bar{\phi}}\right)\left(\frac{\phi}{\bar{\phi}}\right)^{n-1} e^{-\left(\frac{\phi}{\bar{\phi}}\right)} \qquad \textbf{eq. 13}$$

In this manner it has been defined the analytical shape of the function to fit with the curve in Fig. 12b combining the $\overline{\phi}$ and n parameters.

To validate the just presented methodology, such procedure has been applied in this work to test cases characterised by several widely different SRM dimensions, for which the particulate dimensions in combustion chamber represent known data.

Such verifications, together with offering an excellent estimate of the most probable particulate dimensions, have further shown also a good representation of the granulometric representation.

Even if the presented model shows limitations, as a consequence of the adopted simplifications, it constitutes in any case a development in the identification of the most probable granulometry present within the motor to be adopted during the simulation. Although not comprehensive of several important phenomena, it is reminded that the model should be considered as a support to the simulations. Such simulations have the final scope to evaluate the PWO.

6.2 METHODOLOGY VALIDATION

The validation of the methodology employed within the present research to forecast the particulate dimensions within SRM, has been conducted on two motors presenting two different configurations.
The dimensions that the particulate could present in such motors has been evaluated via the exposed methodology and then compared with the real particulate dimensions, known for the two SRM taken in consideration, being:

1. A demonstrator with very reduced dimensions for experimental activities developed by ONERA [23];
2. The full scale configuration of the P230 at instant in time t=87 [s] [39].

For both selected SRM, geometry, ballistics and granulometry are known or simple to determine quantities. Holding very different characteristic dimensions they represent two cases particularly suitable for the validation of the methodology under exam.

6.2.1 ONERA DEMONSTRATOR VALIDATION

The demonstrator taken under examination is employed at ONERA for experimental activities.
As shown in Fig. 20, this demonstrator is composed of several modules for which the coupling makes possible the definition of different lengths.
The considered geometry to validate the procedure is exactly the one indicated in figure, for which all the modules available in the plant have been adopted.

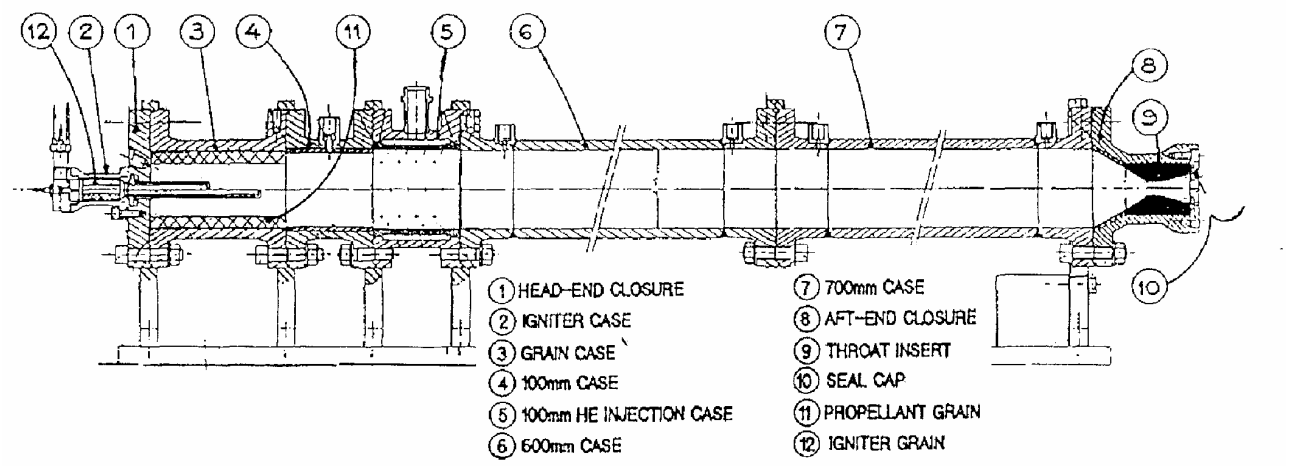

Fig. 20 – ONERA demonstrator for experimental activities

Since the scope of this work is to obtain the particulate granulometry during the first phases of combustion [23], the experimental configuration taken into consideration is the one for which the aluminium droplets, once injected in the motor, undergo break-up processes (primary/secondary break-up) under the actions of the surrounding fluid; however the droplets do not have the time to take part to the entire combustion process because of the immediate cooling effect of a cold helium jet, which subtracting energy makes them solidify (in detail see the module indicated in figure 5).

Thanks to this cooling process it is possible to freeze the dimensions of the particles in the moment when they should be modified by the combustion process. The dimension and the number of cooled particles have been experimentally estimated gathering data regarding their dimensions in two different manners:

1. Via optical laser placed at nozzle exit, monitoring the flow of partially combusted gas and full of cooled particles;
2. Via dedicated "*impactors*" disposed in the combustion chamber, where some sample particles get trapped.

The experiment foresees the engine functioning for a duration of about 5 seconds.

The phases describing the time evolution of the experiment are reported as follows:

- t=0 [s] beginning of data registration;
- t=0.3 [s] helium injection;

- t=1.2 [s] propellant ignition;
- t=3 [s] propellant burn out;
- t=4.4 [s] helium plant cut-off;
- t=5 [s] end of experiment.

The several firing phases are reported in Fig. 21.

As described it is immediate to notice that the useful period to collect data is the one ranging from 1.2 to 3 seconds, which is equivalent to the firing phase at engine regime.

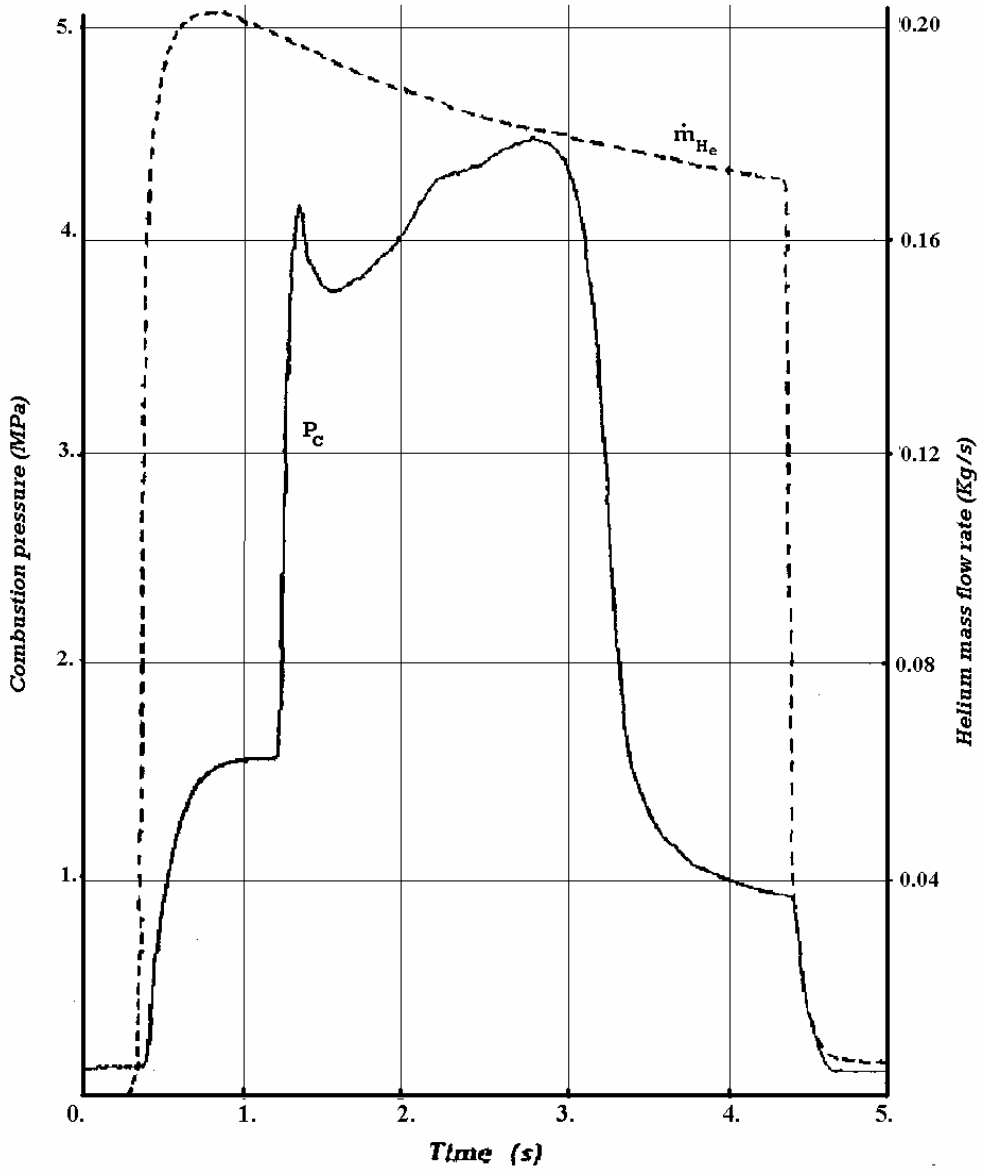

Fig. 21 – Firing phases of the ONERA demonstrator

The validation has occurred with the scope of reproducing the particulate distribution within the engine in four different instants in time during the propellant combustion phase, within the indicated time range.

The moments during which to record the obtained granulometry have been selected for regular intervals within the 1.2 – 3.0 seconds time range as follows:

1. t=1.5 [s];
2. t=2.0 [s];
3. t=2.4 [s],
4. t=2.8 [s].

The ballistics for each of the four moments in time has been partially supplied by ONERA [23] and partially obtained from the information contained in the technical reports. Details are reported in the annex.

In Fig. 25 the particulate distributions obtained by ONERA are reported during firing in the four moments of time considered, superposed to the particulate distributions evaluated in the same moments, via the procedure to be validated.

In the y-axis it is adimensionally represented the volume fraction occupied by the particles.

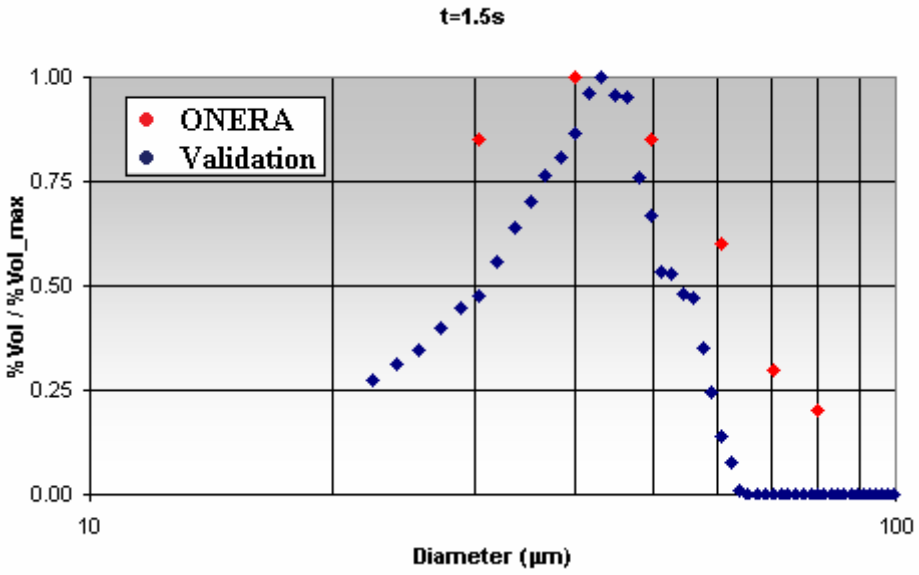

Fig. 22 – Particulate estimated dimensions comparison with respect to the real dimensions t=1.5 [s] (LP2 motor)

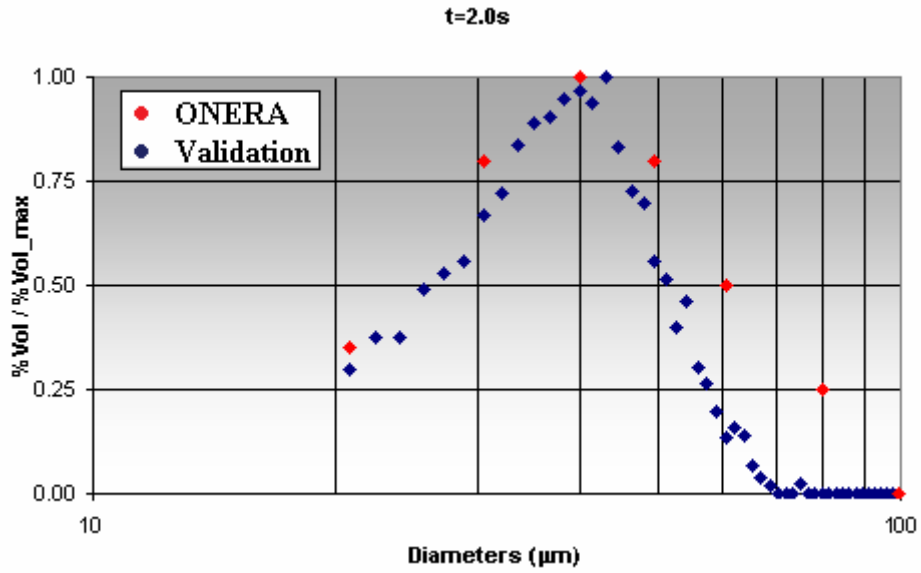

Fig. 23 – Particulate estimated dimensions comparison with respect to the real dimensions t=2 [s] (LP2 motor)

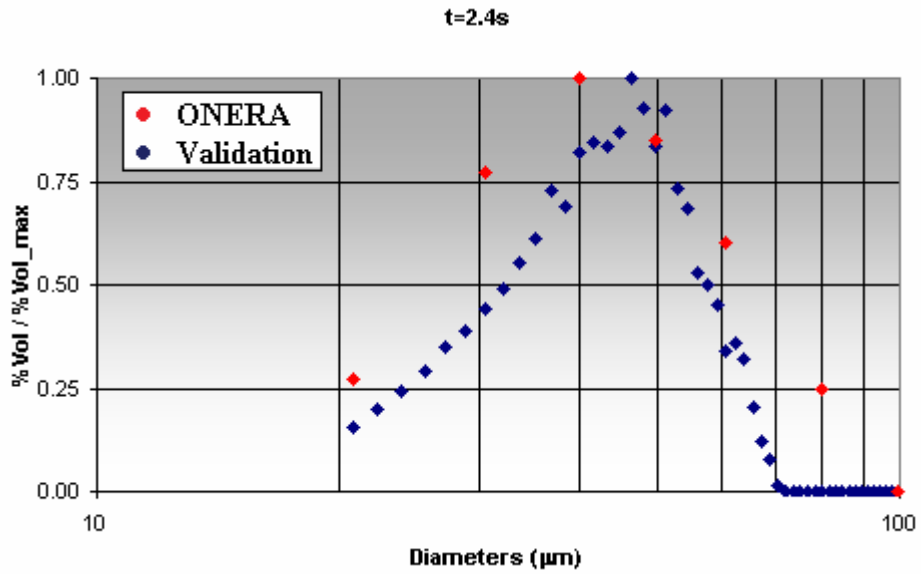

Fig. 24 – Particulate estimated dimensions comparison with respect to the real dimensions t=2.4 [s] (LP2 motor)

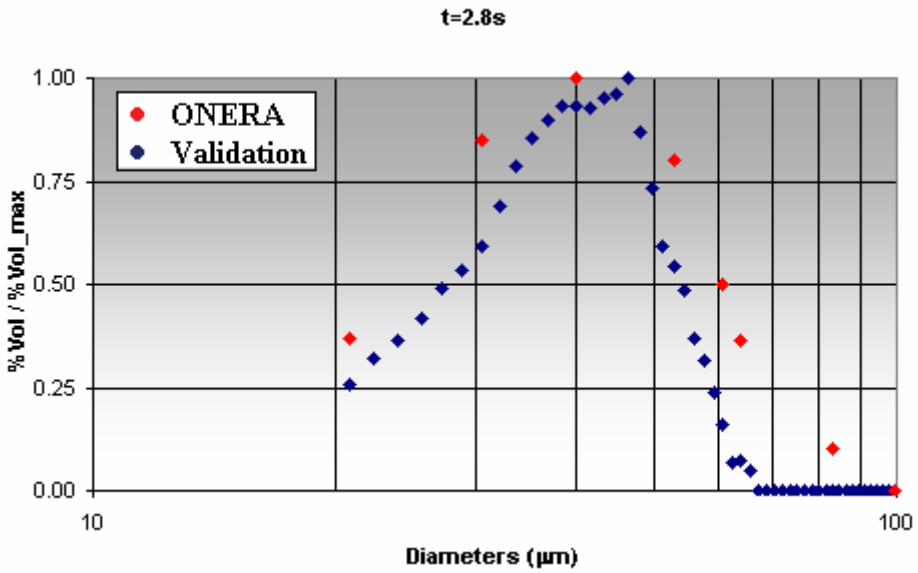

Fig. 25 – Particulate estimated dimensions comparison with respect to the real dimensions t=2.8 [s] (LP2 motor)

The comparisons show not only that the granulometry distribution obtained via the adopted procedure well reproduces the real one, but also that it is possible to identify with a reduced error margin in the zones where the statistical distribution of the particulate volume presents a maximum.
The errors made in the determination of the most probable diameter for each instant of time are reported in Tab. 2.

T [s]	1.5	2.0	2.4	2.8
Error [%]	8	8	16	16

Tab. 2 – Error on the most probable granulometry estimate

6.2.2 VALIDATION FOR THE P230

The second case for which the validation has been performed was selected in such manner that it would be possible to verify the suitability of the procedure to predict a SRM characteristic dimension for a fairly different case from the previous, however representative of the dimensions for which the model should be applied.

For such reason, the selected reference configuration has been the one of the P230 at t=87 [s].

Fig. 26 reports such geometry and the particulate dispersion due to the internal fluid dynamics of the motor.

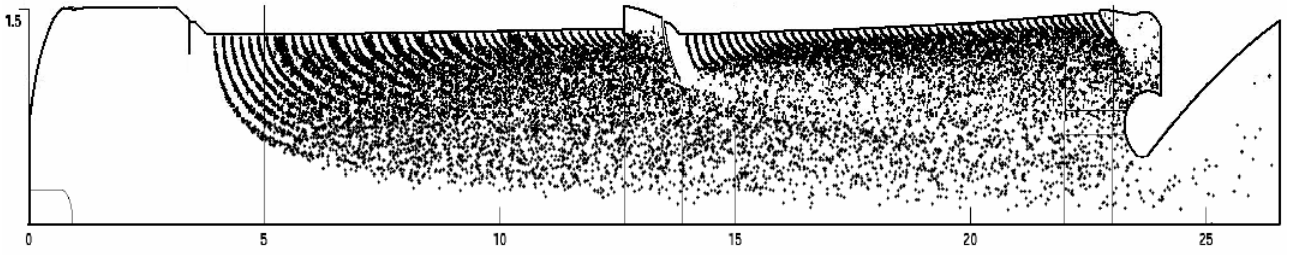

Fig. 26 – P230 geometry adopted for particle dimension validation

In this moment, for such type of engine, the geometry and the ballistics are known, while the particulate distribution is reported in the literature [39].

Superposing the distribution obtained via the process under validation and the diameter distribution supplied by the ONERA reports, it is possible to notice that the granulometry is very well represented in the zone with smaller diameters and in the zone where the diameters indicate a maximum in the statistic distribution of the particulate volume; for such zone the error made is small.

As in the previous case, though if more stressed, the wider diameters are less representative. However, since such representation has been performed in terms of particulate volume associated to each diameter, not just in terms of particle number, it should be reminded that the wider diameter are representative of a very limited number of particles.

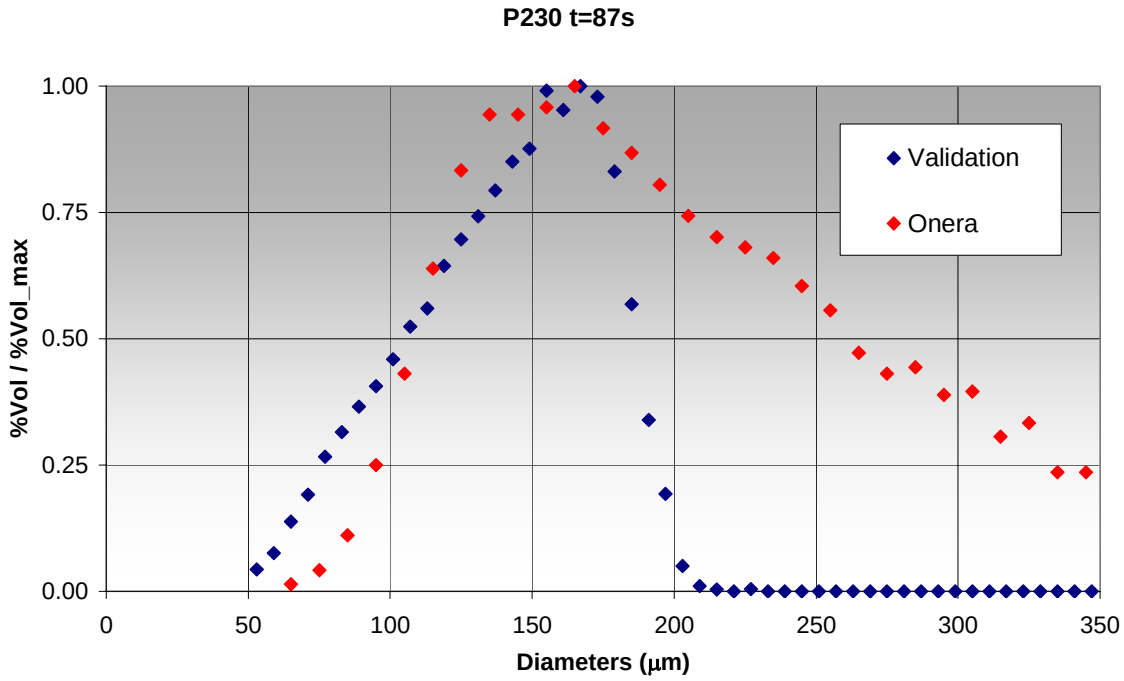

Fig. 27 – Comparison of the estimated particles and the real dimensions (P230 motor)

7 NUMERICAL MODEL

The selection of the appropriate numerical model to be adopted to predict the physical phenomena cannot disregard the intrinsic nature of the flows to simulate. At the aim of identifying the most suitable numerical model, it was necessary to define several characteristics of the flows under investigation and then to supply some simplifications.

It should be reminded that the numerical model employed for this work has been selected in such manner that it could be adopted also during future development, when also particulate combustion shall be taken into consideration.

The following list reports some of the most relevant simplifications adopted within this research:

1. The main gaseous flow has been represented as a continuous phase composed of a unique homogeneous fluid with characteristics reproducing a real gas mixture;
2. The droplets dispersed within the motor have been represented as a discrete phase composed of non reacting particles;
3. Each particle is representative of a certain number of particles holding the same characteristics;
4. The particle-fluid heat exchange could be modelled introducing production terms in the particle energy balance equations [16] (to be considered for future developments).
5. The particle dimension variations could be modelled introducing some dedicated laws [16] (to be considered for future developments).

7.1 NUMERICAL POSSIBLE APPROACHES

In general the fluid dynamic solution of the problems under consideration follows an Eulerian approach. This choice is based on the conception according to which the fluid can be considered as continuous, and its evolution can be described through the Navier-Stokes equations [67].
Also for multiphase flows such choice can be adopted, although with the limitation that the different phases shall be represented as continuous (Fig. 28 (a)). Moreover the interaction of the different phases shall be appropriately modelled through the introduction of phase coupling coefficients [49].
In the present case the hypothesis is introduced that the liquid/solid phase dispersed within the gaseous one represents a discrete system of particles, therefore an Eulerian cannot be employed for the determination of its motion.
In general two types of approaches exist to for the solution of a flow [57]:

- Eulerian approach;
- Lagrangian approach.

The second approach, heavier in terms of computer power required, is applied just for the determination of the motion of discrete phase flows (Fig. 28 (b)). In such manner the particle flow field is represented by their trajectories obtained integrating the associated equations of motion.

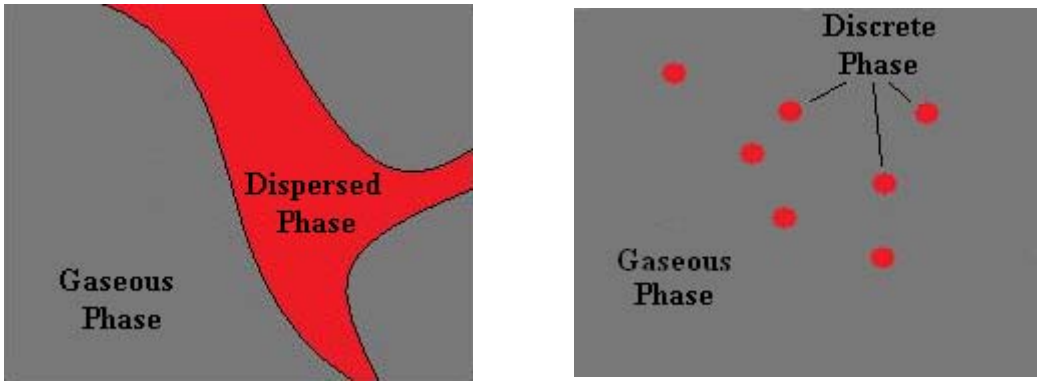

(a) (b)

Fig. 28 – Bi-phase flows. Application of the Eulerian model (a) and Lagrangian (b)

For the case under investigation, the Eulerian approach is not appropriate for the solution, but its adoption is necessary to solve the flow field in which the particles are immersed. Finally, since the flow is composed of a continuous and a discrete gaseous phase, a mixed lagrangian-eulerian approach has

been adopted [60]: the Eulerian approach for the solution of the continuous phase, the Lagrangian one for the discrete phase [17], [44], [66].

The Lagrangian model adopted for the discrete phase, although heavier in terms of computer power required, shows advantages with respect to the Eulerian one, due to the fact that it allows to differentiate the particle dimension, faithfully representing the reality and also to introduce heat transfer models [51].

A further choice that influences the behaviour of the fluid and the particulate regards the phases coupling method [59].
Indeed two main coupling types exist:

- The 1 way coupling, for which it is supposed that the particulate presence offers a negligible effect on the dynamics of the main flow;
- The 2 way coupling, for which the particulate presence holds a significant role on the dynamics of the main flow and vice-versa [68].

Normally the choice of the most suitable model occurs evaluating the Stokes number, which represents the aerodynamic force particle response time to characteristic time of the fluid ratio [18], [19].

$$St = \frac{\tau_R}{\tau_F} = \frac{\rho_P d^2 U}{18 \mu L}. \qquad \textbf{eq. 14}$$

Where U is the characteristic velocity of the fluid, d the particle diameter, ρ_p the particulate density, μ represents the viscosity of the fluid and L the duct characteristic length.
When $St << 1$ the particulate is constantly in equilibrium with the flow, therefore a 1 way approach can be employed. When $St \approx 1$ or higher the 2-way approach is suggested. Since in the present work the Stokes number is about 0.85, such last model is adopted.
In this manner the particle dispersion within the gaseous phase is controlled by the local speed variations due to the turbulent structures, while on the other hand, the particles can influence the turbulence modifying the associated energy [18].
The "two-way" is made possible alternating the calculus of the continuous phase solutions and of the discrete one, depending one on the other, till the point for which the solutions of both phases show negligible differences.

7.2 CFD MODEL SELECTION

The numerical simulations have been performed by means of the commercial Fluent code. Such code employs a finite volumes discretisation and solution technique of the fluid dynamic field.
To solve the conservation of mass and the momentum equations an implicit pressure based algorithm it was selected. Furthermore, the convection terms in the momentum and energy equations were discretised with a second order upwind scheme [52]. The algorithm, named PISO, was employed for the pressure-speed coupling.
The turbulence model adopted is the Monotone Integrated Large Eddy Simulation (MILES) [70].
For those simulations requiring the addition of a discrete phase, the option to have an interaction of the phases by means of the so called "2-way" was chosen in the code, hence taking into account the mutual effects on the motion during the fluid-particle coupling.
Le equations solved by the solver, written for the axis-symmetrical case are:

Mass conservation:

$$\frac{\partial \rho}{\partial t}+\frac{\partial}{\partial x}\left(\rho u_x\right)+\frac{\partial}{\partial r}\left(\rho u_r\right)+\frac{\rho u_r}{r}=S_m \qquad \textbf{eq. 15}$$

Where S_m indicates a mass production, which is equal to 0 in this case $\left(S_m=0\right)$.

Momentum conservation along the axial direction:

$$\frac{\partial}{\partial t}\left(\rho u_x\right)+\frac{1}{r}\frac{\partial}{\partial x}\left(r\rho u_x u_x\right)+\frac{1}{r}\frac{\partial}{\partial r}\left(r\rho u_r u_x\right)=-\frac{\partial p}{\partial x}+\frac{1}{r}\frac{\partial}{\partial x}\left[r\mu\left(2\frac{\partial u_x}{\partial x}-\frac{2}{3}\left(\nabla\cdot\vec{u}\right)\right)\right]$$
$$+\frac{1}{r}\frac{\partial}{\partial r}\left[r\mu\left(\frac{\partial u_x}{\partial r}+\frac{\partial u_r}{\partial x}\right)\right]+F_x \qquad \textbf{eq. 16}$$

Momentum conservation along the radial direction:

$$\frac{\partial}{\partial t}\left(\rho u_r\right)+\frac{1}{r}\frac{\partial}{\partial x}\left(r\rho u_r u_x\right)+\frac{1}{r}\frac{\partial}{\partial r}\left(r\rho u_r u_r\right)=-\frac{\partial p}{\partial r}+\frac{1}{r}\frac{\partial}{\partial r}\left[r\mu\left(2\frac{\partial u_r}{\partial r}-\frac{2}{3}\left(\nabla\cdot\vec{u}\right)\right)\right]$$
$$+\frac{1}{r}\frac{\partial}{\partial x}\left[r\mu\left(\frac{\partial u_x}{\partial r}+\frac{\partial u_r}{\partial x}\right)\right]+F_r \qquad \textbf{eq. 17}$$

Where:

$$\nabla \cdot \vec{u} = \frac{\partial u_x}{\partial x} + \frac{\partial u_r}{\partial r} + \frac{u_r}{r} \qquad \textbf{eq. 18}$$

and the F_r and F_x terms holding information regarding the interaction of the gaseous phase with the discrete one, are the projections along axial and radial directions of:

$$\vec{F} = \sum \left(\frac{18 \mu C_D \, \mathrm{Re}}{\rho_p d_p^2 24} \left(\vec{u}_p - \vec{u} \right) \right) \dot{m} \Delta t \qquad \textbf{eq. 19}$$

Where μ is the viscosity of the fluid, ρ_p the particulate density, d_p the particulate diameter, Re is the Reynolds number, u_p the particulate speed, u the speed of the flow, C_D is the drag coefficient of the particle, $\dot{m}$ is the mass flow rate of the particle and Δt is the time step adopted for the calculation.
On the other hand the particulate equations of motion are:

$$\frac{du_p}{dt} = K_D \left(u - u_p \right) \qquad \textbf{eq. 20}$$

Where the relative particle to surrounding fluid speed is indicated in two brackets and

$$K_D = \frac{18 \mu}{\rho d_p^2} \frac{C_D \, \mathrm{Re}}{24} \qquad \textbf{eq. 21}$$

The particle C_D is calculated by the solver considering its geometry as spherical.

8 SETUP AND POST-PROCESSING

8.1 SIMULATION ORGANIZATION

The influence of the dispersed phase presence during the PWO generation within the P230 motor has been one of the main objectives of the present research. In particular, the P230 booster is representative for the description of the phenomenon both for its size and for the presence of the discrete phase.
An important aspect that needs to be further investigated is the behaviour of PWO involved in cases where the geometry of the engine is reduced in size. Considering the methodologies described in the previous paragraphs, it was possible to face the solution of the engineering problems raised.

The simulations were organized in order to obtain a first series of results showing the effects of the variations in the characteristic levels of the PWO in solid rocket motors without introducing any dedicated model for the presence of the particles.
Then, for each scaled configuration, the most suitable granulometry to adopt have been evaluated, and finally such inert granulometry has been introduced in the particle setup and the effects of its presence have been studied on the fluid dynamics of the scaled and un-scaled motor.

Summarising, the analyses conducted on the P230 motor were:

1. 1:1 scale PWO simulation without particle adoption;
2. 1:2.5 scale PWO simulation without particle adoption;
3. 1:5 scale PWO simulation without particle adoption;

4. Particle dimension definition for 1:1 scale;
5. Particle dimension definition for 1:2.5 scale;
6. Particle dimension definition for 1:5 scale;

7. 1:1 scale PWO simulation with particle adoption;
8. 1:2.5 scale PWO simulation with particle adoption;
9. 1:5 scale PWO simulation with particle adoption.

8.2 SETUP

8.2.1 ADOPTED MESH

The mesh is composed of about 400,000 quadrilateral cells. It is quite regular in the zones close to the grain, in particular in the S3 zone (the grain located between the FTP and the nozzle), which is important for the evolution of vortex structure, strongly linked to the PWO transportation.
For the full scale configuration, the typical cells dimension in the vortex generation zone is about 2.5 [mm], whereas it assumes 4.5 [mm] values along the S3 grain. For the scaled cases also the mesh dimension scales proportionally to the scale factor.

In the figure it is reported the mesh in the zone where:

A – the vorticity is generated;

B – the acoustic signal is generated;

C – the acoustic signal is recorded.

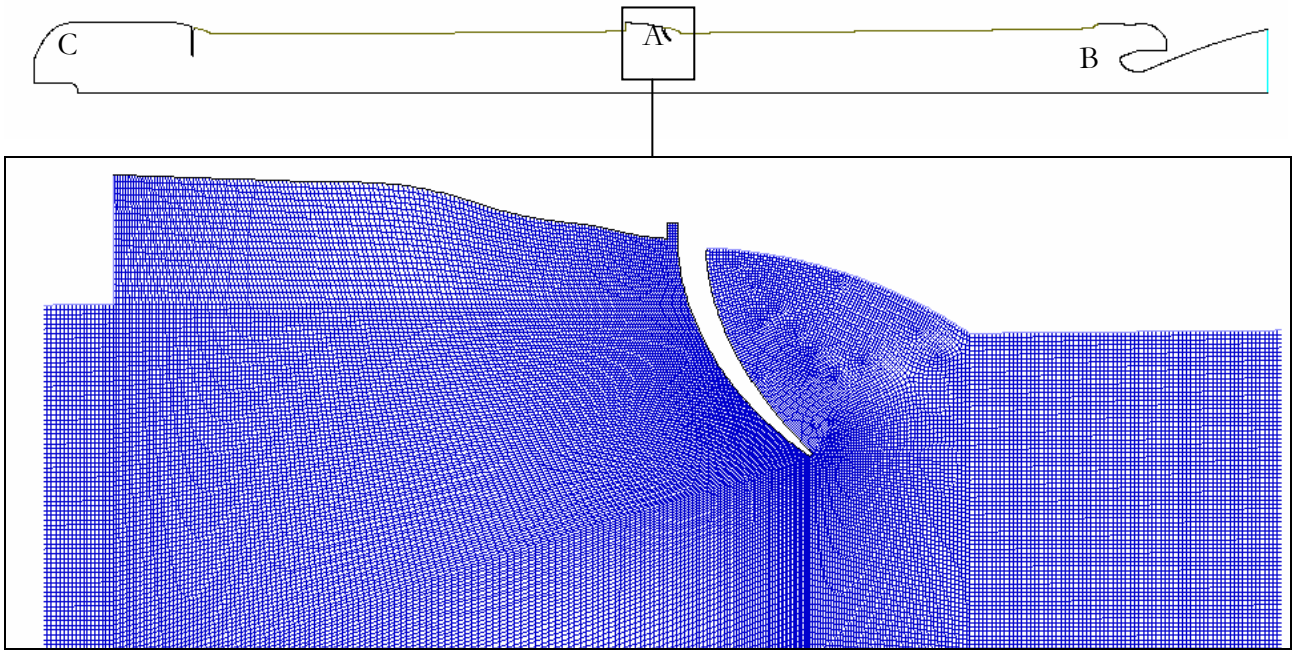

Fig. 29 – Mesh in the vortex generation zone

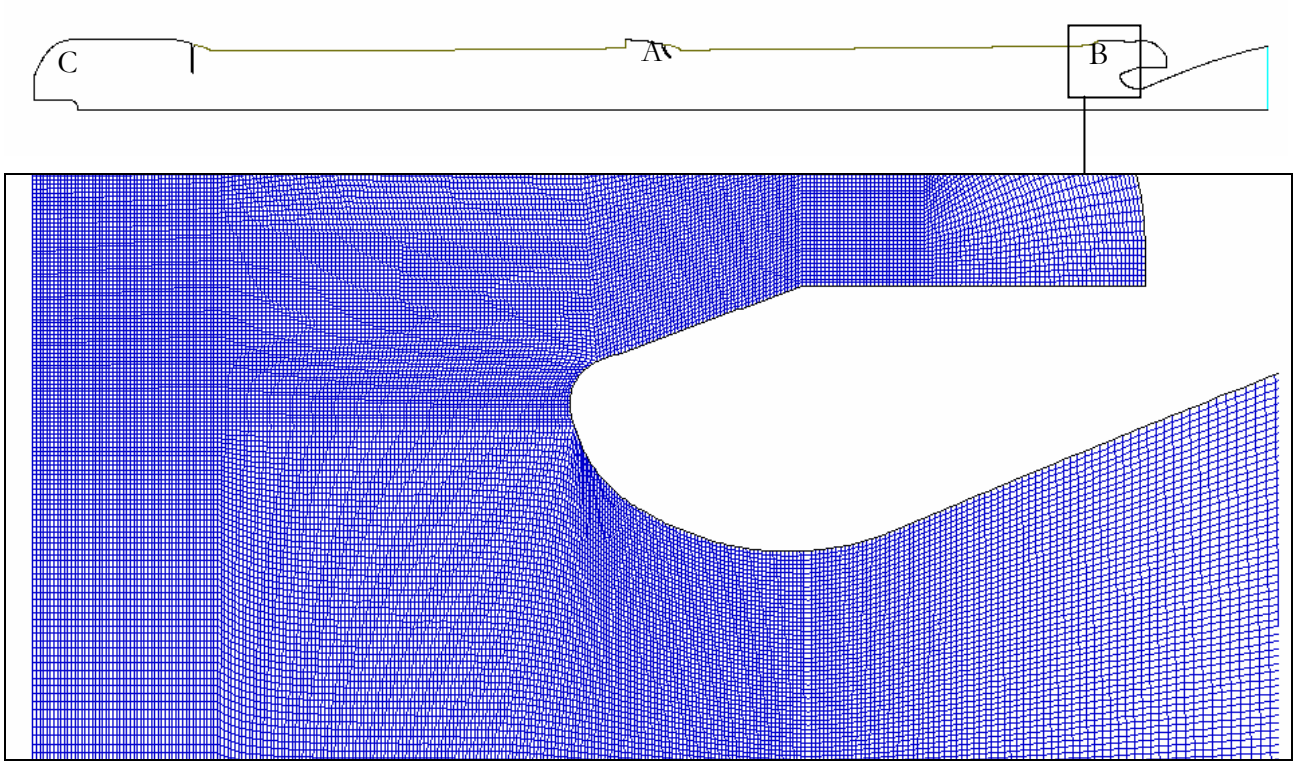

Fig. 30 – Mesh close to the nozzle head

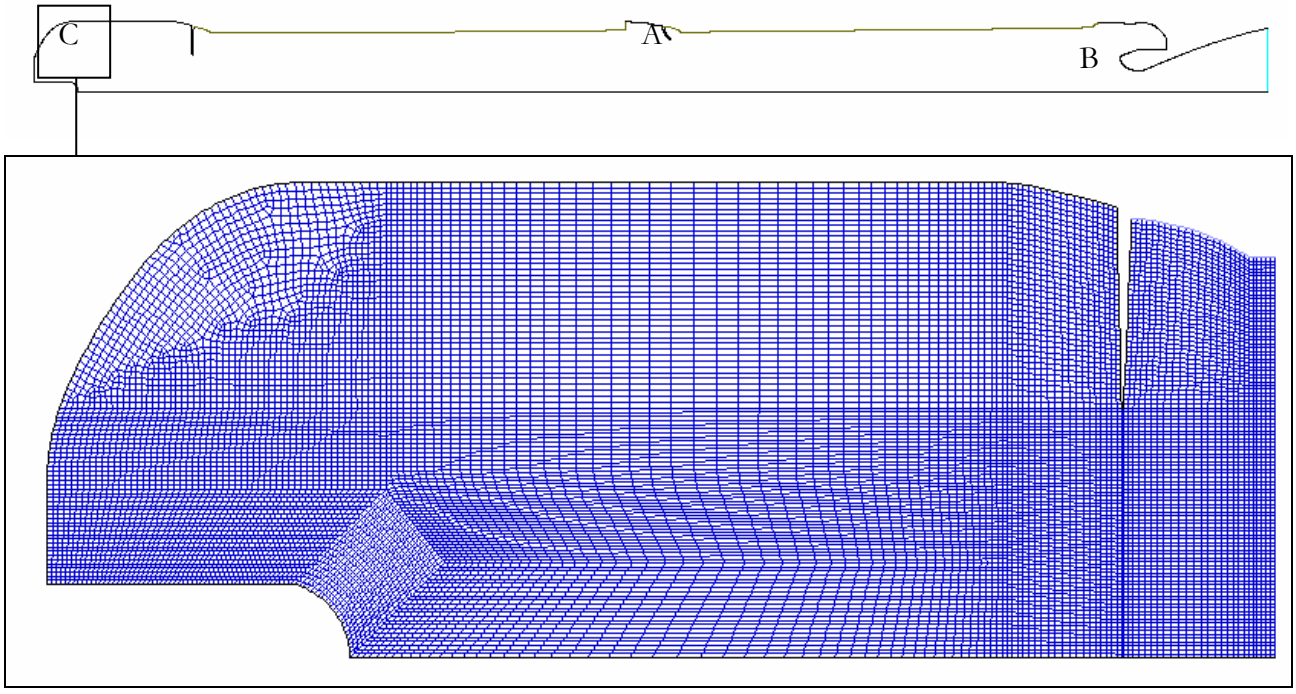

Fig. 31 – Mesh close to the motor head

The mesh sensitivity has not been conducted in this work since the same mesh has already been studied and validated in the literature [41].

8.2.2 DATA MONITORING

Data monitoring is a task to be carefully handled in order to obtain a good estimate of the frequency and the amplitude spectrum of the signal. Because of the complexity of the phenomenon, the simulated transient has been chosen to be quite wide, in order to stabilise the oscillations and to begin the data capturing only when the fluid and the PWO show a stationary behaviour.

The acquisition of the pressure signal occurred in different parts of the combustion chamber through the use of several virtual numerical probes (Fig. 32) that fixed the positions in the domain on which the pressure signal recording instantaneously occurs. In particular, the results presented are related to the probe placed at the head of the engine defined in figure as "**A**", which is reached by the pressure signal after that such perturbation has been travelling through the entire combustion chamber.

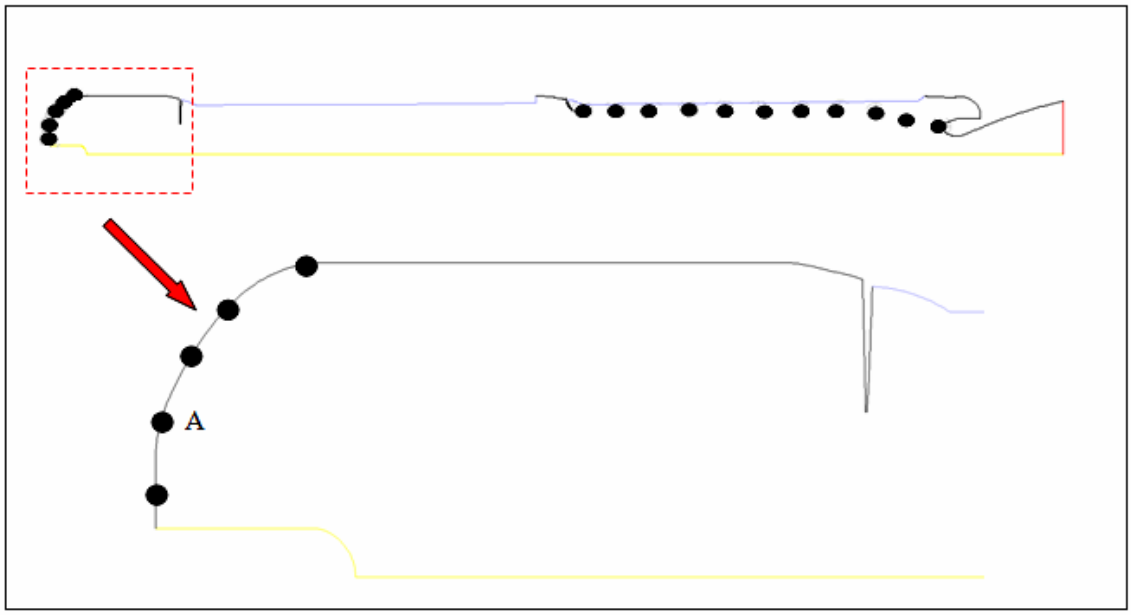

Fig. 32 – Numerical virtual probe position inside the motor

8.2.3 DATA PROCESSING

The study of the PWO frequency response is based on the analysis conducted by means of the spectral Fast Fourier Transform (FFT) and on the entire energy bandwidth.

The FFT operates on a signal containing information on the instantaneous pressure recorded in a certain position of the flow field.
In order to adequately represent the PWO evolution process it is necessary that the signal contains a trend of pressure variations which is stationary, e.g. downstream of transient fully developed.
Usually the signal is characterized by a first part, which is precisely the transition, and a second part which is the steady signal that can be processed (Fig. 33).

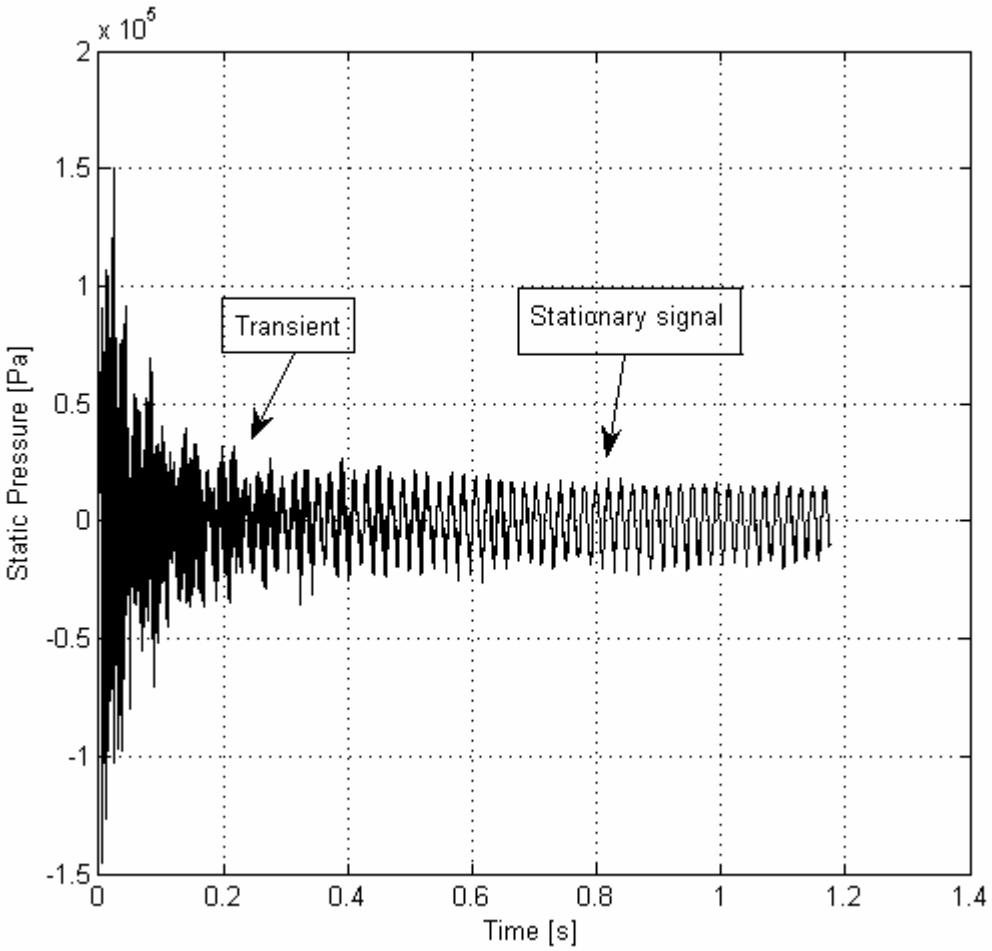

Fig. 33 – Example of pressure signal

Whereas the analysis performed by means of the FFT produces a peak distribution such as the one reported in Fig. 34.

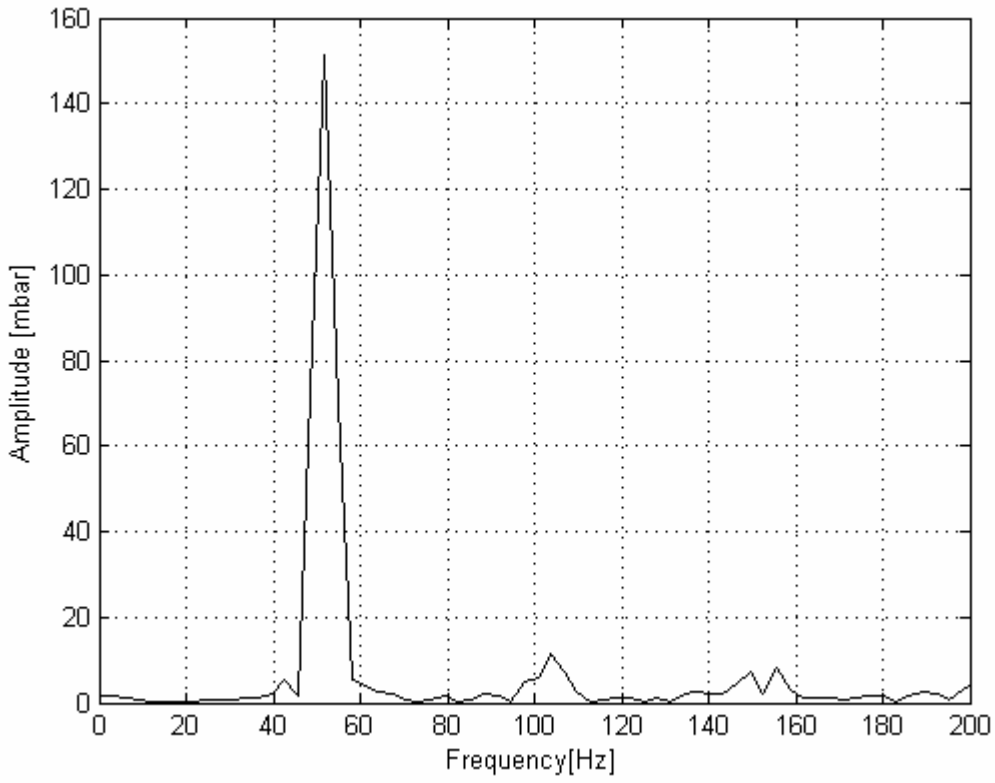

Fig. 34 – Example of FFT

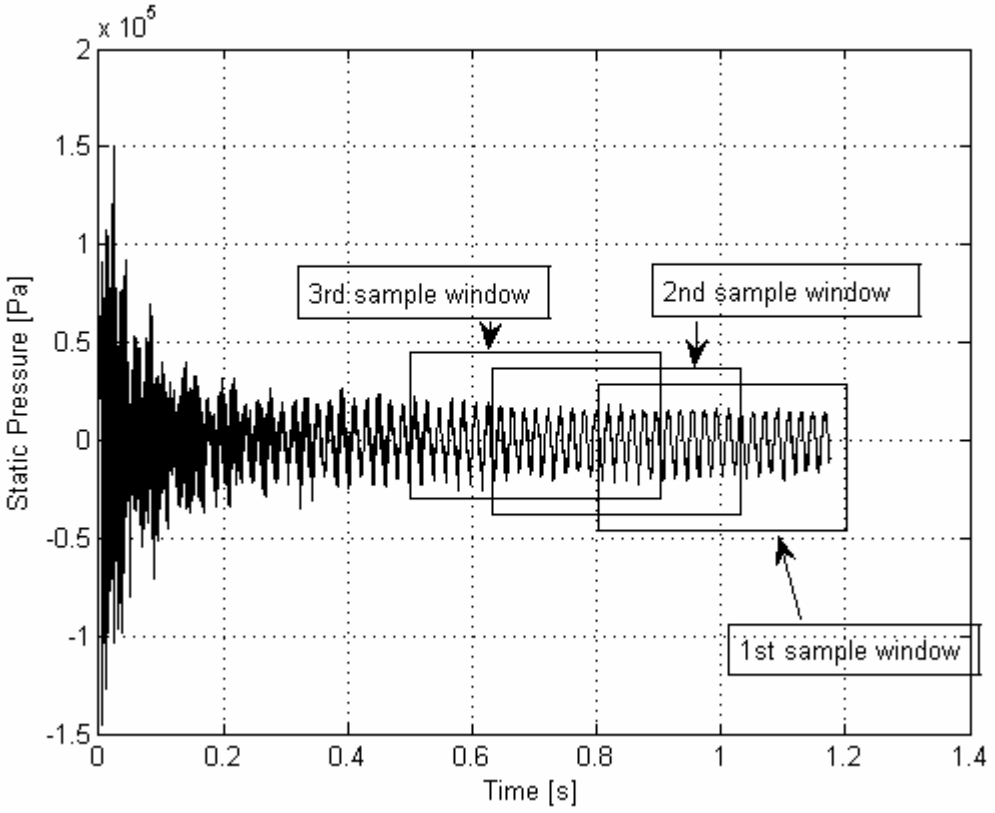

Fig. 35 – Data sampling windows

Considering the fact that the signal analysis is not based on the entire range of data available, but analyses only those contained in a window of samples (Fig. 35), during the signal evolution behaviour of the peak amplitudes can be followed by shifting the position of the sampling window.
Representing the progress of the first peak frequency in this manner (Fig. 36), it is easier to understand when a signal has become stationary. In that case the range of amplitudes in which peaks vary can be identified.

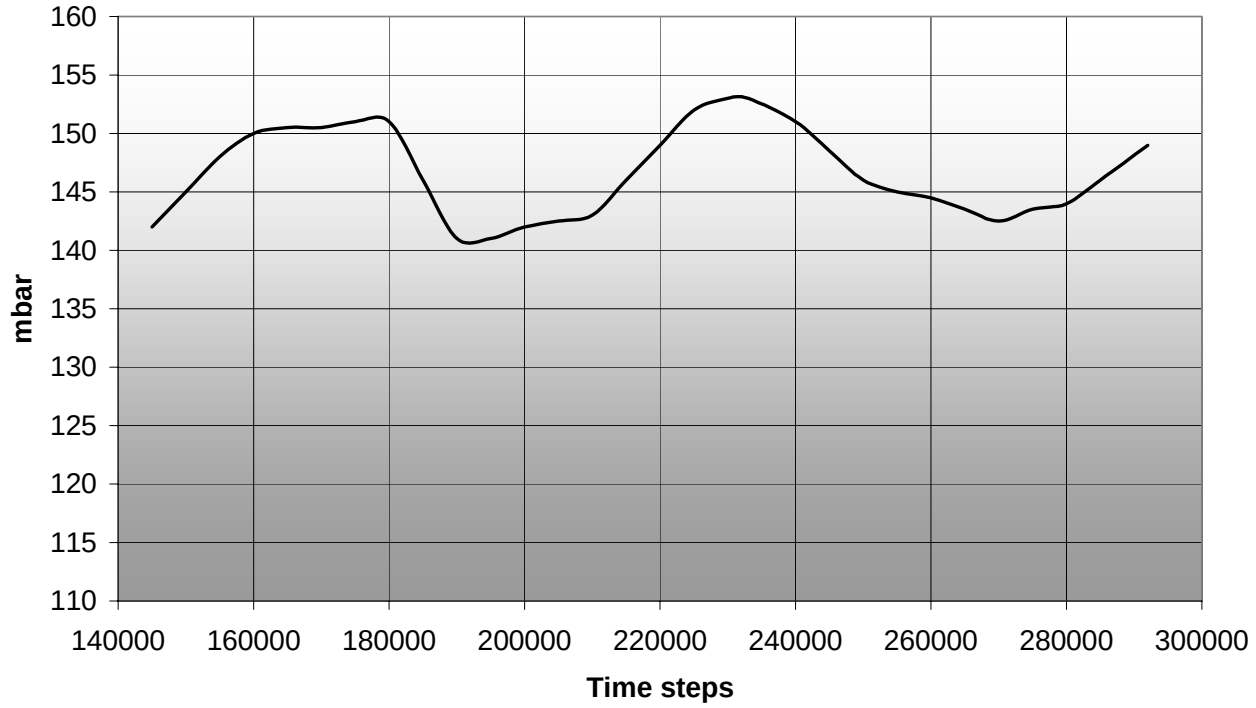

Fig. 36 – Example of PWO amplitudes behaviour during the steady phase

Typically, in this work the windows of samples contain 2^{15} (32,768) values. For a 1:1 scale, in which the time step is defined as 2.5e-5 [s], it represents an interval of time of about 0.82 [s].
Since in this work, the time step is decreased proportionally with the scale factor, the sample windows reduce their amplitude by the same entity (see Tab. 3)

Scale	1:1	1:2.5	1:5
Interval sampling [s]	0.8192	0.3277	0.1638

Tab. 3 – Interval sampling

8.3 COMPUTER POWER

It should be reminded that the efforts made to implement the numerical simulations described so far are highly remarkable. Indeed, such simulations showing the PWO levels are only the results of a wide amount of numerical work performed in order to find the most suitable and reliable setups, to define the validation processes, to determine the granulometry of each configuration, etc.
In order to run such simulations two clusters composed of the following machines have been employed:

- ✓ 4 OPTERON - Each machine containing 4 processors and 8G of RAM;
- ✓ 4 OPTERON - Each machine containing 4 processors and 4G of RAM;
- ✓ 2 XEON - Each machine containing 8 processors and 8G of RAM;
- ✓ 1 XEON containing 8 processors and 16G of RAM.

The total amount is a set of 54 processors and 36G of RAM.

Typically each simulation containing the discrete phase performed on two XEON machines was able to solve about 5,000 time-steps each day.

9 RESULTS

The engine taken as reference case is the P230 motor at time instant equal to t=89 [s].
Such decision has been taken for several reasons: the present motor is widely employed in the aerospace field, furthermore the present engine is the one employed by SNPE in order to perform some preliminary analyses on the PWO levels for both the full scale and the scaled configuration of the same motor.
This chapter shows the results in terms of size of the discrete phase, fluid dynamic fields, but especially the PWO obtained for various configurations.
Comparisons of the PWO and fluid dynamic fields obtained in different cases will be commented in the last paragraph.

9.1 1:1 SCALE

The first analysed configuration is the one related to the full scale dimension (Fig. 37). As already indicated above, for this configuration, simulations were performed first without the introduction of the discrete phase, then the particle size has been evaluated by adding a discrete phase and finally employing the presence of the inert discrete phase.

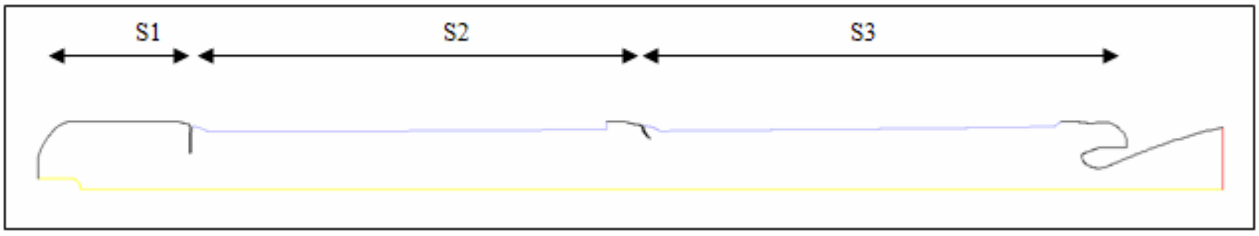

Fig. 37 – Longitudinal section of the motor

9.1.1 PWO WITHOUT DISCRETE PHASE

In this first series of numerical simulations, PWO were evaluated without the presence of additional phases. The fluid is considered as a single phase and the properties of the used gas reproduce the characteristics that actually the gas holds during engine operation.

Actually, this simplification regarding the elimination of the reacting particulate from the flow theoretically eliminates a part of the fuel, which is responsible for a strong raise in temperature in the combustion chamber. Hence, at the aim of obtaining reliable results, not only in terms of engine internal fluid dynamics, but especially in terms of PWO, it was necessary that the removal of the discrete phase would not involve a change in total temperature and total energy present in the motor during engine operations.

For this reason, the numerical simulation of the flow in this first case was carried out by reproducing the conditions in the combustion chamber taking into account also the energy transferred in the combustion process of particle.

The values in terms of amplitude and frequency obtained in this case are shown in the following table.

	Data analysis using FFT		Integral energy analysis
	Frequency (Hz)	Amplitude (mbar)	Amplitude (mbar)
1st mode	20.7 ± 1.2	148.7 ± 6	153.8
2nd mode	40.1 ± 1.2	15.3 ± 5	19.8
3rd mode	61.0 ± 1.2	12.0 ± 4	12.3

Tab. 4 – Results for the 1:1 scale – single phase case

A typical plot representing the spectrum of frequencies and amplitudes for this case is shown in Fig. 38. In such plot it is possible to observe quantitatively all the information regarding the PWO frequencies and amplitudes in the field.

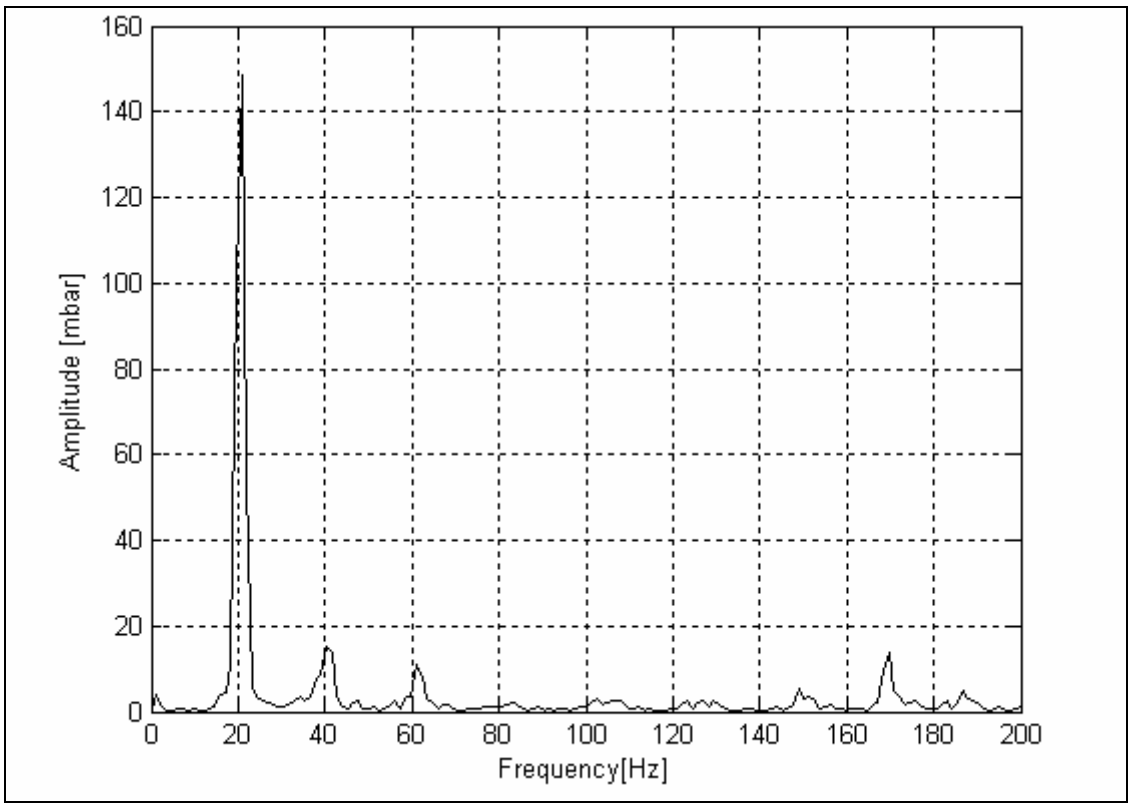

Fig. 38 – Amplitudes and frequencies – 1:1 Scale - Single phase

The fact that the simulation has reached steady state is visible both by the pressure signal shown in Fig. 39,

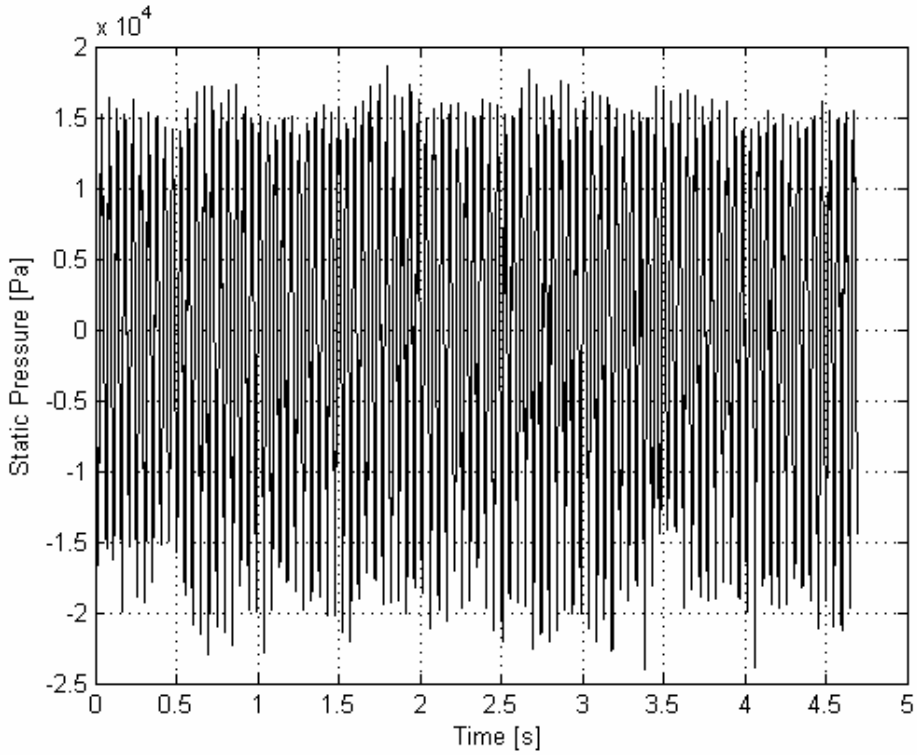

Fig. 39 – Pressure signal

and by following the trend of the maximum amplitude of the first oscillation frequency shown in Fig. 40.

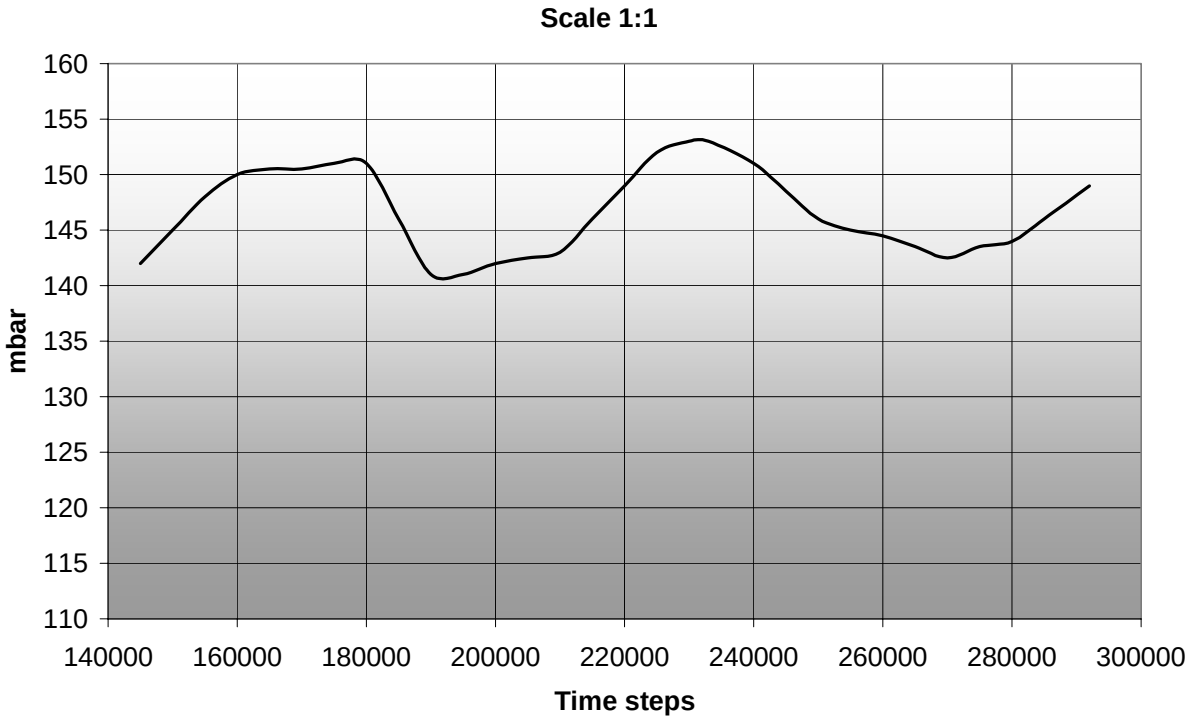

Fig. 40 – First frequency amplitude

In Fig 41 a snapshot of the fluid dynamic field during operation is shown. It is possible to notice that the vortex structures are generated in correspondence of the FTP, travelling downstream and getting aggregated into larger structures. When such periodically generated structures hit the nozzle head, they transfer energy to the acoustic field. This behaviour makes possible to observe the oscillating pressure peaks.

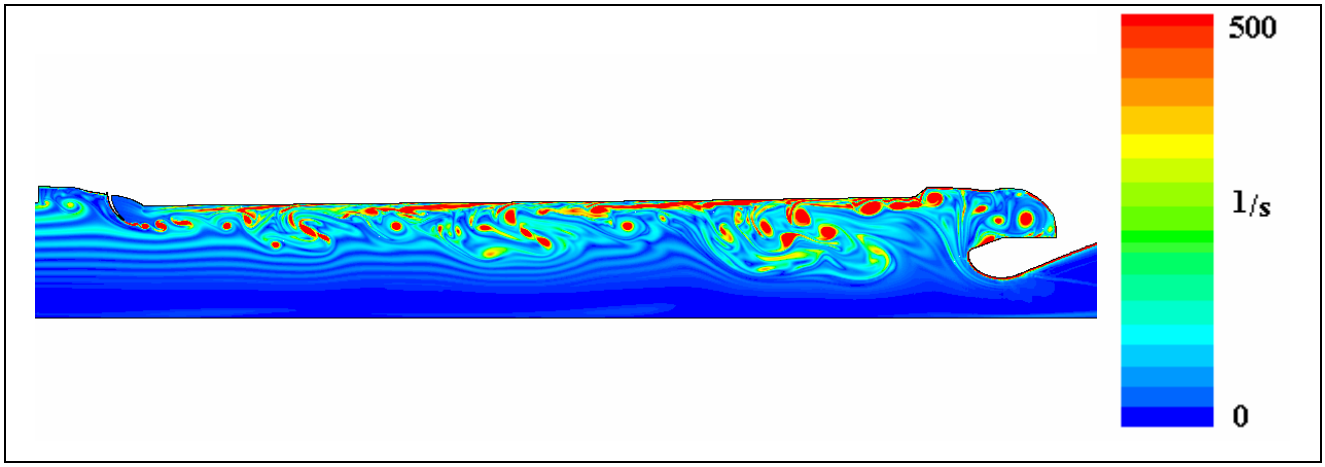

Fig. 41 – Vortex structures in 1:1 motor without particulate

As mentioned above, the vortex structures are the main responsible for the generation of pressure disturbances. During the analysis of the results of this reserarch, the fields of vorticity are shown several times as their shape and evolution may provide important information on the specific structures to investigate.

These data were then considered as the basis for the comparison with the further simulations in which the discrete phase is introduced.

9.1.2 DISCRETE PHASE DIMENSIONS EVALUATION

At the aim of introducing a discrete phase in the fluid dynamics field, its size distribution must be known. In chap. 6 the methodology used for determining the most probable particle size has been illustrated. Such methodology is now applied to the first case for which the PWO oscillation calculation is needed.

The geometry of the motor at t=89 [s] is known and it is reported in Fig. 37. Actually, only for the calculation of the most probable particle sizes, this geometry is reproduced eliminating the nozzle and its head. This removal has been necessary because the aim of such intermediate step is to obtain the initial dimension of the particle only inside of the combustion chamber. Whereas, taking into account also the nozzle, the results would be influenced also by the dynamics occurring in that zone (Fig. 42).

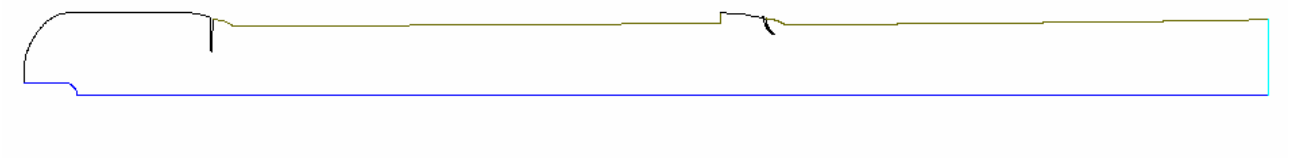

Fig. 42 – Truncated longitudinal section of the motor

Indeed, the critical size of the particles must be determined within the combustion chamber, because it is the maximum size, associated with the particles, during their stay in the engine. Considering also the nozzle, the particles passing through the throat and then along the diverging part, considerably accelerate. In this manner, the critical stress on the particle would define critical diameters much smaller than the ones hitherto obtained in the combustion chamber, and the granulometry obtained in the engine would be replaced by the most critical one achieved in the nozzle, which is not the scope of this analysis.

The next step concerning the particle granulometry evaluation regards the adoption of a diameter distribution such as the one indicated in Fig. 43. In this manner a fixed number of particles has been associated to each representative diameter present in the combustion chamber.

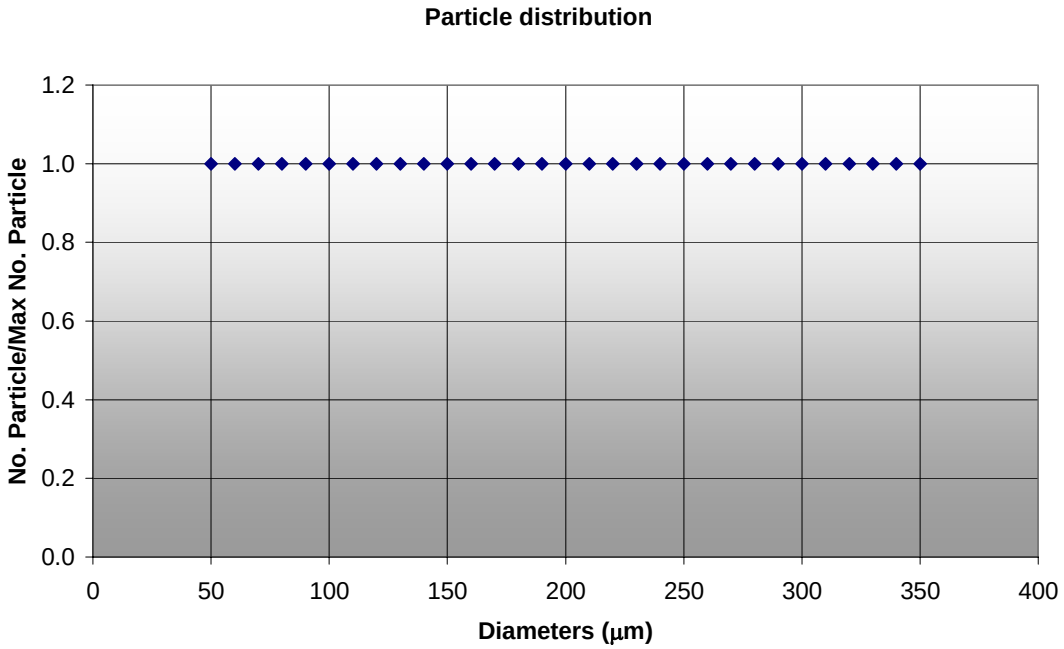

Fig. 43 – Input particle distribution

Performing numerical simulations and processing data as described in section 6.1, the new particle size distribution, represented in terms of number of particles associated with each diameter, is shown in Fig. 44.

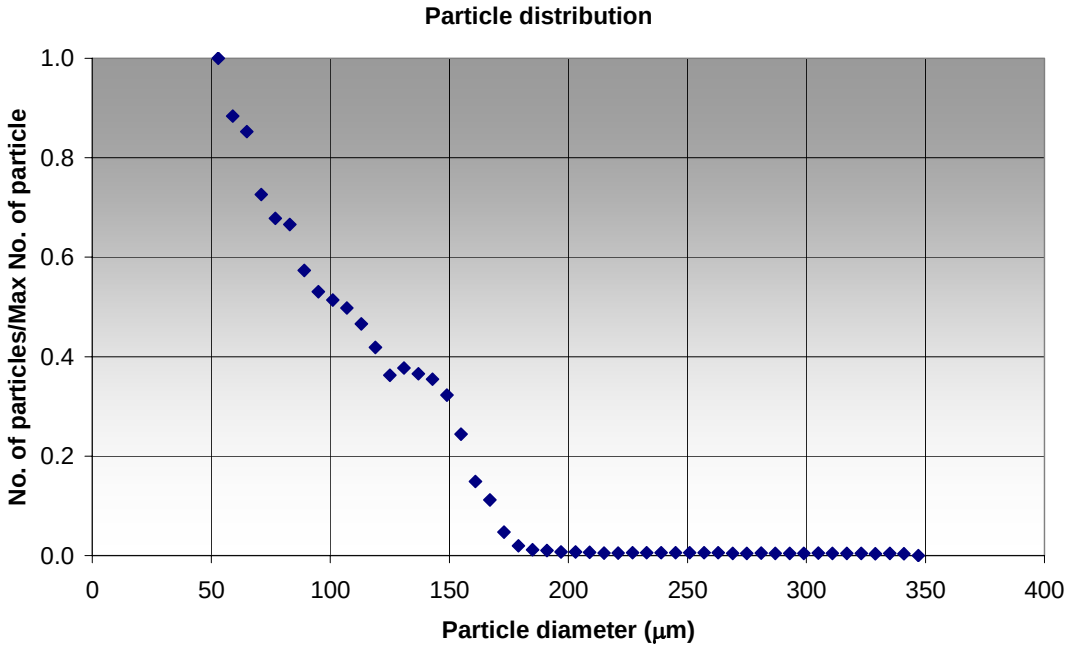

Fig. 44 – Output particles distribution

Observing the previous figure, it is visible that all the particles having a diameter larger than 190 μm have suffered a break and have therefore been scaled by assigning them a diameter equal to the

maximum calculated along the trajectory. This reduction in diameter has meant that the number of particles with smaller diameters increase in number at the expense of particles with larger diameter, as indeed shown in Fig. 44.

In previous cases shown during validation of the methodology, granulometric distributions were represented in terms of mass fraction associated to each diameter. This type of representation was adopted in those cases only because the scientific work reported results only in that unit. Hence, in order to compare the results, it was necessary to adapt to that form.

In this case and in the subsequent ones, in order to represent the particle size distribution, a different form has been assumed. It has been indeed reported, as a function of the diameter, the number of particles instead of the mass fraction.

Using the values of $\overline{\phi}$ and n the Rosin-Rammler function (eq. 10), that best approximates the curve numerically obtained, is defined.

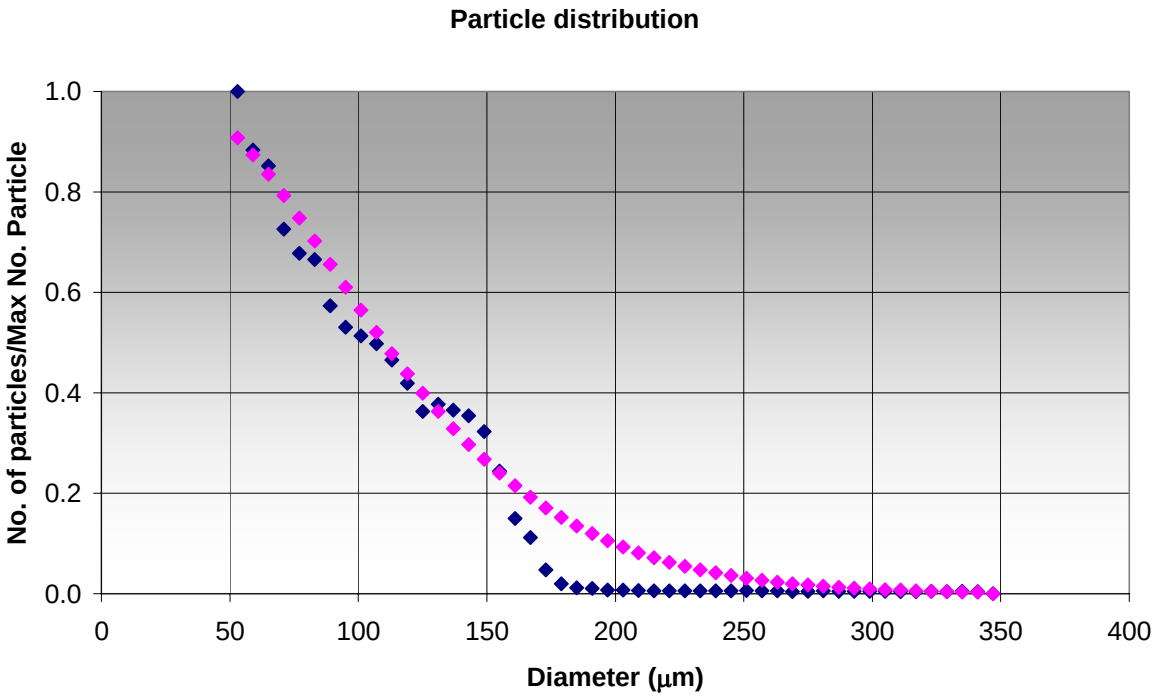

Fig. 45 – Overlapping of output particle / best fit function

For the curve reported in Fig. 45, the $\overline{\phi}$ and n values are:

$$\overline{\phi} = 9.0\text{E-}5 \qquad n=1.45.$$

9.1.3 PWO WITH INERT PARTICULATE

In this first numerical simulation performed with the use of a discrete phase, the ballistics of the engine has not been altered with respect to the case without particles, the discrete phase has been modelled as indicated in earlier chapters (particularly in Chap.6), while the fluid in which the discrete phase is immersed is a gaseous phase holding properties reproducing the actual gas characteristics achieved during engine operation.

This means that the amount of heat that the discrete phase, due to its combustion, should transfer to the gas is already forfeited by the gas, which is injected into the combustion chamber. This avoids the direct exchange of energy between the particles and fluid.

For this reason, the numerical simulation of the flow in this first case was carried out by taking as an input the conditions within the combustion chamber induced also by particulate combustion, while not implementing this exchange.

The values obtained by the analyses of the results performed on this simulation are reported in Tab. 5.

	Data analysis using FFT		Integral energy analysis
	Frequency (Hz)	Amplitude (mbar)	Amplitude (mbar)
1st mode	17.1 ± 1.2	75.7 ± 27	99.5
2nd mode	35.8 ± 1.2	24 ± 7	35.0
3rd mode	58.6 ± 1.2	9.5 ± 3	14.0

Tab. 5 – Results for the 1:1 scale – bi-phase case

From a first quick analysis it can be seen how the amplitudes of the first peak are reduced compared to the case without particles. This result is in line with the results reported in the literature concerning the PWO damping in the presence of inert phases.

Amplitudes and frequencies are visible from the graph in Fig. 46.

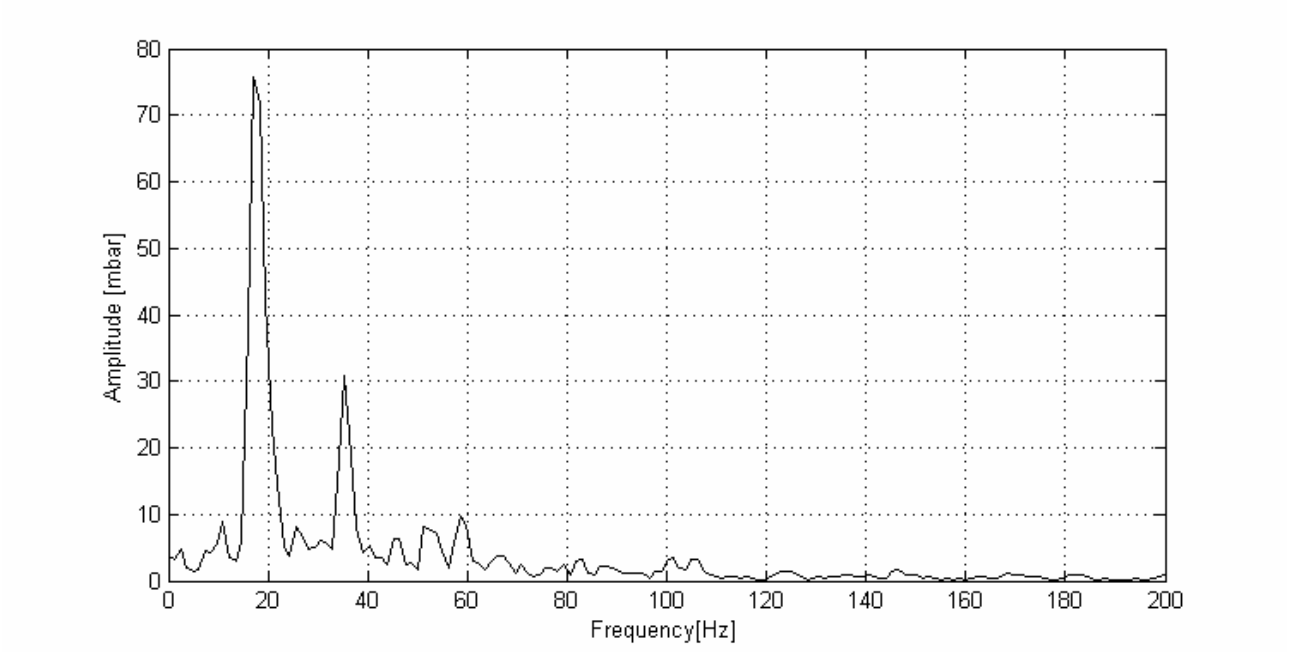

Fig. 46 – Amplitudes and frequencies plot – 1:1 scale case with inert particulate

The signal, shown in Fig. 47, shows the evolution of the pressure on the engine head over a wide range of time in which it was possible to sample the pressure changes needed to evaluate the PWO. The signal shows a transient of about 2 seconds and a steady phase of about 3 seconds.

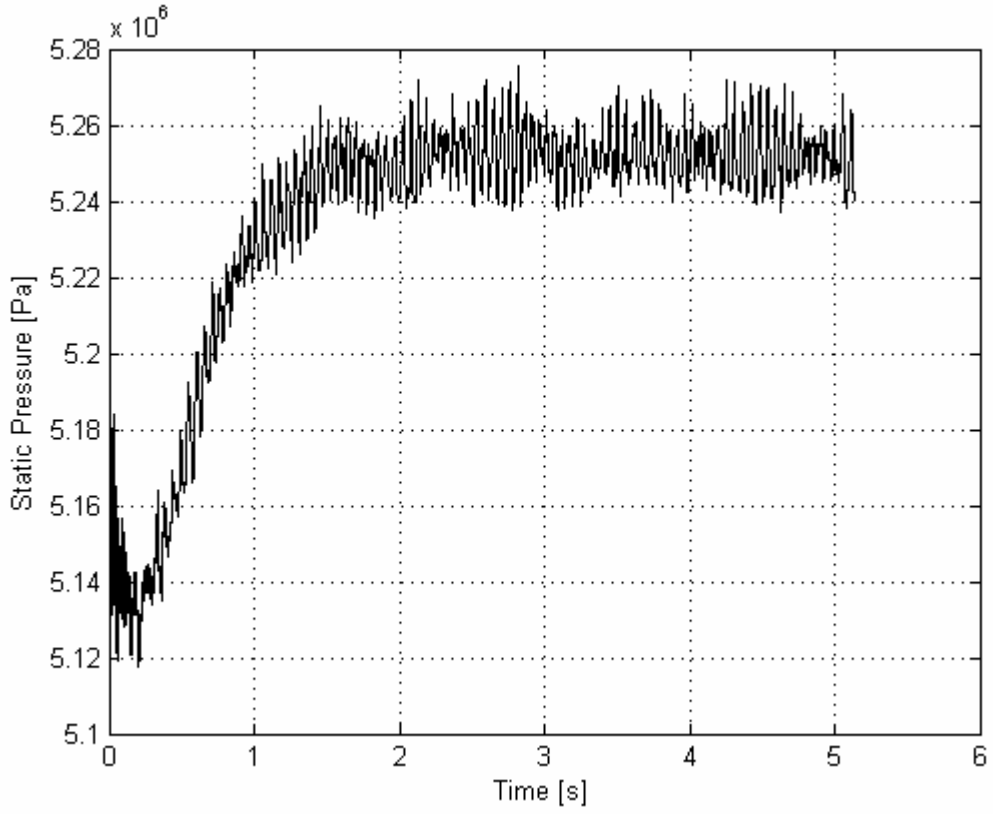

Fig. 47 – Pressure signal. Case with inert particles

The evolution of the maximum amplitude of the first frequency of oscillation is shown in Fig. 48, from which it can be also noticed the increase in amplitude of the error bars with respect to the single-phase case.

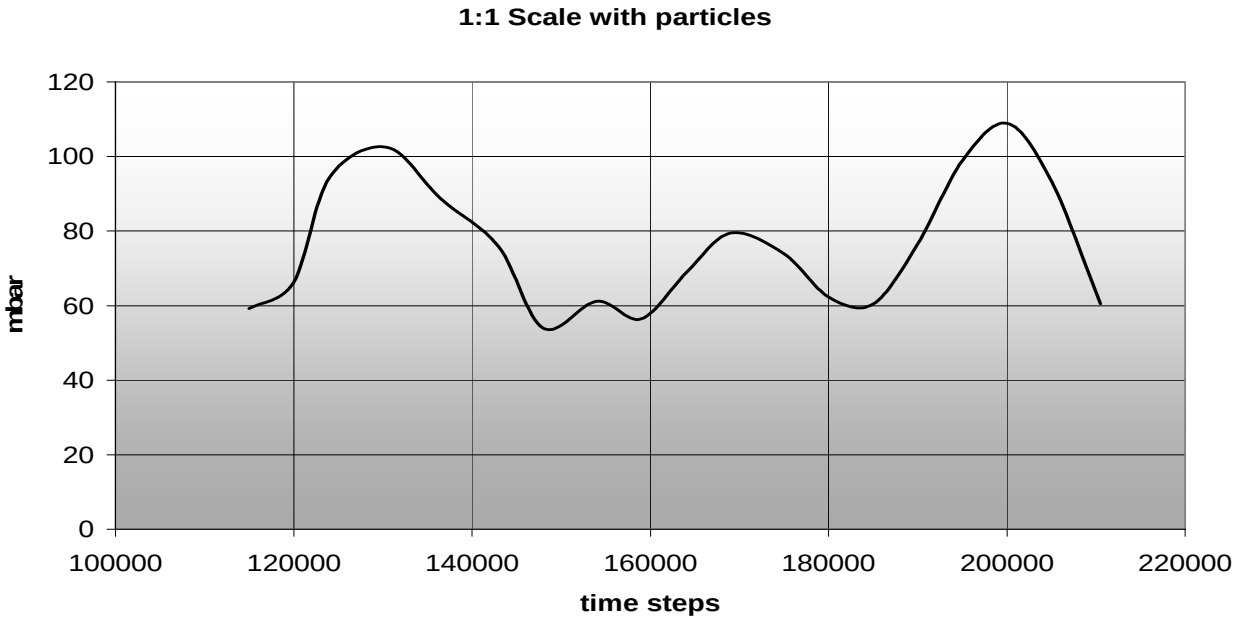

Fig. 48 – Behaviour of first frequency amplitude

Another peculiarity that can be noticed from Fig. 46 is the presence of noise which increases the difficulty to distinguish the peaks of the oscillations (especially the lower ones), if compared to the case in which the discrete phase was not present. Generally, the case employing inert particle shows a greater presence of noise. From Fig. 49 it can be noticed how the presence of particles modifies the vortex structures, which in this case show a much more fragmented geometry with respect the previous case, where the particulate was not adopted.

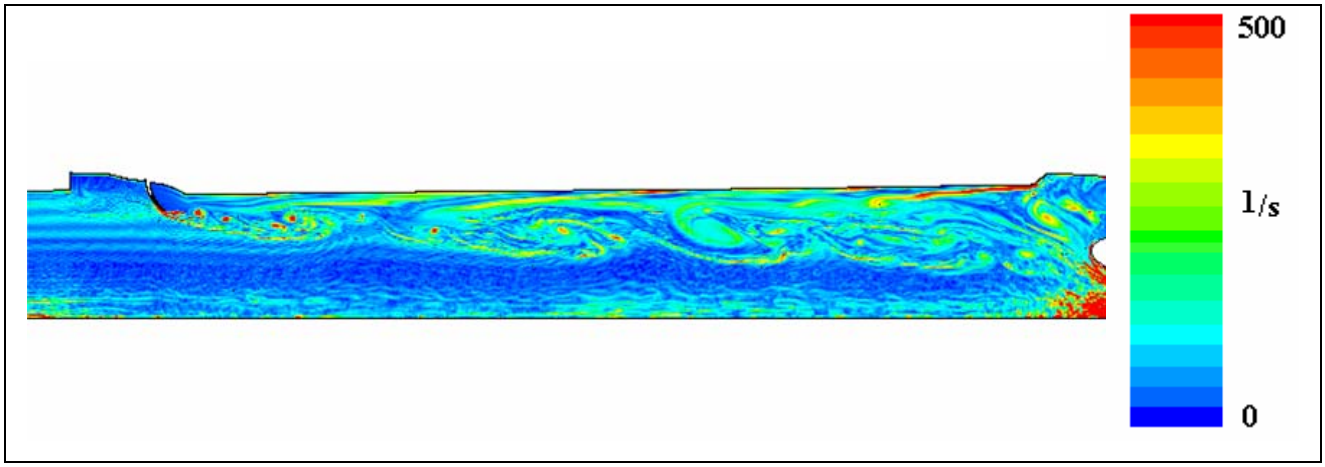

Fig. 49 – 1:1 scale with particle. Vorticity

The particles, responsible for this fragmentation, as shown in Fig. 50, are mainly densified on the surface of the grain, corresponding to the areas where the generation of vortex shedding occurs.

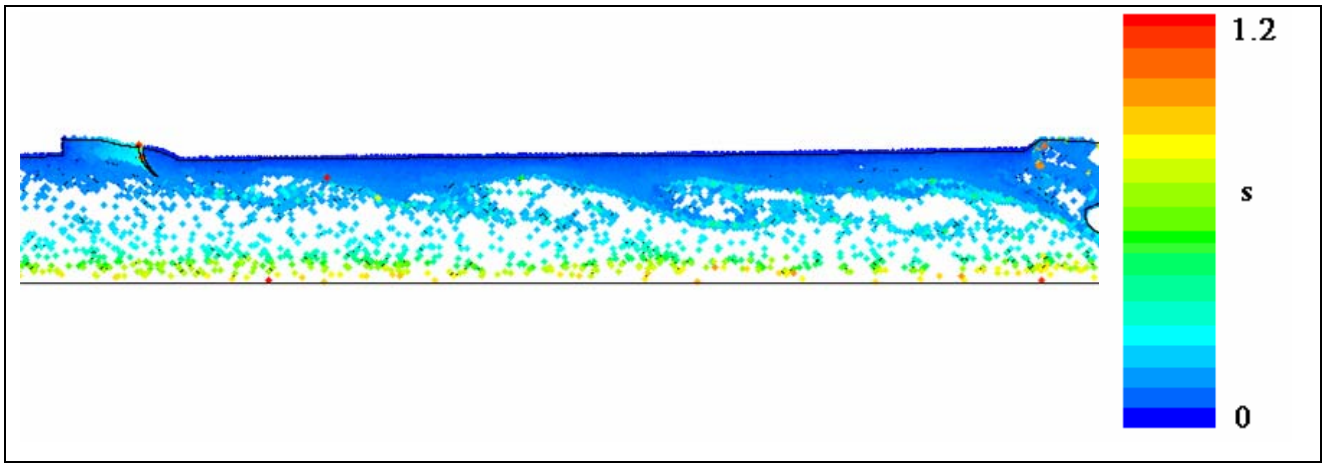

Fig. 50 –1:1 scale with particles – Coloured according to the residence time

Moreover, observing Fig. 51, it can be noticed that the particles move with more difficulty towards the centre of the engine, remain confined within the area near the grain (i.e. in the zone where parietal vorticity is concentrated), and influence the vorticity structures (see Fig. 41). Hence, in the case for which the particulate is employed, the parietal and obstacle vorticity are modified by the presence of inert particles, which subtract momentum and energy from the fluid. Being characterized, in this way, by lower energy levels, the fluid field can transfer a lower amount of energy to the acoustic field making the particle acting therefore as dampers for the PWO. This phenomenon agrees with the ones observed and reported in literature [53].

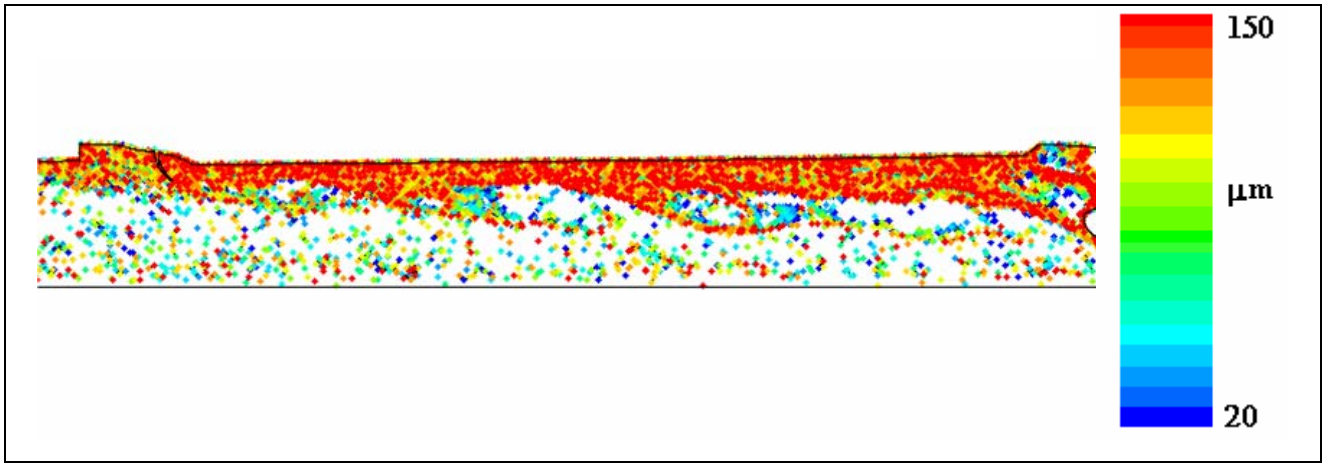

Fig. 51 – 1:1 scale with particles – Coloured according to the particle diameter

The strong interaction between the fluid and the particles can be seen both in Fig. 49, in which the damping effect that the particles produce on vortex structures can be noticed, and in Fig. 51 in which it is shown that the motion of particles is deflected because of the vorticity in which particles are immersed.

9.2 1:2.5 SCALE

The second analysed configuration has regarded the 1:2.5 scaled engine. As performed for the larger scale, on this configuration the simulations were performed first without the introduction of the discrete phase, in order to assess the possible existence of phenomena simply due to the scaling process of the engine. Then the calculations for the size determination of the discrete phase have been performed and finally, the addition of the presence of the reacting discrete phase has been adopted in order to obtain the PWO levels.

9.2.1 PWO WITHOUT DISCRETE PHASE

The manner in which this calculation has been conducted is identical to the one used in the 1:1 scale. The geometry is indeed exactly the same, unless the scale factor, and the internal ballistics scale time is representative of the one occurring in a full scale.
Amplitudes and frequencies are visible in Fig. 52. The plot is taken in an intermediate instant during the stationary sampling phase.

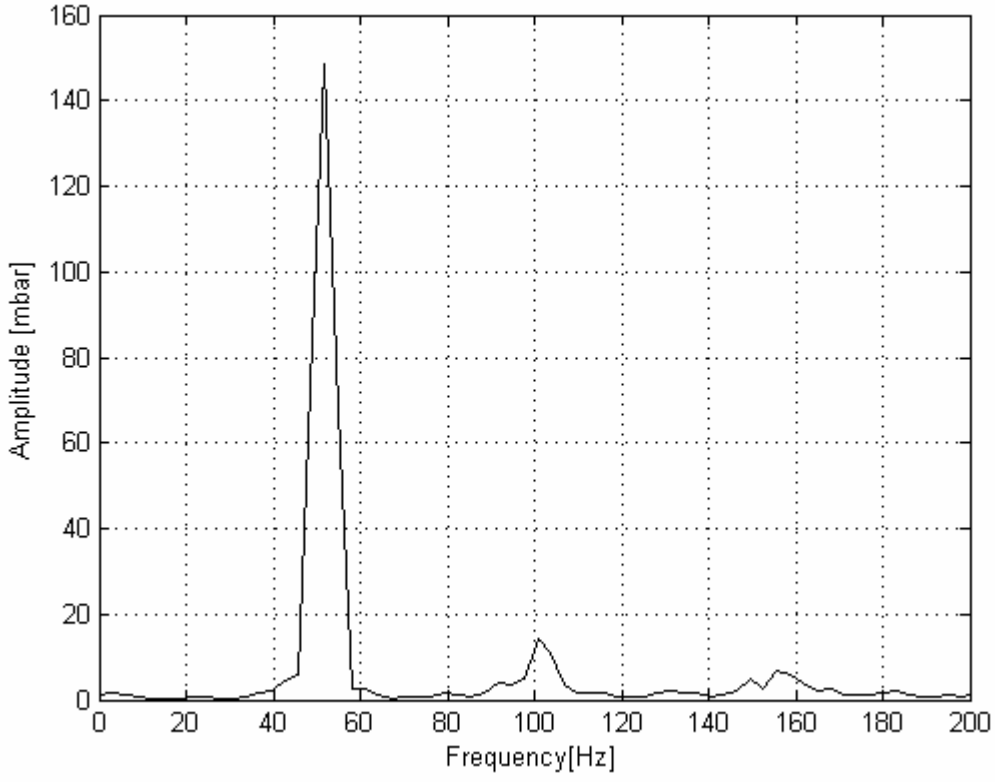

Fig. 52 – Amplitudes and frequencies of pressure signal

A more detailed analysis of the frequencies and of the amplitudes is reported in Tab. 6.

	Data analysis using FFT		Integral energy analysis
	Frequency (Hz)	Amplitude (mbar)	Amplitude (mbar)
1st mode	51.9 ± 3.1	148.7 ± 10	150.1
2nd mode	100.7 ± 3.1	13.5 ± 7	16.2
3rd mode	155.6 ± 3.1	11.8 ± 3	13.0

Tab. 6 – Amplitudes and frequencies – 1:2.5 scale

Moreover, the trend of the peaks of the first oscillation frequency, during the stationary sampling phase, is shown in Fig. 53. It can be seen from this figure that the peaks monitoring includes a wide range of time, estimated to be about 1.2 [s].

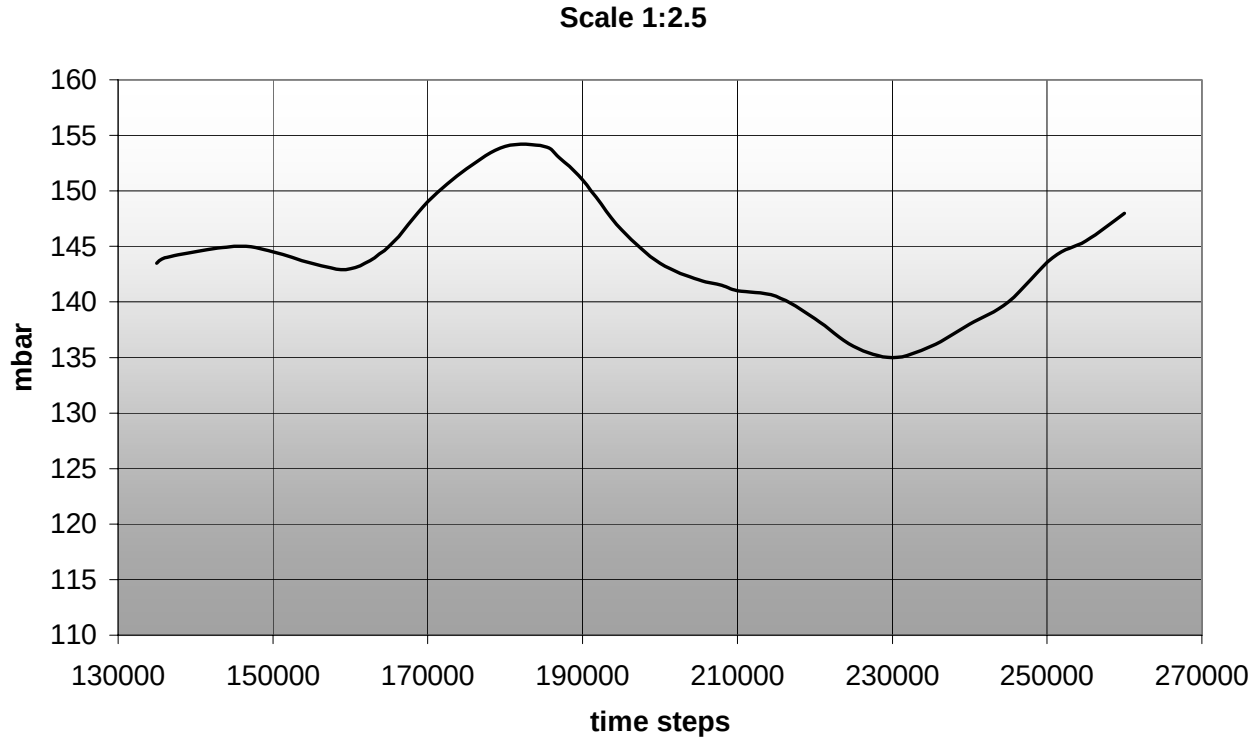

Fig. 53 – First frequency's amplitude behaviour

The signal from which the frequencies are derived is shown in Fig. 54.

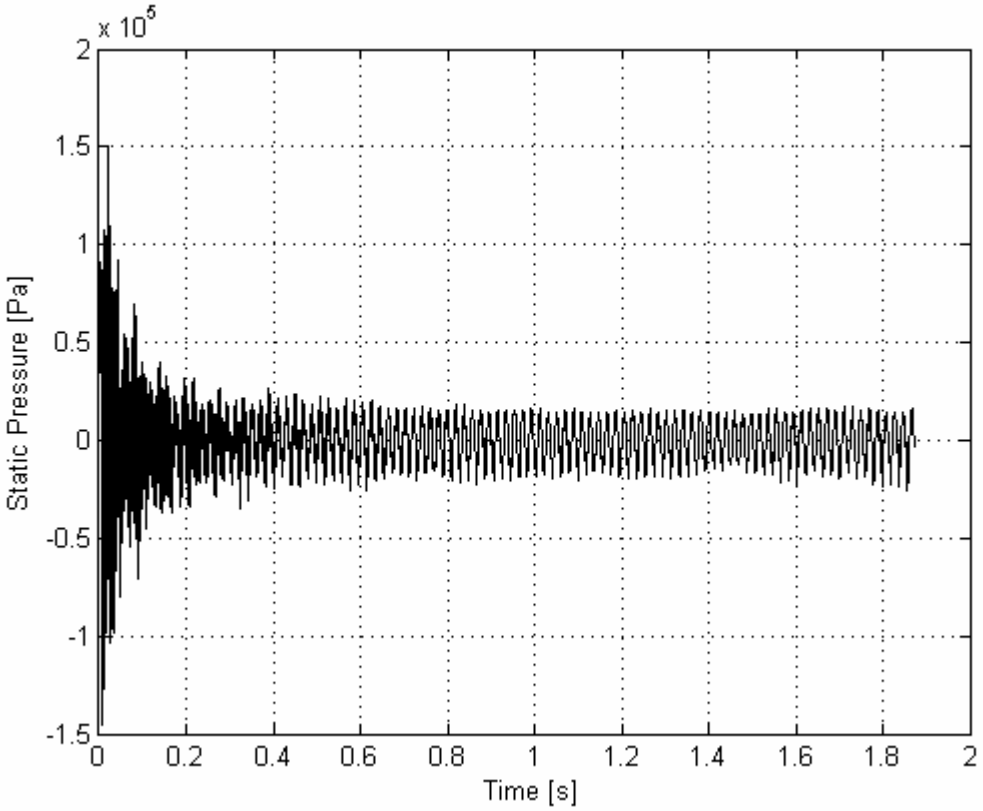

Fig. 54 – Pressure signal

Again, observing the field of vorticity, groups of vortex structures can be seen, generated by the obstacle, travelling towards the head of the nozzle and interacting with other vortexes generated near the grain (parietal vortex).

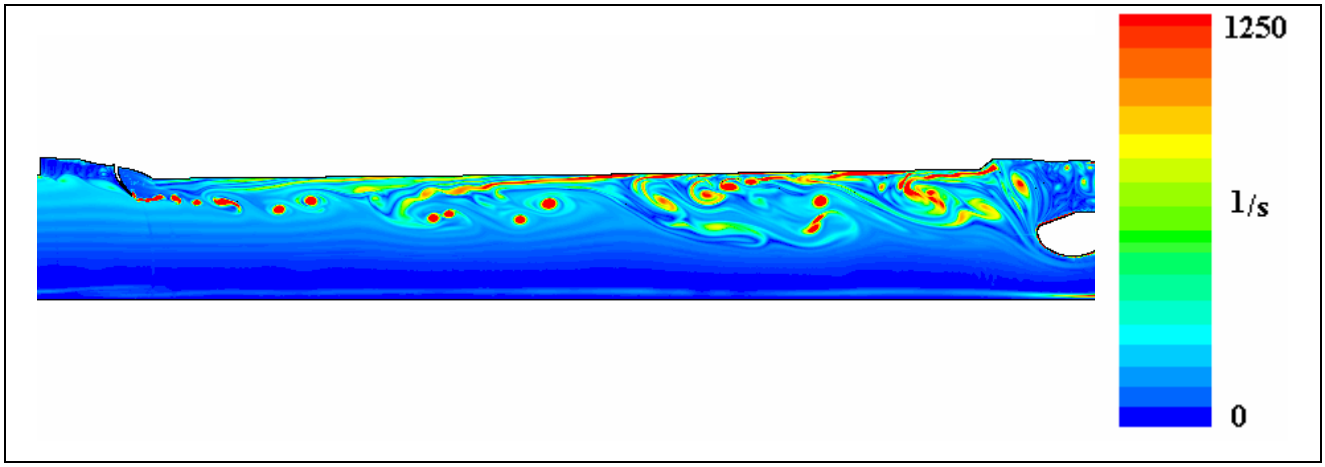

Fig. 55 – Vortex structures in 1:2.5 motor without particulate

9.2.2 DISCRETE PHASE DIMENSIONS EVALUATION

At the aim of introducing a discrete phase in the fluid dynamic field, its size distribution must be known. In chap. 6 the methodology used for determining the most probable particle size has been illustrated and already used in the previous calculation (1:1 scale). Such methodology is now applied to the 1:2.5 case for which the PWO oscillation calculation is needed. As already mentioned, for these calculations the nozzle has to be removed from the field so that the results can be representative of the particle size in the combustion chamber and not affected by the fluid flowing through the nozzle.

Performing the numerical simulations and processing the data as suggested in paragraph 6.1, the new obtained particle distribution is reported in Fig. 56.

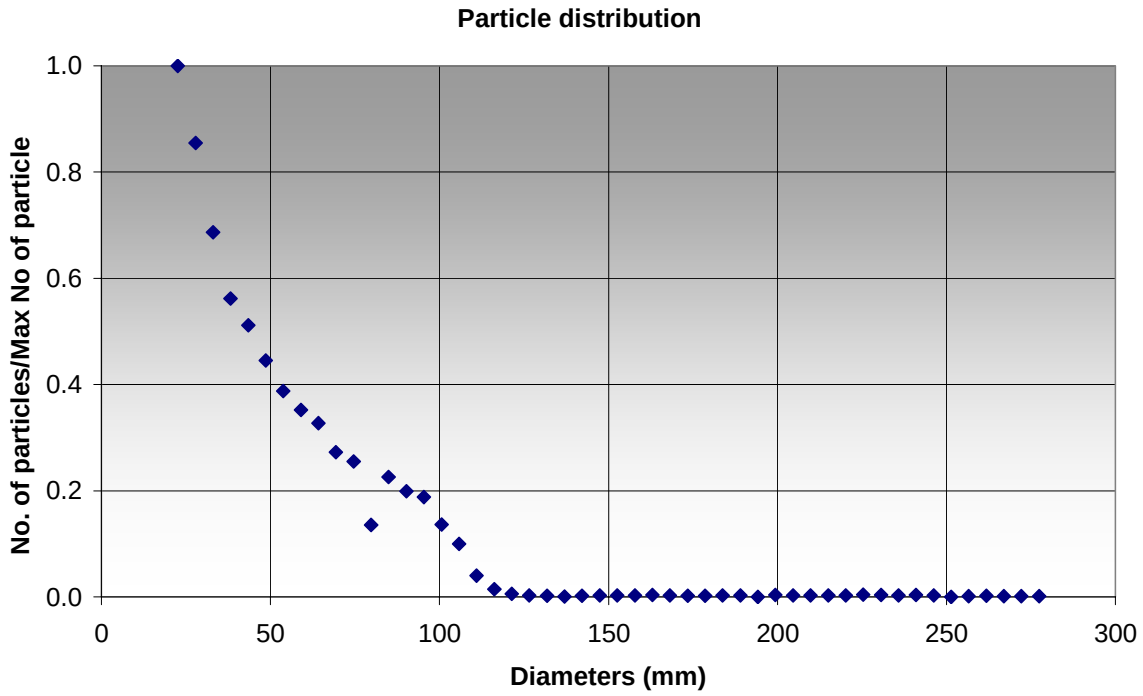

Fig. 56 – Output particle distribution

Observing the previous figure, it is visible that all the particles having a diameter larger than 120 μm have suffered a break and have therefore been scaled by assigning them a diameter equal to the maximum calculated along the trajectory. Using the suitable values of $\bar{\phi}$ and n, the Rosin-Rammler function (eq. 10), that best approximates the curve numerically obtained, is defined.

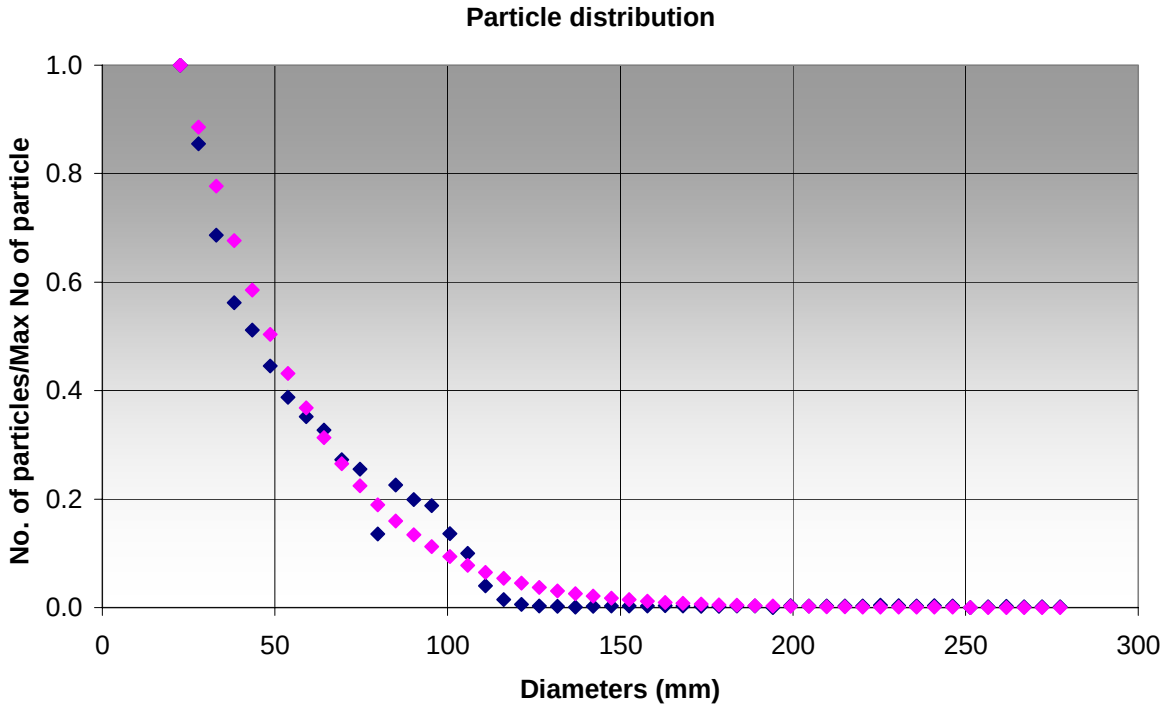

Fig. 57 – Overlapping of output particle / best fit function

For the curve represented in Fig. 57 the values of $\overline{\phi}$ and *n,* which better define the best fit are:

$\overline{\phi}$ = 3.7E-5 n=1.15

9.2.3 PWO WITH INERT PARTICLE

The manner in which this calculation was conducted is identical to the one adopted in the 1:2.5 case without particulate. The geometry is indeed exactly the same, and the internal ballistics, scaled proportionally to the scale factor, is representative of what occurs in the real scale.
The main difference regards the introduction of the inert discrete phase.
Also in this case the input granulometry has been previously calculated using the procedure indicated in chap. 6 and shown in the previous paragraph.

Amplitudes and frequencies are visible in Fig. 59, where PWO are shown during an intermediate instant of time taken during the stationary sampling phase.

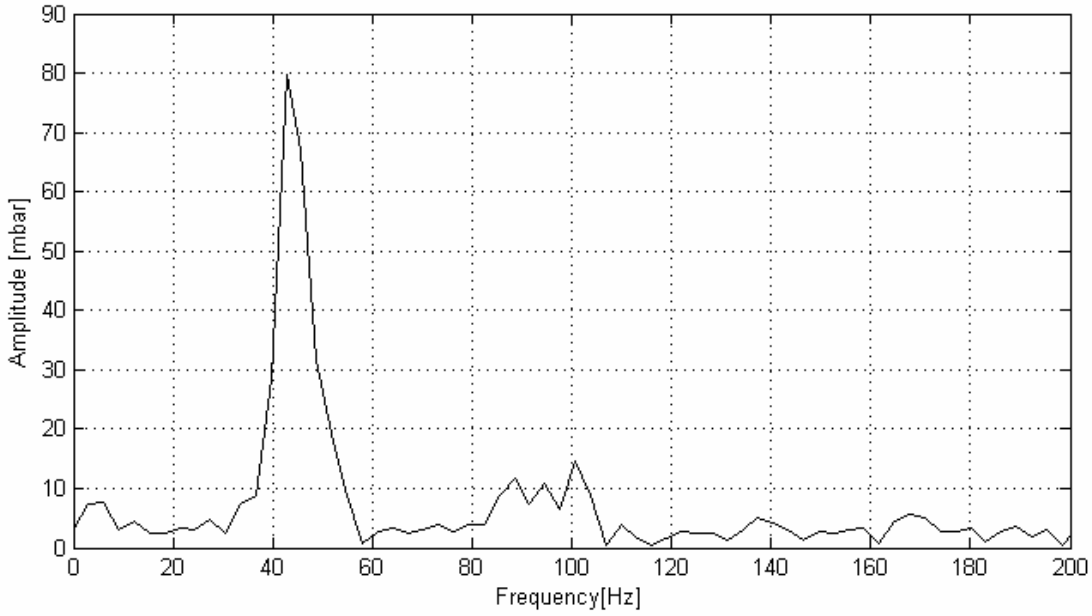

Fig. 58 – Amplitudes and frequencies of the pressure signal

Also in this case the pressure oscillations are affected by the presence of the inert phase.
It can be indeed noticed that the amplitude associated with the first frequency is well below the level obtained when the particles had not been introduced in the flow.

A more detailed analysis of both frequencies and amplitudes is reported in Tab. 6.

	Data analysis using FFT		Integral energy analysis
	Frequency (Hz)	Amplitude (mbar)	Amplitude (mbar)
1st mode	42.7 ± 3.1	70.0 ± 30	95.1
2nd mode	100.7 ± 3.1	17.5 ± 3	23.5
3rd mode	167.8 ± 3.1	8.0 ± 2	10.5

Tab. 7 – Amplitudes and frequencies – 1:2.5 scale. Case with discrete phase

Again, as seen in the full scale configuration with particulate, the error bar is quite wide, whereas the amplitudes of the 2nd and 3rd frequencies do not suffer from the introduction of the second phase.
Finally, the evolution of the peaks of the first oscillation frequency during the stationary sampling phase is shown in Fig. 53. It can be seen from this figure that the monitoring of the peaks included a fairly large time, estimated in about 1.2 [s].
The first frequency peak amplitude shows average values of about 70 [mbar] (Fig. 59)

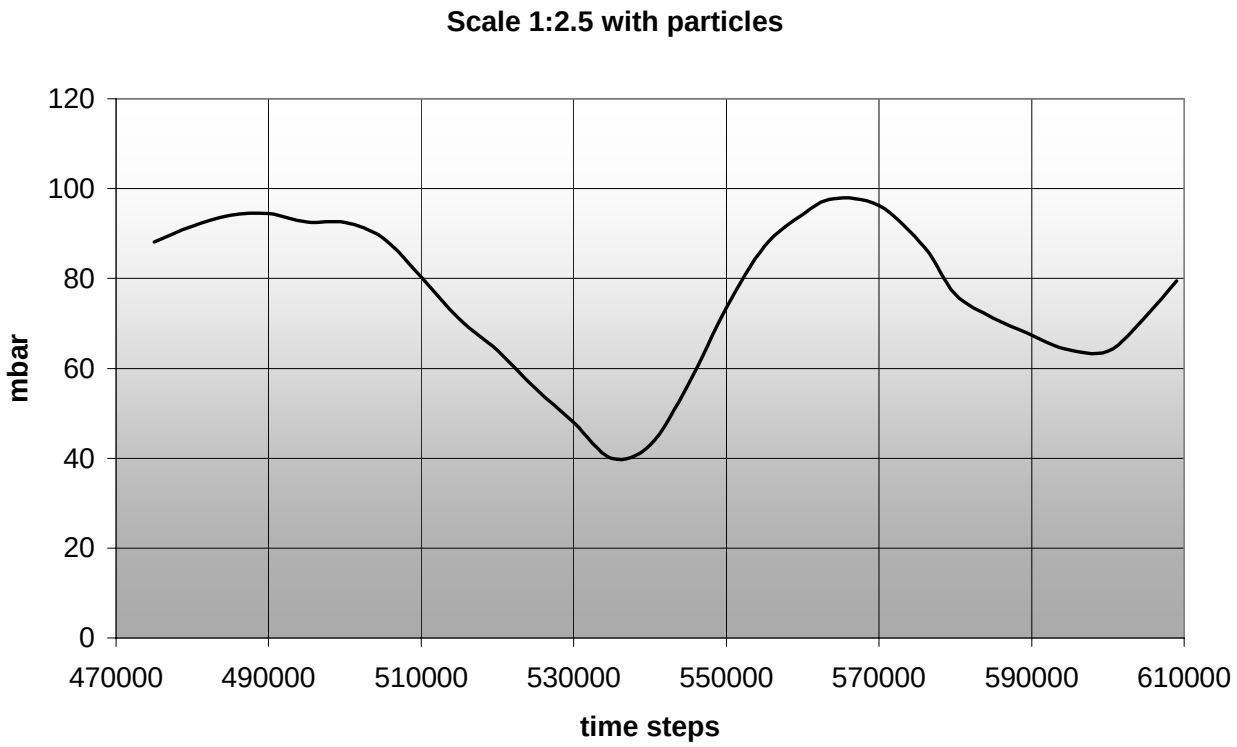

Fig. 59 – First frequency amplitude behaviour

The signal from which the frequencies are derived shows a rather long stationary phase, as shown in Fig. 60.

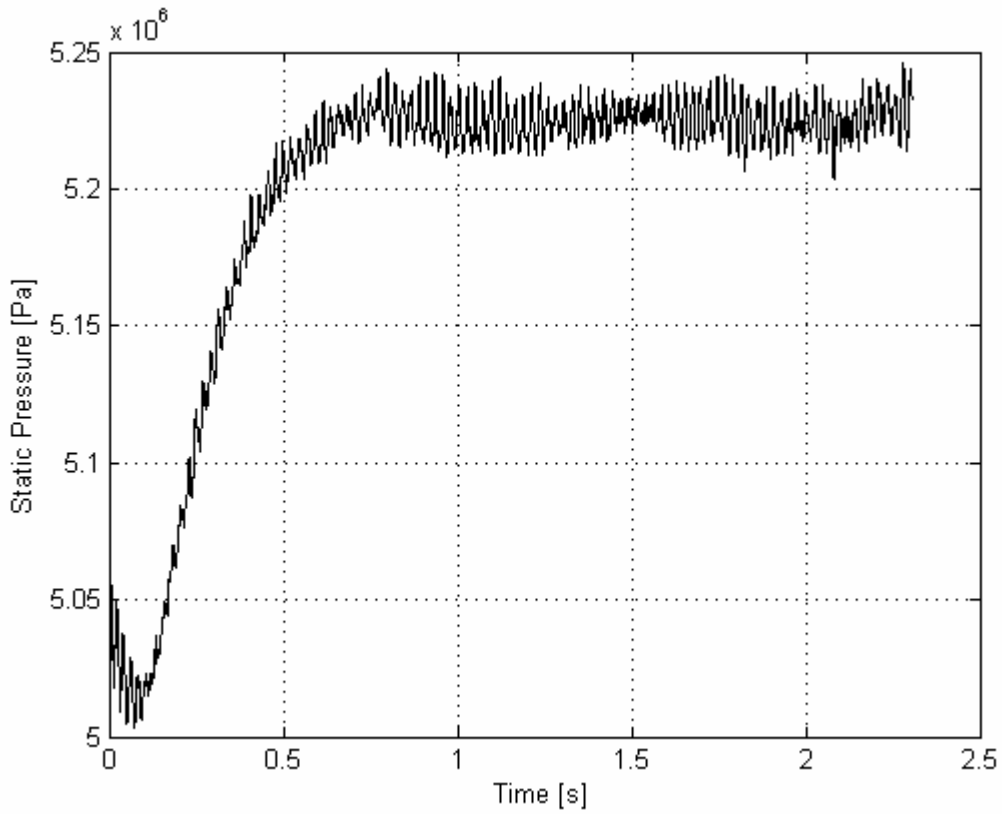

Fig. 60 – Pressure signal

From the plot in Fig. 61 it can be seen once again how the presence of the particles strongly modifies vorticity structures if compared with the case where the particles were not introduced.

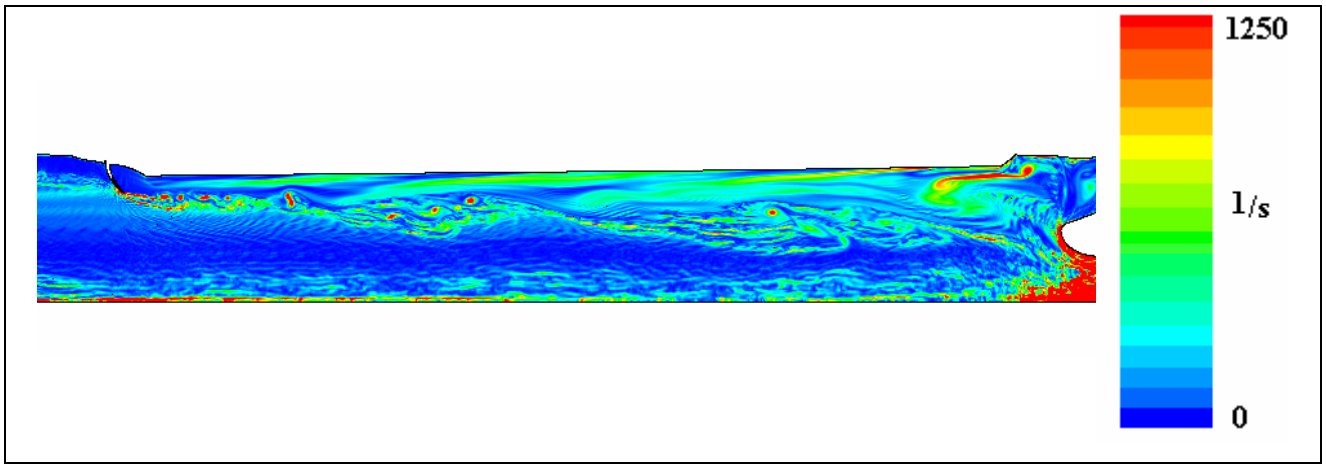

Fig. 61 – 1:2.5 scale with particles. Vorticity field

As in the 1:1 case, and as shown in Fig. 50, the discrete phase is densified mainly on the grain surface, influencing the generation and motion of the vorticity generated on the wall.

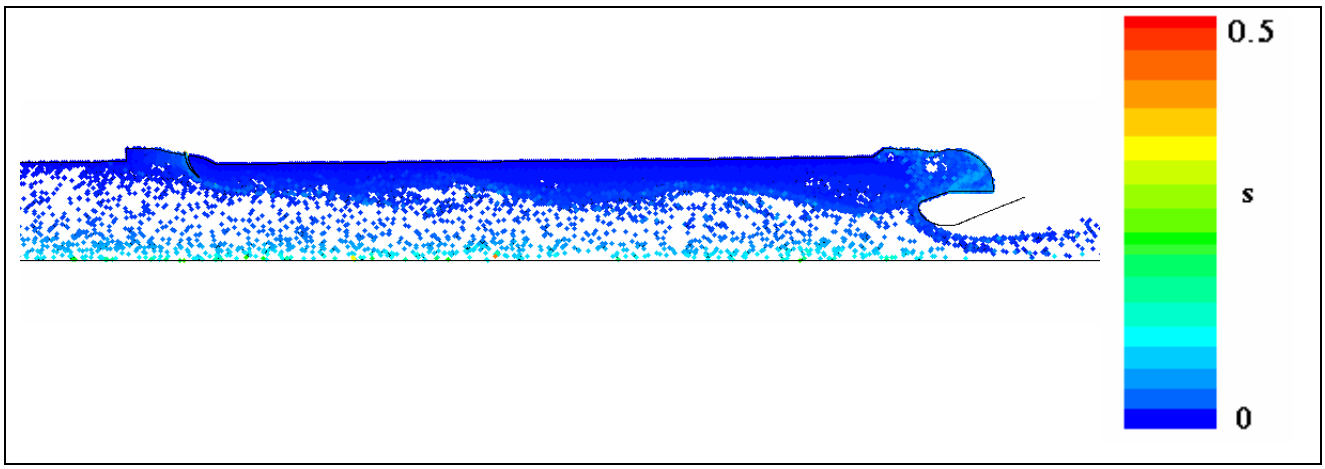

Fig. 62 – 1:2.5 scale with particles – Coloured according to the residence time

Observing the position of the particulates, it should also be noticed that in this occasion (Fig. 62), the particles inside the chamber, independently of their diameter, tend to remain confined in the area near the grain, i.e. the area where the parietal vortex shedding occurs. As already noticed these vorticity interacts with the vorticity generated by the FTP obstacles and influences the vorticity field present in the combustion chamber (see Fig. 61).

Hence, in the case of presence of particulate, the vorticity close to the wall and the vortexes travelling towards the nozzle are modified by the particles, which subtract momentum from the fluid and behaving as PWO dampers.

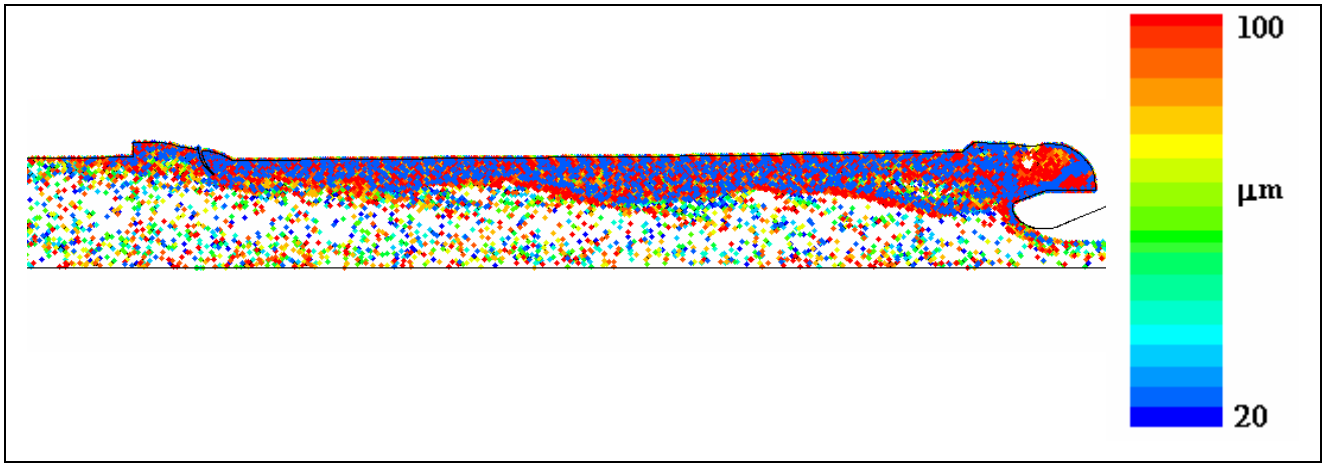

Fig. 63 – 1:1 scale with particles – Coloured according to the particle diameter

9.3 1:5 SCALE

The third analysed configuration is related to the 1:5 scaled engine. This is a fairly important case because, as explained in the next chapter, the PWO behaviour is not in line with the one anticipated by the previous two simulations.

9.3.1 PWO WITHOUT DISCRETE PHASE

The manner in which this calculation has been conducted is identical to the one adopted in the 1:1 and 1:2.5 scale cases. The geometry is indeed exactly the same, unless the scale factor, and the internal ballistics is proportionally scaled to the scale factor and representative of full scale ballistics.
The amplitudes and frequencies are visible from the plot shown in Fig. 64, which represents these quantities in an intermediate instant of time while the stationary phase of the sampling

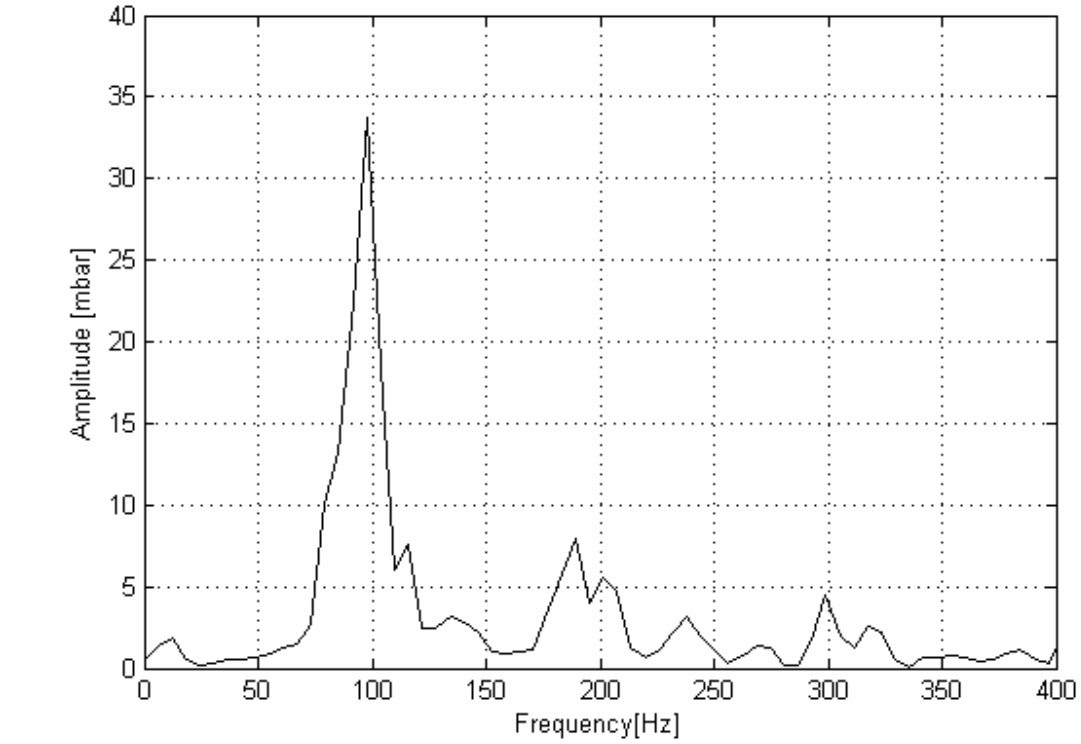

Fig. 64 – Amplitudes and frequencies of the signal

A more detailed analysis of amplitudes and frequencies is reported in Tab. 8.

	Data analysis using FFT		Integral energy analysis
	Frequency (Hz)	Amplitude (mbar)	Amplitude (mbar)
1st mode	97.6 ± 6.1	31.0 ± 12	39.5
2nd mode	189 ± 6.1	17.0 ± 12	20.1
3rd mode	299 ± 6.1	7.1 ± 4	8.0

Tab. 8 – Amplitudes and frequencies – 1:5 scale

Finally, the evolution of the peaks of the first oscillation frequency, during the stationary phase of sampling, is shown in Fig. 65. It can be seen from this figure that the monitoring of the peaks included a wide range of time, estimated to be about 0.45s

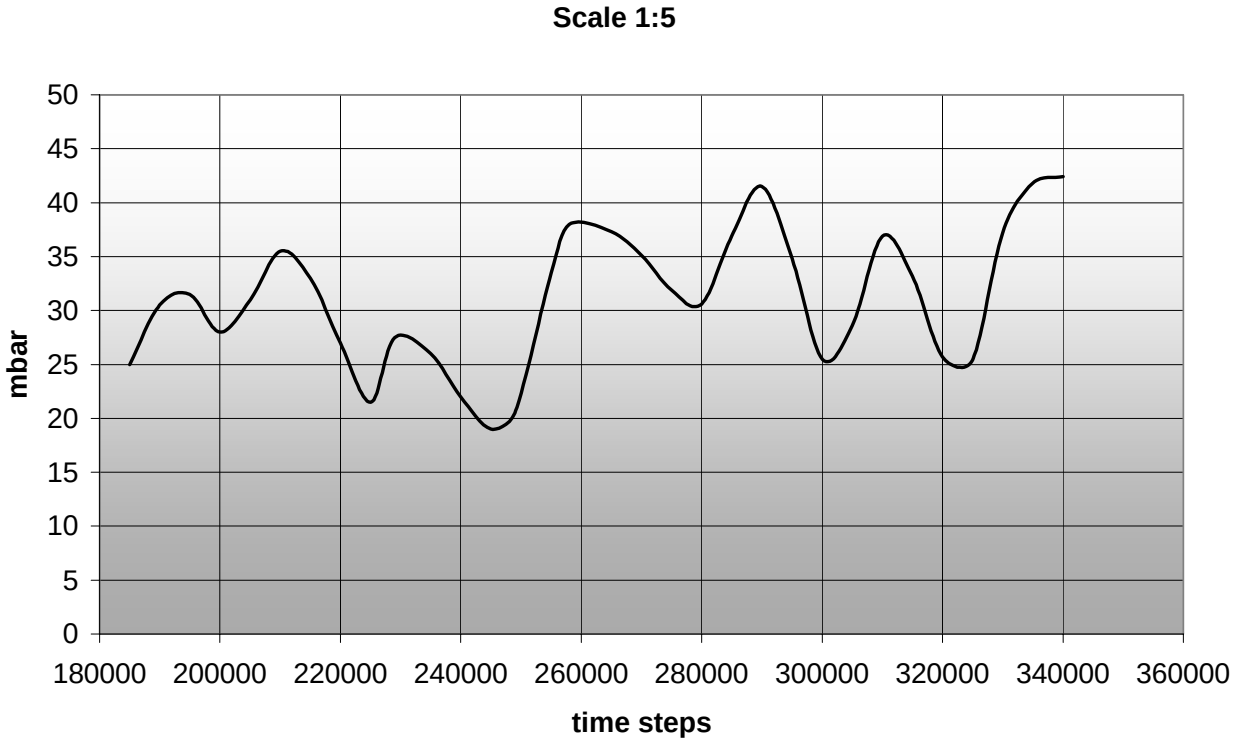

Fig. 65 – First frequency's amplitude behaviour – 1:5 Scale

The signal from which frequencies are derived also presents a long stationary phase, as shown in Fig. 66.

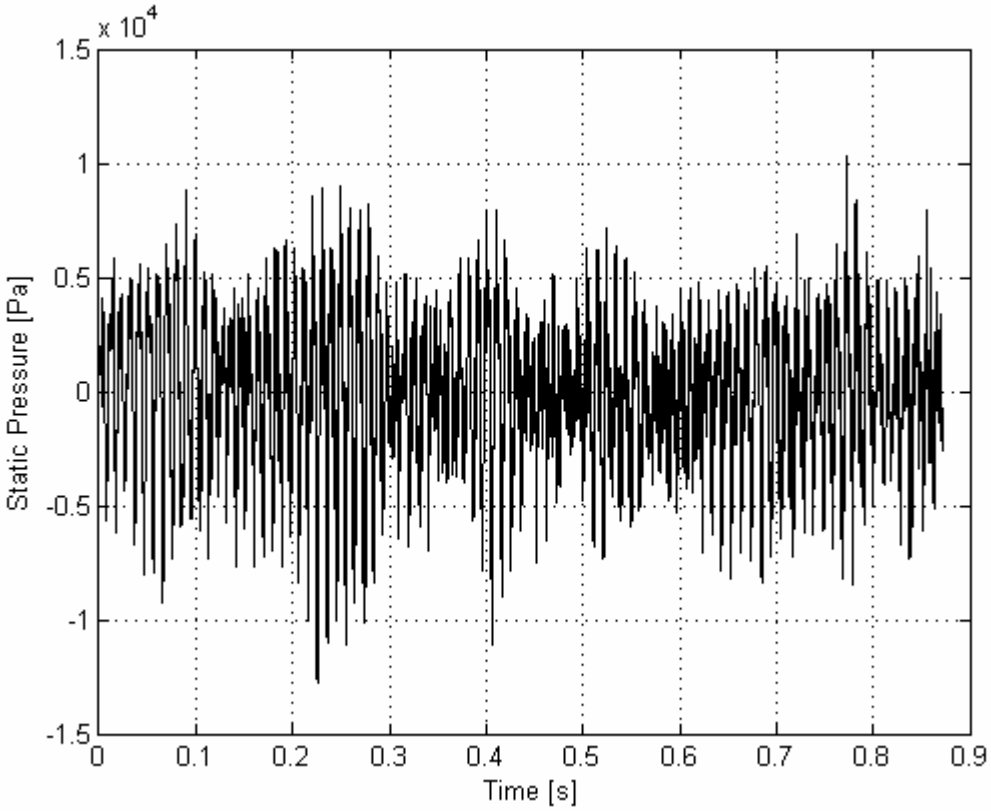

Fig. 66 – Pressure signal – 1:5 scale

Also in this last case, the vorticity field is reported in (Fig. 67). Observing this figure it can be seen that the absence of discrete phase enables vorticity structures to keep their shape without being fragmented. Despite this, in this case the amplitude of the first peak, as shown in the above table, shows a dramatic collapse.

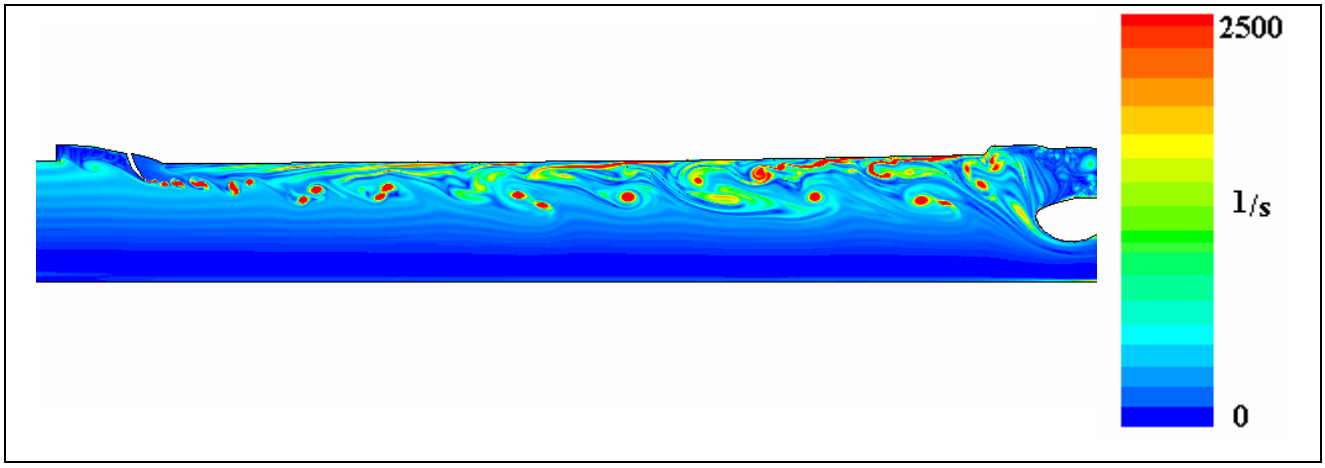

Fig. 67 – Vorticity fields for 1:5 case

9.3.2 DISCRETE PHASE DIMENSION EVALUATION

In order to introduce the discrete phase in the flow field, the methodology discussed in chap.6 must be applied. The adopted geometry is the one scaled by a factor 1:5, for which the particle dimension need to be found.

Performing the numerical simulation and process data as described in paragraph 6.1, the new particle size distribution obtained is shown in Fig. 68.

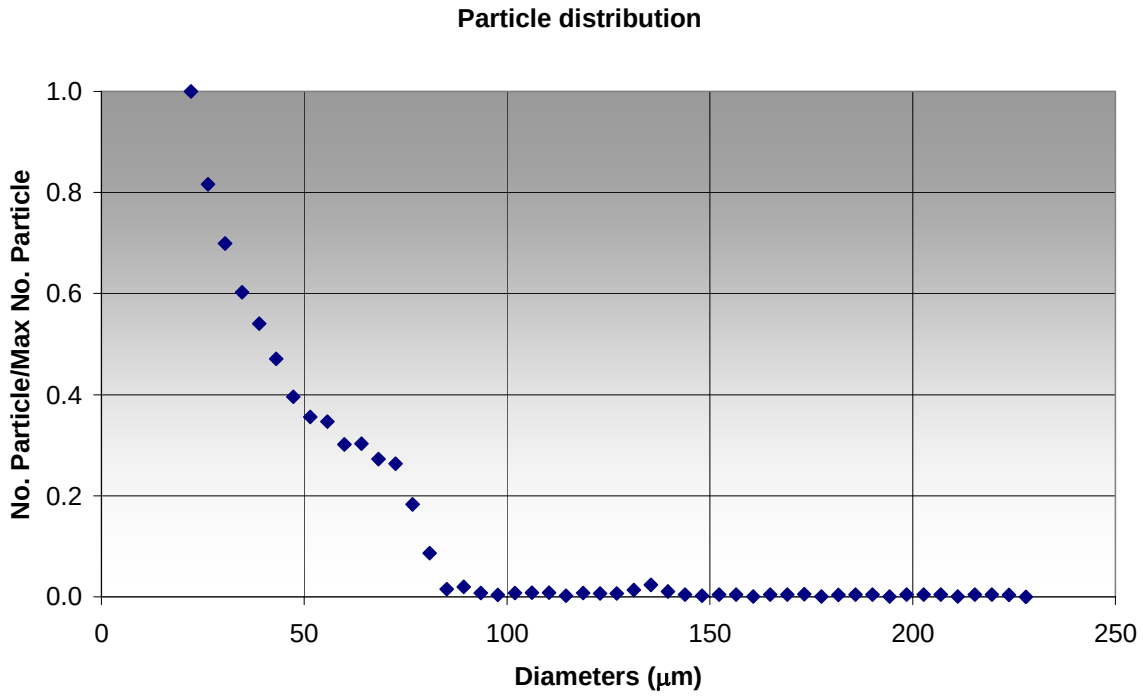

Fig. 68 – Granulometric output distribution

Observing the previous figure, it is visible that all the particles having a diameter larger than 90 μm have suffered a break and have therefore been scaled by assigning them a diameter equal to the maximum calculated along the trajectory. Using the suitable values of $\bar{\phi}$ and n, the Rosin-Rammler function (eq. 10), that best approximates the curve numerically obtained, is defined.

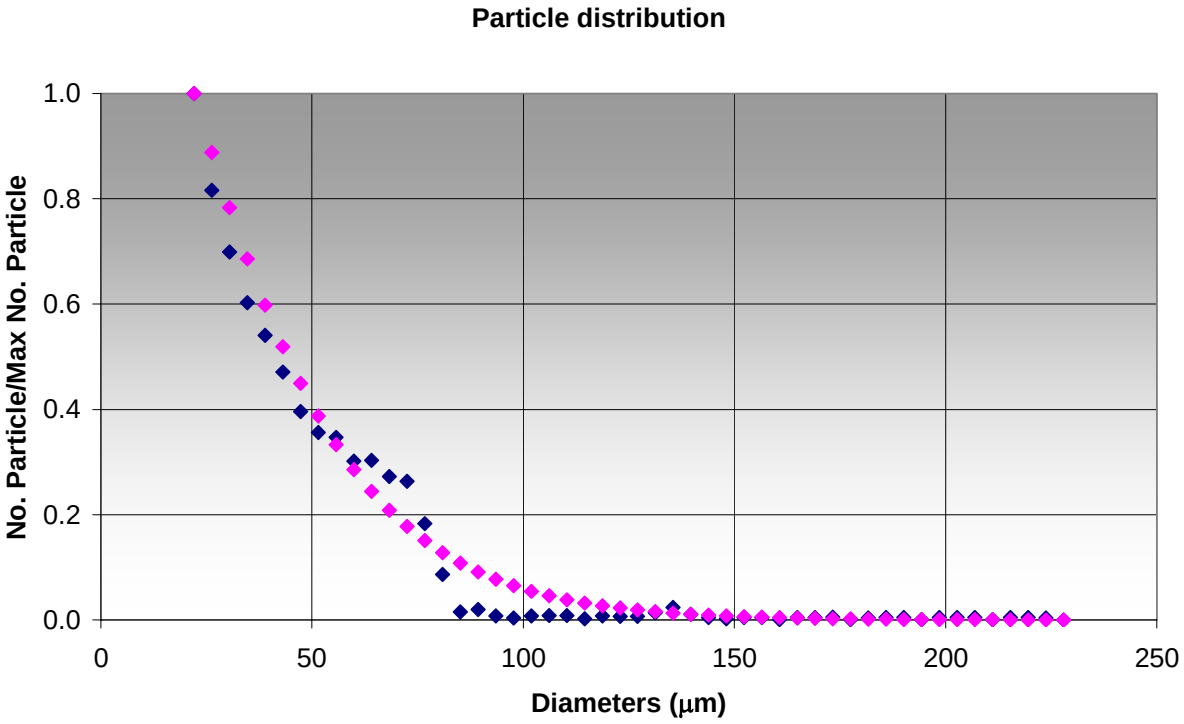

Fig. 69 – Overlapping of output particle / best fit function

For the curve represented in Fig. 69 the values of $\overline{\phi}$ and n, that better define the best-fit function are:

$\overline{\phi}$ = 3.2E-5 n=1.15

9.3.3 PWO WITH INERT PARTICLES

The manner in which it this calculation has been conducted is the same adopted in the case in scale 1:2.5 and 1:1. Indeed the full scale geometry has been re-employed and appropriately scaled, and the internal ballistics is representative of the full scale configuration.
The main difference compared to the 1:5 scale single-phase case (par.9.3.1) concerns the introduction of the inert particulate.
Also in this case the input granulometry has been previously calculated using the procedure indicated in chap. 6 and shown in the previous paragraph.

Amplitudes and frequencies are visible in Fig. 70, where PWO are shown during an intermediate instant of time taken during the stationary phase of sampling

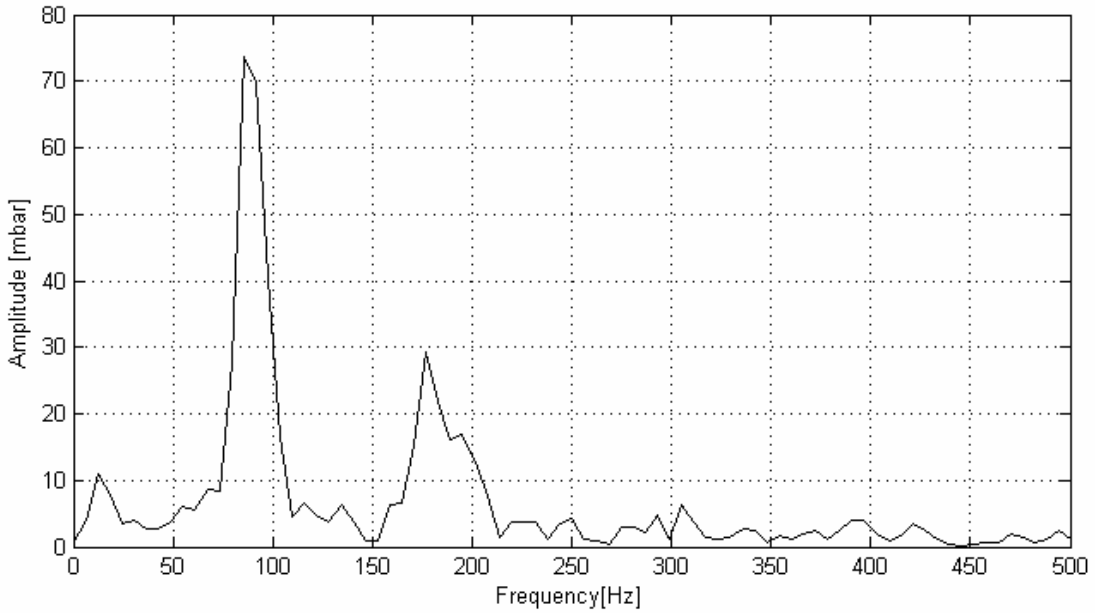

Fig. 70 – Amplitudes and frequencies of pressure signal

In this case the pressure oscillations are affected by the presence of an inert phase in a quite different manner if compared with the effect induced on the PWO by the particles injection at larger scales (1:1 and 1:2.5). The presence of particles, in this case, reactivates the first peak that now shows amplitudes values in line with the two-phase simulations of cases in 1:1 and 1:2.5 scale.

A more detailed analysis of frequencies and amplitudes is reported in Tab. 9.

	Data analysis using FFT		Integral energy analysis
	Frequency (Hz)	Amplitude (mbar)	Amplitude (mbar)
1st mode	85.5±6.1	67.2 ± 20	93.8
2nd mode	177.0±6.1	23.0 ± 10	39.8
3rd mode	305.2±6.1	7.0 ± 3	8.3

Tab. 9 – Amplitudes and frequencies – 1:5 scale – Case with dispersed phase

Finally, the evolution of the amplitude peaks of the first frequency, during the stationary phase of sampling, is shown in Fig. 71. It can be seen from this figure that the monitoring of the peaks includes a wide range of time, estimated at about 0.25s.

The peak of amplitude corresponding with the first frequency indicates that its average value is about 67mbar. Again, from the analysis made during the stationary phase a remarkable fluctuation on the PWO level can be found.

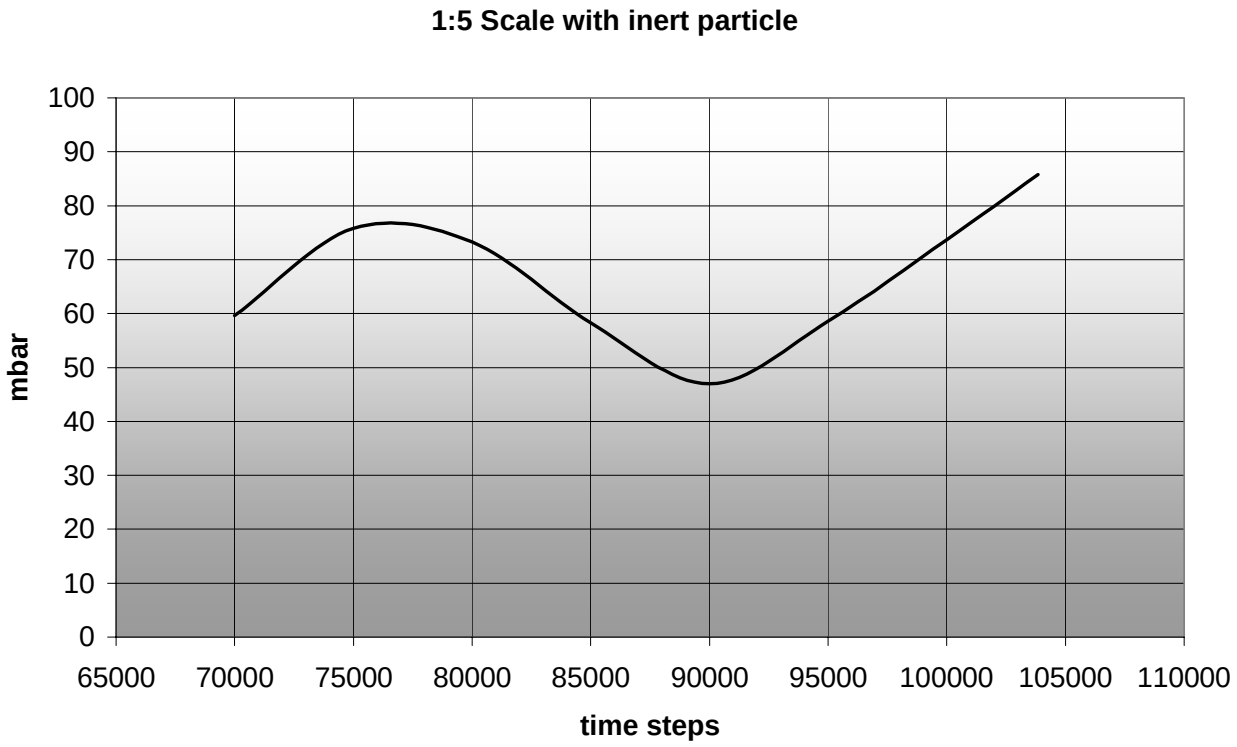

Fig. 71 – First frequency's amplitude behaviour

The pressure signal is shown in Fig. 72.

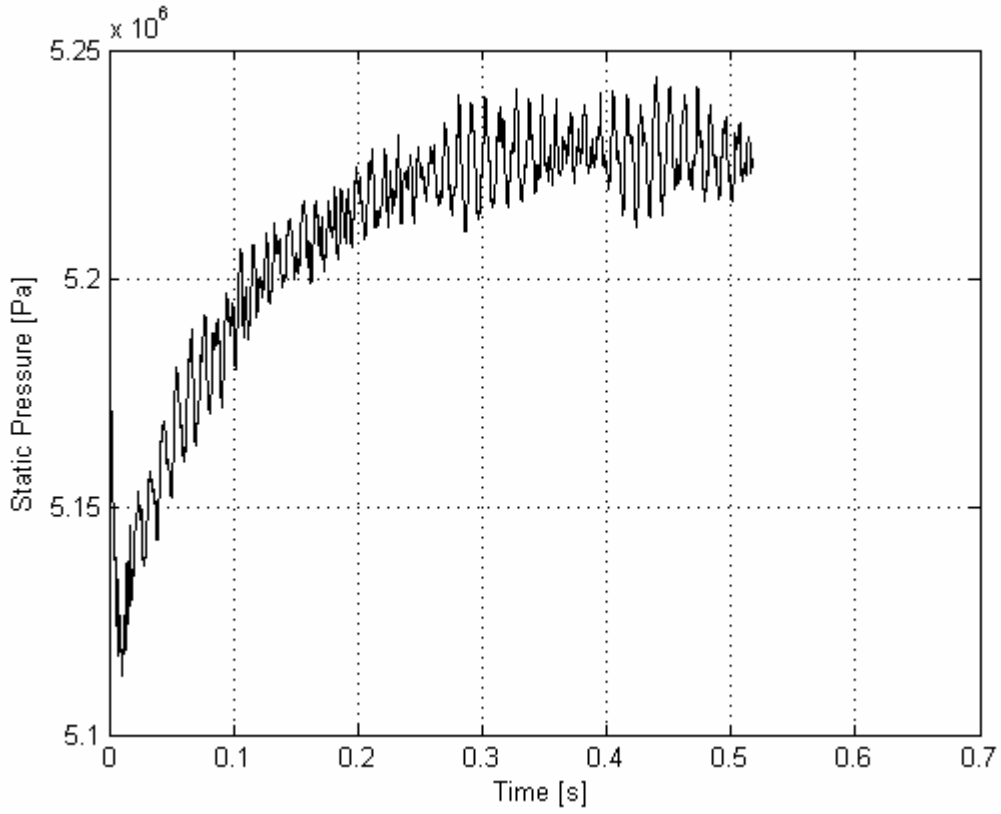

Fig. 72 – Pressure signal

From Fig. 73 it can be seen that, once again, the presence of particles strongly modifies the vorticity structures if compared with the previous case where the discrete phase was not employed.

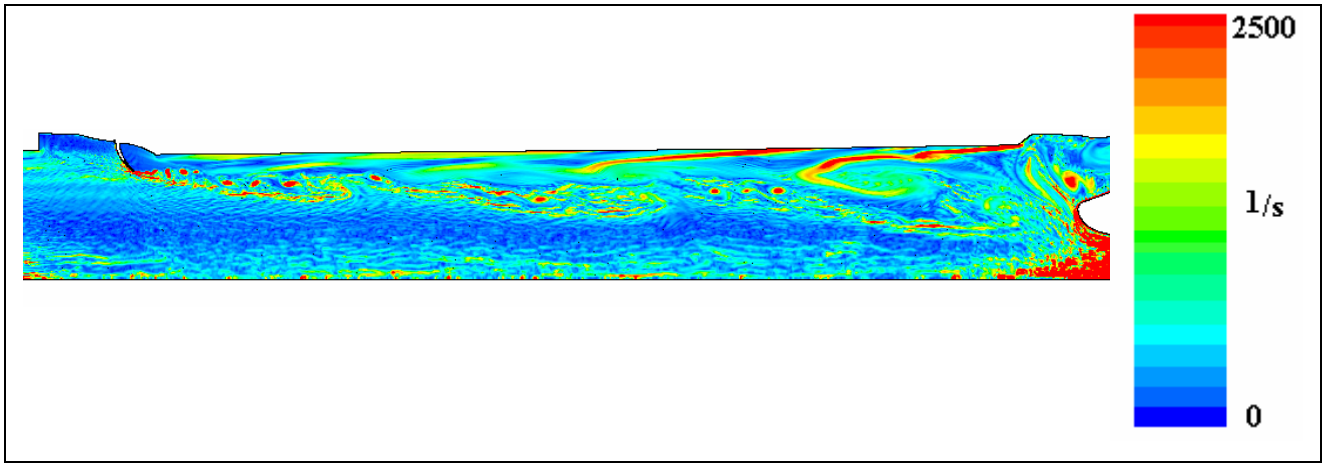

Fig. 73 – 1:5 scale with particles. Vorticity field

Particulate, in fact as shown in Fig. 74, is accumulated on the surface of the grain.

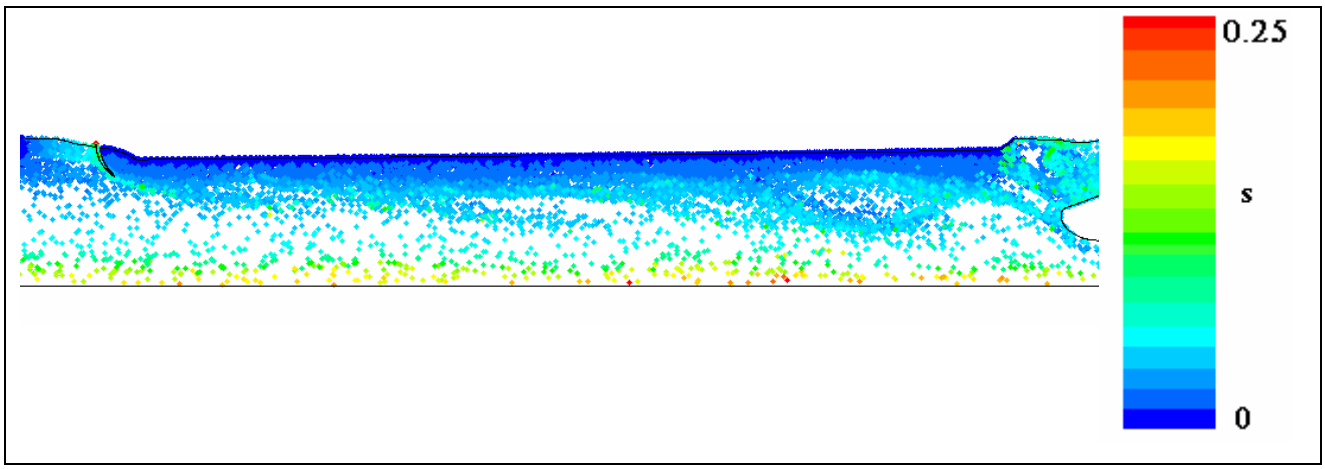

Fig. 74 – 1:5 scale with particles – Coloured according to the residence time

It should again be noted that, observing the position of particles (Fig. 75) inside the chamber, regardless of their diameter, they tend to stay confined in the area near the grain that is the area where a parietal vortex shedding is generated.

However, in this case, the discrete phase can not be considered as a PWO damper since its employment caused a rising in the first frequency level of PWO.

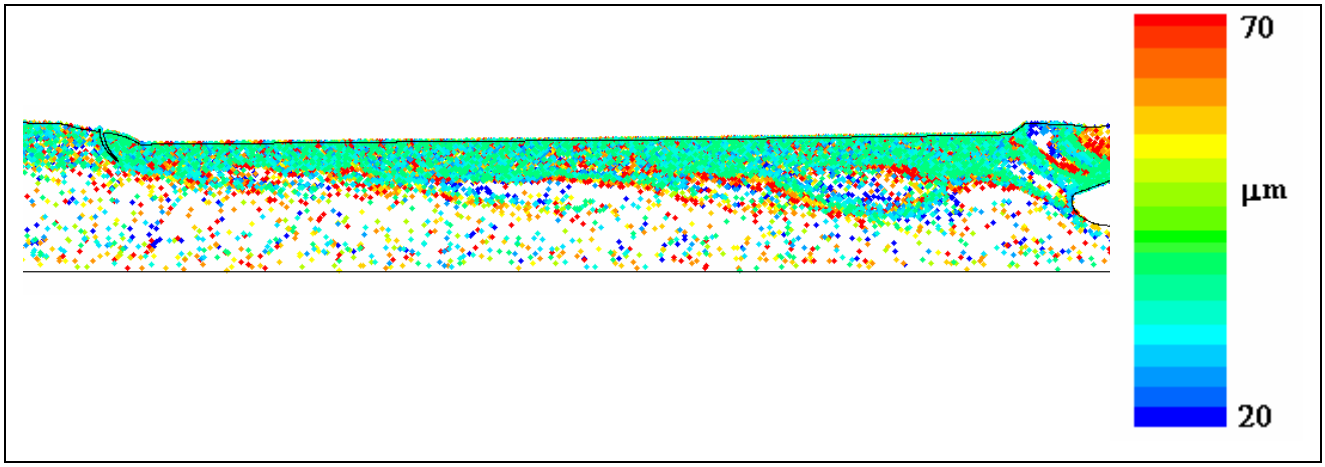

Fig. 75 – 1:2.5 scale with particles – Coloured according to the particle diameter

9.4 COMPARISONS

In this section the results obtained applying the methodologies and the setup shown in previous chapters have been collected. These results were also compared in order to highlight the dependency of PWO to the geometrical configuration and fluid dynamic variations simulated inside the engine. As stated above, attention was focused on the effects induced on the PWO due to geometric scaling engine, the presence of particles, and the coupling of these two phenomena.

In the results comparison, for simplicity it is taken as a reference configuration the 1:1 scale, in which the setup of the fluid does not take into account the presence of inert particles.
The results were compared firstly assessing the effect of geometric scaling, then considering the presence of particulates.

Following that order, some plot and tables of PWO frequencies/amplitudes in different geometric configurations, regardless of the presence of particulates are reported.
In the table only the amplitudes/frequencies of the first peak are included.

Scale	Data analysis using FFT		Integral energy analysis
	Frequency (Hz)	Amplitude (mbar)	Amplitude (mbar)
1:1	20.7 ± 1.2	148.7 ± 6	153.8
1:2.5	51.9 ± 3.1	148.7 ± 10	150.1
1:5	97.6 ± 6.1	33.7 ± 9	39.5

Tab. 10 – Comparisons: effect of geometrical scaling on a mono-phase case

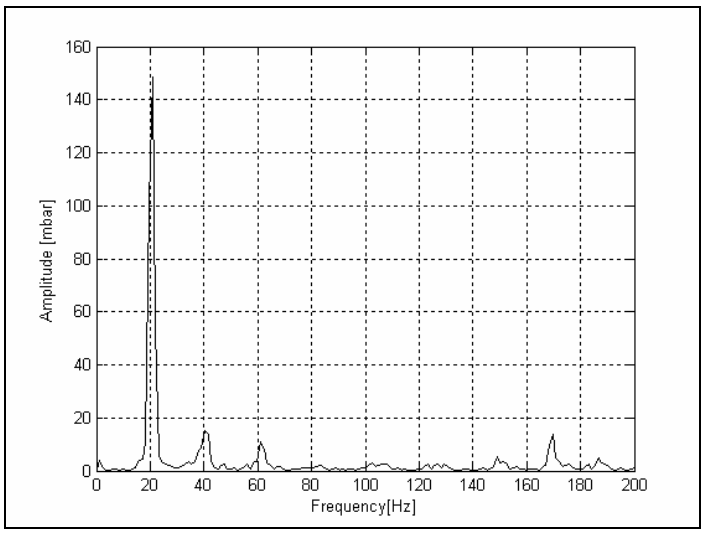

Fig. 76 – Amplitudes and frequencies – 1:1 scale – Single phase case

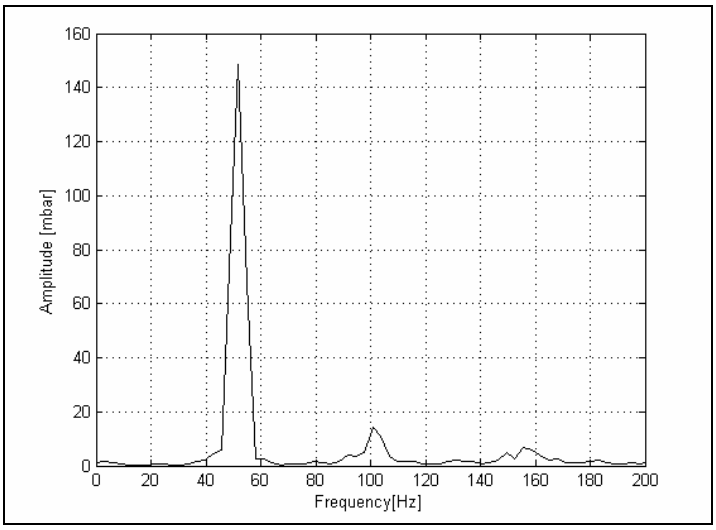

Fig. 77 – Amplitudes and frequencies – 1:2.5 scale – Single phase case

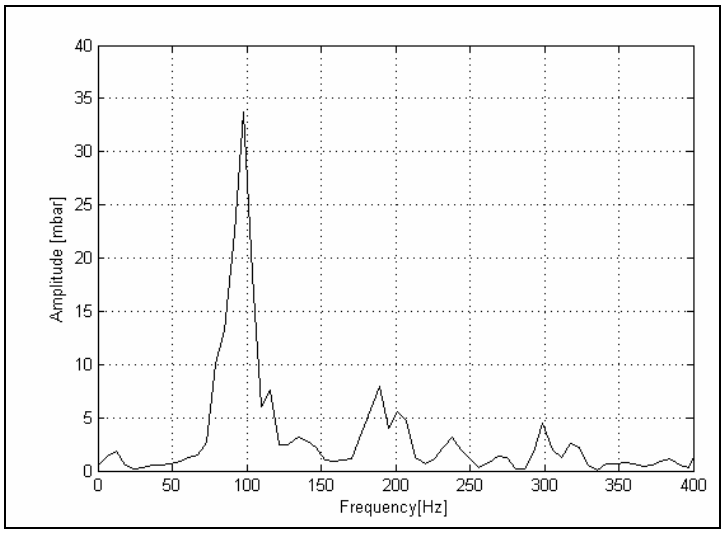

Fig. 78 – Amplitudes and frequencies. 1:5 scale – Single phase case

From this first comparison, for what concerns frequencies, a strong correlation with the adopted scale factor can be found. The frequency variations are indeed proportional to the scale factor. This behaviour depends on the length of the engine that has to be crossed by the pressure signal: this distance is shortened just by the scale factor, the travel time it takes for the signal cross the chamber is reduced and the frequency, hence, increased.

For what concerns the amplitudes, results show that their values are constant for the first two scales (1:1 and 1:2.5), whereas in the 1:5 scale it can be observed a quite dramatic reduction. This behaviour raised the idea about the existence of a scale phenomenon.

In order to test whether this effect was real or not, the presence of particulate was added later in the setup of numerical simulations.

Since the amount of mass of particulates in the propellant is considerable (about 20% of the total weight of propellant) it has been assumed that this additional element, present during engine operation, could modify the calculation of the dynamic fluid, hitherto considered as a single phase, hence the fluid dynamics of the flow inside the combustion chamber. The first result obtained and shown regards the comparison between the PWO's on the full scale (1:1) configuration considered with and without the adoption of the particulates.

1:1 Scale	Data analysis using FFT		Integral energy analysis
	Frequency (Hz)	Amplitude (mbar)	Amplitude (mbar)
With part.	20.7 ± 1.2	148.7 ± 6	153.8
Without part.	17.1 ± 1.2	75.7 ± 27	99.5

Tab. 11 – Comparisons: effects of particulate adoption in 1:1 scale

From Tab. 11 it can be noticed that the introduction of the single particle produces a strong decreasing of amplitudes. This damping effect is thought to be due to the energy that the fluid dynamic field uses to transport inert particles along the motor (i.e. transforming momentum of the fluid to momentum of particles), rather than using to amplify the sound field oscillation.

In addition, the frequencies suffer a slight decrease. Again, the reason lies in the slowdown suffered by the vortexes, which transport energy towards the head of the nozzle (see Fig. 8 in chap.4.1). Such slowdown is caused by the transfer of kinetic energy from the fluid dynamic field in favour of the motion of particles. In this manner a vortex, proceeding slowly, hits the head of the nozzle releasing energy to the acoustic field at slightly lower frequencies.

The results obtained on all three scales taken into account by introducing in the calculation also the presence of particulates are shown below.

As before, in the summary table are reported only the behaviour of the first frequencies, while the plot shows also the evolution of the amplitudes associated with the higher frequencies.

Scale	Data analysis using FFT		Integral energy analysis
	Frequency (Hz)	Amplitude (mbar)	Amplitude (mbar)
1:1	17.1 ± 1.2	75.7 ± 27	99.5
1:2.5	42.7 ± 3.1	70.0 ± 30	95.1
1:5	85.5±6.1	67.2 ± 20	93.8

Tab. 12 – Comparisons: effect of geometrical scale. Bi-phase case

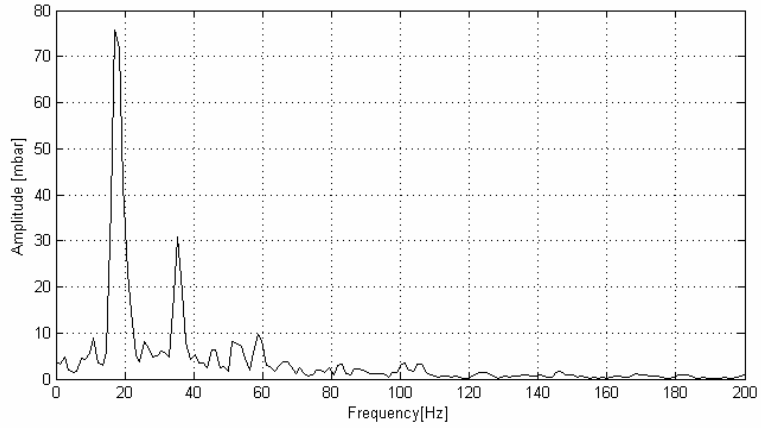

Fig. 79 – Amplitudes and frequencies. 1:1 scale – bi-phase case

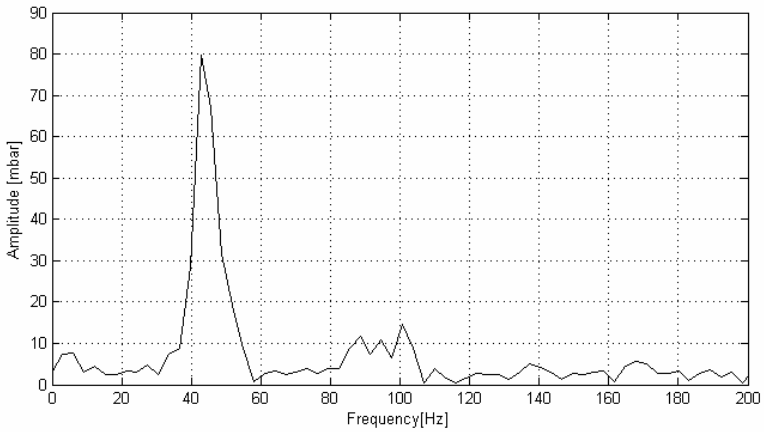

Fig. 80 – Amplitudes and frequencies. 1:2.5 scale – bi-phase case

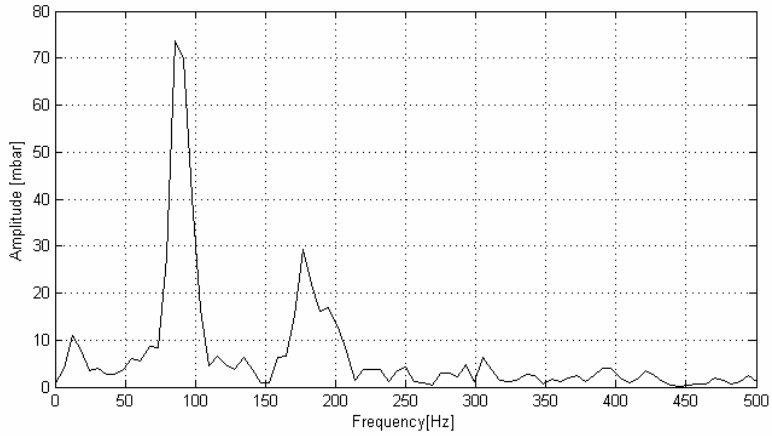

Fig. 81 – Amplitudes and frequencies – 1:5 scale – bi-phase case

Regarding the frequencies of oscillation, in these cases a good correlation with the scale factors has been found.

Amplitudes of oscillation show, instead, a rather more interesting behaviour. Indeed, despite the effect of damping due to the presence of particles which reduces the intensities of the ODP in cases 1:1 and 1:2.5, the amplitudes for present case employing particulate are approximately constant for all scale factors taken into consideration, including the factor 1:5 (for which the amplitude in the case without particles have shown a dramatic decreasing).

This means that presence of inert discrete phase during scaled engine operation, or generally inside a small dimension motor, play a fundamental role at the aim of PWO evaluation. Results suggest that for particular motor sizes, in order to avoid the scale phenomenon observed in chap.9.3.1, particle injection is needful.

In the following two plots, vorticity fields for the scale 1:1 in absence and in presence of particulates have been represented and compared. From this comparison it can be seen how the vortex structures in the presence of particulates are fragmented.

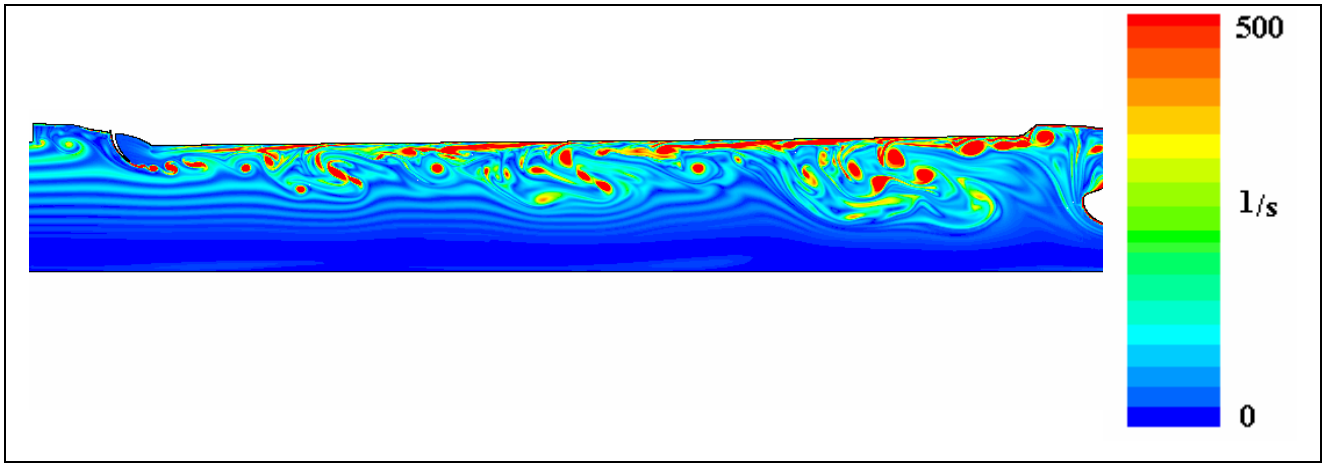

Fig. 82 – Vorticity field in 1:1 scale motor without particles

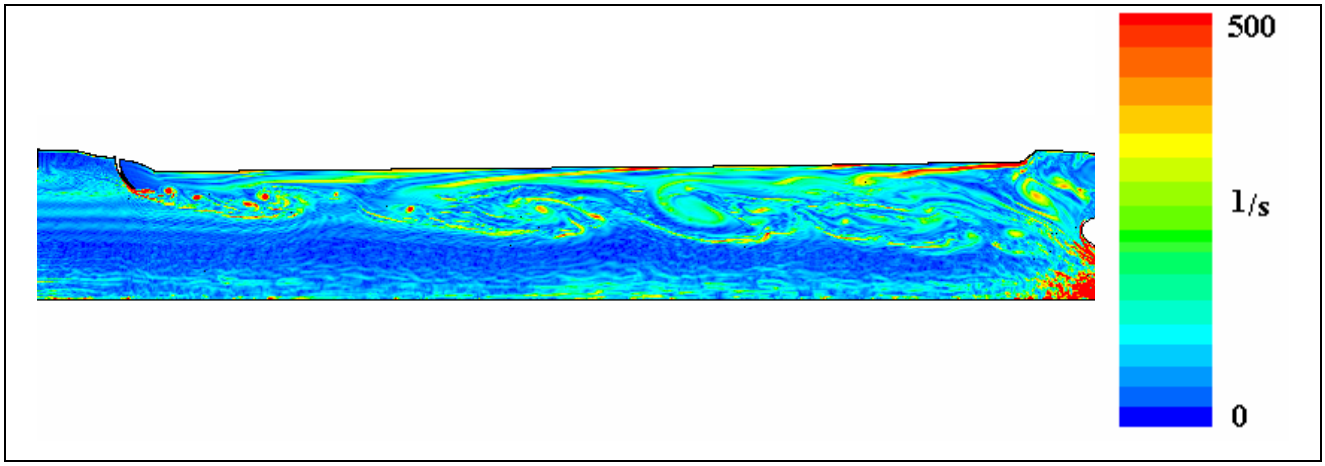

Fig. 83 – Vorticity field in 1:1 scale motor with particles

Similarly for the other two scales, the fields of vorticity obtained with the setup with discrete phase show again a very strong fragmentation of the structures which contain energy to be released to the acoustic field.

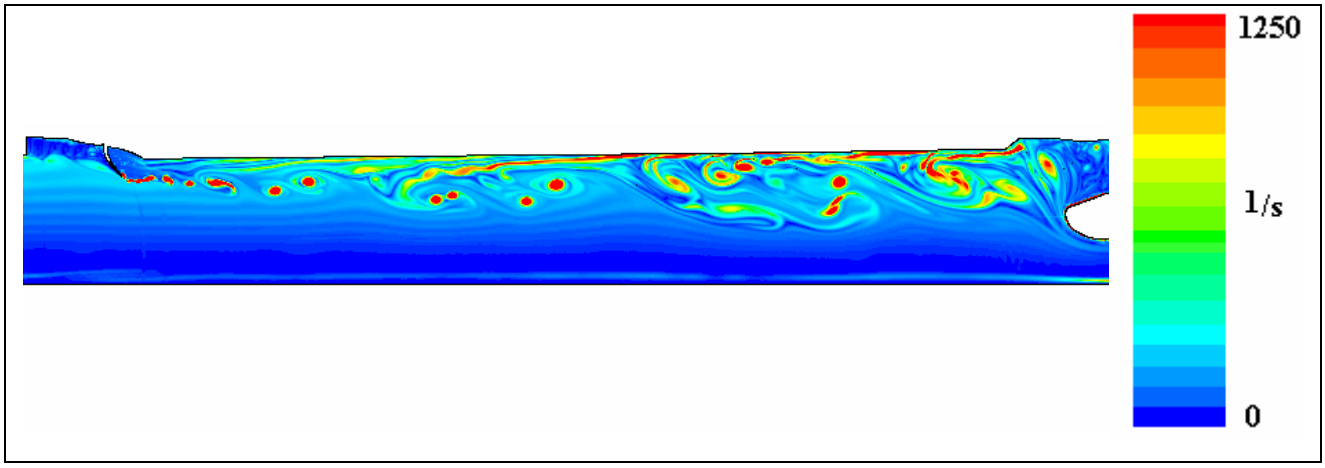

Fig. 84 – Vorticity field in 1:2.5 scale motor without particles

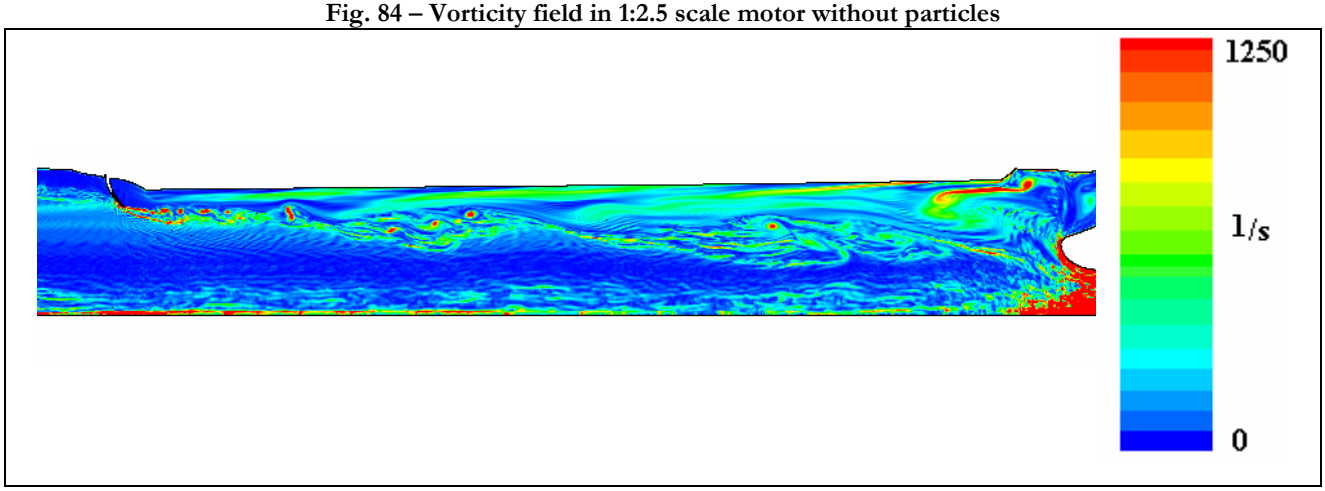

Fig. 85 – Vorticity field in 1:2.5 scale motor with particles

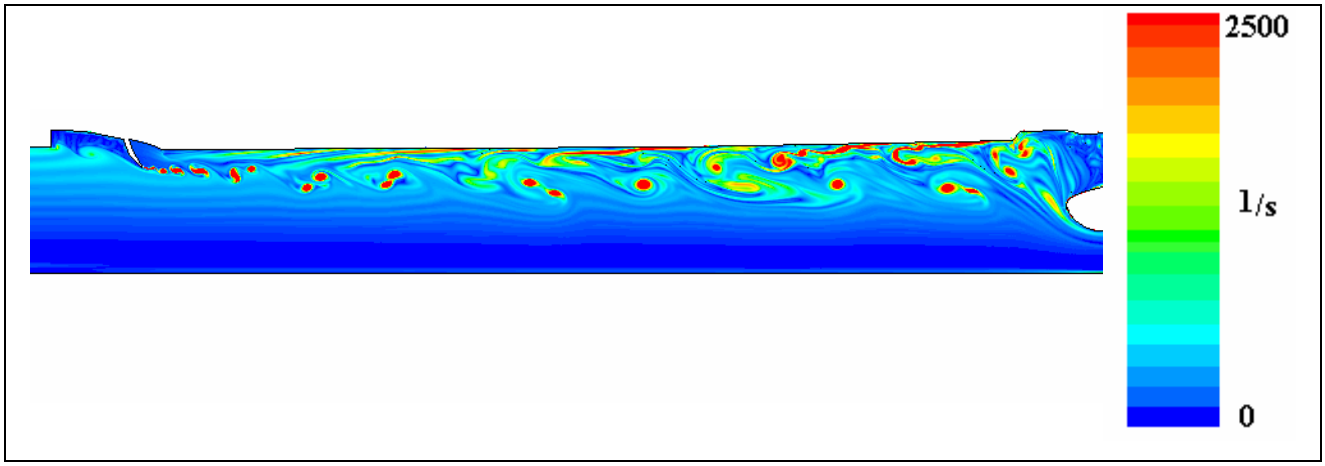

Fig. 86 – Vorticity field in 1:5 scale motor without particles

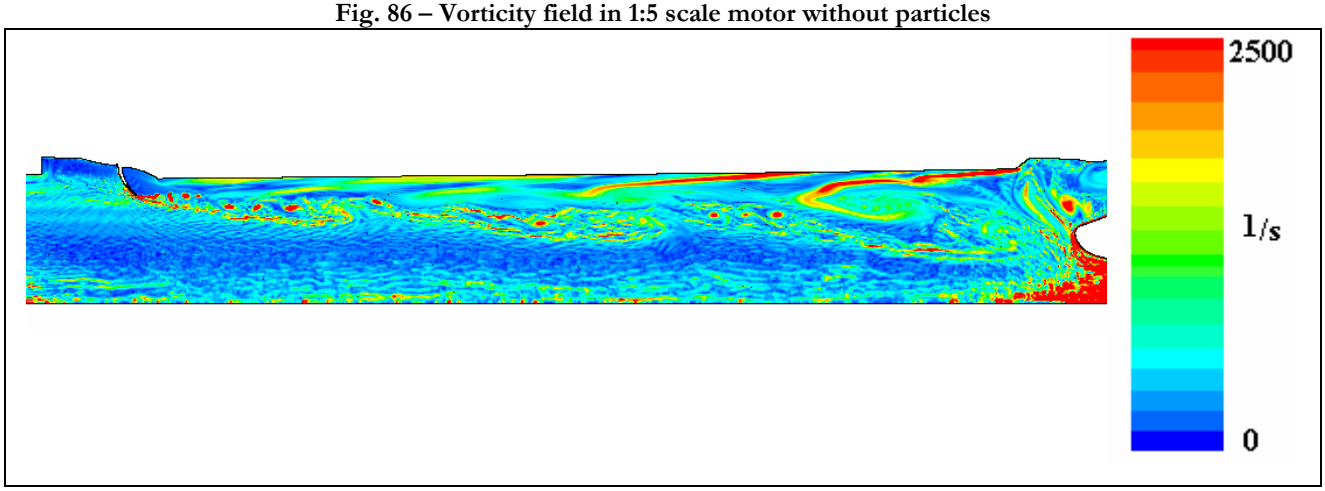

Fig. 87 – Vorticity field in 1:1 scale motor with particles

Since the fluid dynamics observed in the 1:5 scale shows homothetic transformation, the phenomenon observed related to the peak variation is most likely due either by the process of energy transfer that occurs between the vortices and the acoustic field, or by effect due to the presence of gradient which in the 1:5 case are more intense than in larger scales.

Even if the setup for which the particulate has been adopted resulted in the elimination of the scale effect problem, the PWO levels are not yet representative of the real phenomenon because of the already described effect of damping introduced by particulates presence.

For this reason the present work should be extended by studying the effects brought by the combustion of particulates. A first theoretical approach to the problem of combustion of particulate (distributed combustion) has already been developed in this work and reported in the Annex. Numerical simulation using these models are however still not ready. Since for this next step, external subroutines to implement in the commercial code have been developed, a rising of computational effort, already very high, is expected.

10 CONCLUSIONS

The main objective of the present work has been the investigation of pressure waves oscillation (PWO) when two fundamental characteristic parameters of the motor vary:

1. The combustion chamber characteristic dimensions;
2. The multiphase nature of the flow passing through the chamber (due to the presence of solid/liquid particulate, which is considered as inert within this research).

The results show that both the geometric scaling and the presence of multiphase flows play a fundamental role in the PWO evaluation.

For the description of the acoustic PWO phenomenon the analyst and the designer should typically take into account the frequency and the pressure signal amplitude parameters, evaluated and measured in an experimental manner first and then numerically at a significant section of the flow field inside the combustion chamber.

When experimental data miss, or however when such information is limited, normally one takes advantage of numerical estimates of the frequency and amplitude parameters numerically obtained through the adoption of validated codes, considered for the several scales of interest.

According to the analysis of the results it is possible to notice that the frequency peak acoustic parameter generated in the combustion chamber is strongly related to the scale of the considered solid rocket motor (SRM). This can be stated both for simplified and comparative simulations, for which the particulate is not considered present in the flow, and also for more complex simulations for which inert particulate is introduced.

On the other hand, considering the parameters describing the acoustic phenomenon intensity, thus the **amplitude of the pressure signal peak**, it has been observed that in the first simulated single-phase cases (i.e.: **without inert particulate**) the levels of the first PWO peak did not show significant variations as a function of the characteristic geometric dimensions, up to a critical scale factor, in such case ranging between 1:2.5 and 1:5. Under this range the values of the acoustic scale signal achieved were damped with respect to the ones discovered for the real booster considered (**P230 in real scale 1:1**). This led to think of the existence of a critical scale factor, under which the intensity of the acoustic PWO phenomenon tend to decay.

On the other hand, the subsequent simulations performed for the several scales (1:1, 1:2.5 and 1:5) **introducing the inert particulate within the numerical modelling**, show that for engine dimensions higher than the critical ones, the levels of the first PWO amplitude peak, receive a uniform damping, therefore holding maximum levels which are lower than the ones obtained without introducing particulate in the flow.
This can be caused by a particulate energy absorption phenomenon, which should be kept active at the expenses of the surrounding flow. Instead, for scales below the critical ones, the amplitude corresponding to the first peak frequency are reactivated, allowing to obtain also for the 1:5 scale PWO levels in line with higher scales.
Hence, this indicates that the presence of particulate contributes to eliminate or shift the scaling criticality encountered for simulations without particulate.

However the reasons of such physical behaviour are not completely clear yet; therefore within this work it is indicated that the direction to follow in order to better understand the phenomenon passes through the study of the particulate influence on the energy transfer processes between the fluid dynamic field and the acoustic one.

ANNEX

Within the present Annex several explicative analytical and numerical steps and methods of calculation required in support of the actual research are reported in order to describe the modelling of several physical phenomena under consideration.
Furthermore, the first chapter reports on a preliminary study related to the combustion and shape evolution of the particulate.

I DISCRETE PHASE MODELLING – SHAPE EVOLUTION

According to the physics described in chapter 4, and the related phenomena observed, the reader comprehends that a full and complete analysis would require to also consider the particulate during its combustion, its related evolution, while taking into account that it represents even an energy source [45].
The particle combustion represents a very complex topic. It involves several chemical and physical phenomena which are tightly coupled [65].
Indeed, after the break-up of the liquid alumina film, which is generated on the grain surface that generates a droplets distribution (phenomenon called *primary break-up*), and the successive break-up of the drops due to the motion of the fluid in which they are immersed (phenomenon called *secondary break-up*), the remaining particles suffer a further transformation, which is operated by the combustion.
The Al particles, being in a fluid for which the temperature is higher than the Al boiling temperature (T_{boil}-Al=2790K [10]), start to vaporise (Fig. 88). The gaseous Al, expelled from the particle, immediately meets the oxidiser in gaseous phase present close to the particle, reacts and releases heat towards the surrounding environment. The chemical reaction occurring between Al and oxidiser generates a new product (Al_2O_3 or alumina – T_{fus}=2328K [11]), which deposits on the particle surface producing a liquid layer [12].

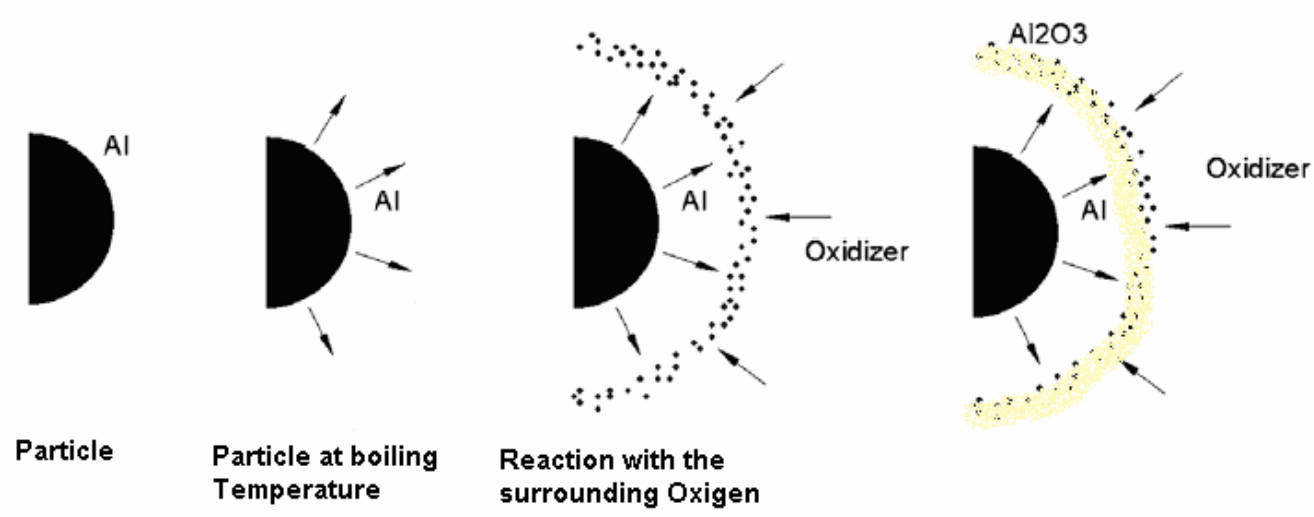

Fig. 88 – Alumina production

Due to the relative velocities between the fluid and the particle, such alumina layer is removed and transported towards the back side of the particle. The accumulation of alumina in this zone generates a new spherical shape as shown in Fig. 89 [13], [14], [15].

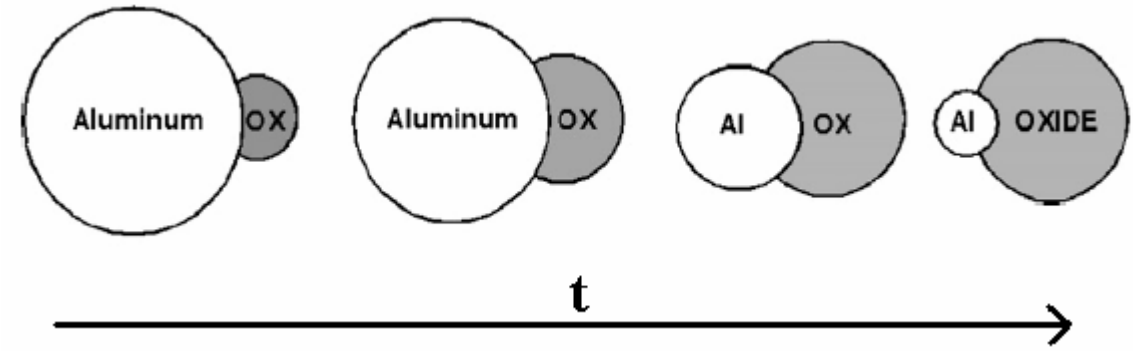

Fig. 89 – Particle shape evolution phenomenon

The mentioned transformation occurs during the travel of the Al/alumina particle along the combustion chamber and increasing the distance from the surface from which it has been detached (Fig. 9).

Since an exact reproduction of the wide range of the occurring phenomena cannot be simulated due to the high computational cost, in this preliminary study only the main effects of the distributed combustion have been introduced.
Considering the several phenomena occurring during combustion, the ones introduced in this work are representative only for:

1. the thermal exchange between particle and surrounding fluid;

2. the mass exchange between particle and surrounding environment;
3. the particle diameter variation.

Even though the previous listed arguments are tightly linked to each other, in this work they are separately treated.

I.I THERMAL EXCHANGE

During Al combustion inside the SRM a large number of chemical reactions occurs simultaneously involving many elements.
The oxygen, hydrogen, carbon, fluorine, chlorine, only to list the elements present in larger quantities, react with Al producing several intermediate compounds. Such compounds participate to a various number of reactions either transferring or absorbing energy until the combustion process is concluded. The end of the combustion process is reached when either the entire amount of Al contained in the particle has been transformed in Al_2O_3 [31], otherwise when the residual mass is so negligible that it is impossible to meet the oxidiser and react.
In the present work the combustion is not a goal whereas the combustion effects need to be introduced. For this reason a simplification has been introduced assuming that the particle combustion is ruled by a single reaction, which is representative of the entire process:

$$2Al + 3/2\ O_2 \rightarrow Al_2O_3\ (\Delta H_C = -387.325\ Kcal/mol = -1619\ KJ/mol) \qquad \textbf{eq. 22}$$

where ΔH_C indicates the heat released during the reaction [31].
This balance reaction contains two important data about the models to introduce:

- the heat release rate;
- the mass transfer rate.

In other words, this balance reaction contains information regarding the fact that the release of each 1619 [KJ] to the surrounding environment, occurs in parallel to the the transformation of 2 Al moles in an oxide mole.
The direct consequence is that, during the reaction process, the continuous mass transformation (Al consumption and proportional oxide production Fig. 89) occurs along with a proportional energy release.

This means that the mass transfer and the heat transfer phenomena are tightly linked. Hence, the knowledge of the amount of mass instantly released from the particle is necessary to estimate the amount of energy (heat) instantly transferred from the particle to the surrounding gas [36]

$$\dot{q} = \dot{m} \cdot \Delta H_C \qquad \textbf{eq. 23}$$

At this stage of the study, due to the large importance of the role played by the heat transfer inside this process, it is necessary to fix some details about the effective energy levels reached during combustion. It has to be undertaken that the H_c value, represents a net energy contribution provided from the particle to the surrounding gas. For a correct evaluation of the thermal phenomena regarding the particle combustion it should be considered that not the entire amount of heat produced during the combustion is transferred to the fluid. Indeed, a fraction of the energy needs to be used in order to increase the Al temperature towards the temperature of the surrounding gas.

It should be noticed that the reaction provides the rate of heat released for the Al considered in gaseous phase, hence there are not any other contributions to be removed from the balance (such as for example the vaporisation heat).

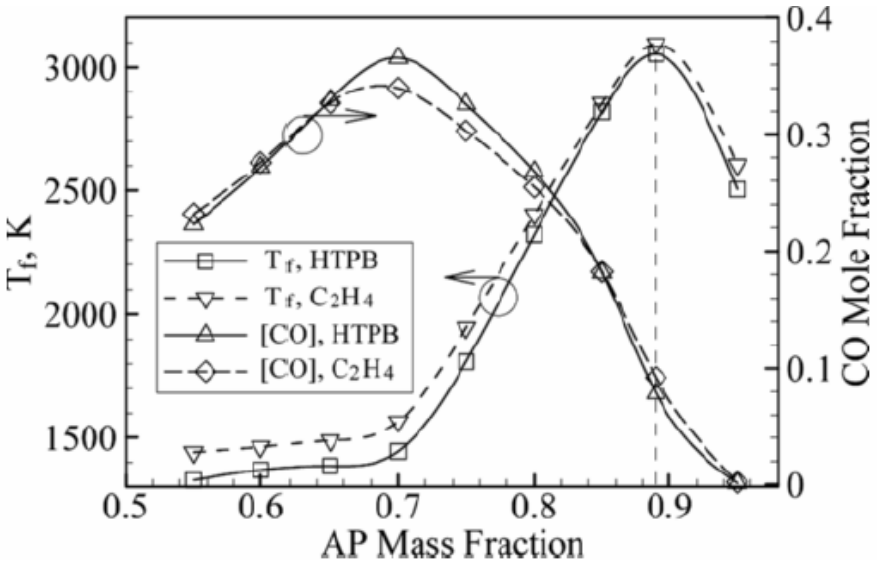

Fig. 90 – Temperature contribution inside the engine due to the AP fraction

Moreover it should be considered that the amount of mass that receives heat from the Al combustion (i.e. the gaseous phase) is not 100% of the mass introduced from the propellant during combustion, because this value takes into account also the mass of Al itself, which is 18% of total mass that must be, hence, subtracted.

The equation describing such energy transfer process is:

$$\dot{m}_p \left(\Delta H - c_{p\_vap\_Al} \cdot \Delta T_{Al\_vap} \right) = 0.82 \cdot \dot{m}_f c_{pf} \Delta T \qquad \textbf{eq. 24}$$

where $\dot{m}_p$ is the particle towards the gaseous phase mass flow rate, ΔH is the particle combustion enthalpy, $c_{p\_vap\_Al}$ is the Al specific heat in gaseous phase and ΔT_{Al_vap} is the increase of temperature suffered by the gaseous Al in order to elevate its temperature from the boiling till the equilibrium temperature present in the chamber during combustion.

The balance can be rewritten in terms of particle mass, which, at regime, enters and leaves the engine. The two quantities are different since during combustion a remarkable part of the particle mass is transformed in gaseous mass. Indicating with

$$\Delta H_{tot} = \Delta H - c_{p\_vap\_Al} \cdot \Delta T_{Al\_vap} \qquad \textbf{eq. 25}$$

The balance can be rewritten as:

$$0.82 \cdot \dot{m}_f c_{pf} \Delta T = \left(\dot{m}_{p\_IN} - \dot{m}_{p\_OUT}\right)\Delta H_{tot} = \left(1 - \frac{\dot{m}_{p\_OUT}}{\dot{m}_{p\_IN}}\right)\dot{m}_{p\_IN}\Delta H_{tot} \qquad \textbf{eq. 26}$$

Which, in terms of diameter is:

$$0.82 \cdot \dot{m}_f c_{pf} \Delta T = \left(1 - \frac{\rho_p \frac{4}{3}\pi\left(\frac{\phi_{fin}}{2}\right)^3}{\rho_p \frac{4}{3}\pi\left(\frac{\phi_{in}}{2}\right)^3}\right)\dot{m}_{p\_IN}\Delta H_{tot} = \left(1 - \frac{\phi_{fin}^3}{\phi_{in}^3}\right)\dot{m}_{p\_IN}\Delta H_{tot} \qquad \textbf{eq. 27}$$

Recalling again that the incoming particle mass is 18% of the total amount of injected mass

$$\left(\frac{0.82}{0.18}\right)c_{pf}\Delta T = \left(1 - \frac{\phi_{fin}^3}{\phi_{in}^3}\right)\Delta H_{tot} \qquad \textbf{eq. 28}$$

Assuming that the combustion consumes the entire Al particle, hence the Al final diameter is null, from eq. 28, the heat balance would result,:

$$\left(\frac{0.82}{0.18}\right)c_{pf}\Delta T = \Delta H_{tot} \qquad \textbf{eq. 29}$$

or

$$\Delta T = \frac{\Delta H_{tot}}{\left(\frac{0.82}{0.18}\right)c_{pf}} \qquad \textbf{eq. 30}$$

I.I.I COMBUSTION CHAMBER TEMPERATURE ESTIMATE

In order to estimate the validity of the proposed model, one can suppose to apply this equation to the validation case conducted on P230 presented at par.6.2.2.

To evaluate the ΔT generated by the adoption of the particle, it is necessary to know the combustion chamber temperature during engine operation, that according to ballistic data provided by AVIO is evaluated to be about 3,230 [K], and the temperature obtainable deactivating the energy produced by the particle combustion (temperature obtained by only HTPB and AP combustion).

Before proceeding with the calculation, some considerations have to be presented: inside the SRM the HTPB even participating to the combustion does not release much energy. It behaves essentially as a matrix, a sort of glue that keeps the AP and Al grains bonded, whereas the actual heat production occurs by means the AP combustion.

In case an additional different fuel mass is added inside the propellant at the expense of the AP itself (in the present case Al), the percentage of AP decreases inducing a consequent reduction of the temperature obtainable by its combustion. Obviously, in order to obtain an advantage in terms of higher temperature levels reachable in the engine, the combustion of the added fuel has to provide an amount of energy which is higher than the one lost by AP removal.

In order to evaluate the adiabatic flame temperature produced by AP, the graph shown in Fig. 90 has been considered. It reports the adiabatic flame temperature (T_{ad}) as function of the percentage amount of AP present in the engine. Moreover, to evaluate the ΔH_{tot} value defined in eq. 25 the following Al characteristic data are required:

c_p of Al in gaseous phase: 769 J/Kg-K

ΔT_{Al_vap} is 3240-2790=450K.

By solving eq. 30, a ΔT equal to 1777 [K] has been obtained.

1400 [K]	+	1777 [K]	=	3177 [K]
Propellant adiabatic flame temperature without particle		temperature increase due to particle combustion		Average fluid temperature

The difference with the temperature actually present within the combustion chamber is about 57 [K], meaning an error of 1.7 [%].

I.II PARTICLE TO FLUID MASS EXCHANGE

The mass exchange is a fundamental process during combustion. Indeed, it is tightly connected with both thermal exchange and diameter evolution.

The amount of mass, $\dot{m}$, which can be instantly burned can be mathematically indicated by two main parameters:

1. the first parameter, which is indicated with $B_{0,q}$, is a function of some chemical and physical characteristics such as:
   - stoichiometry of the reaction;
   - heat released by each mole product;
   - particle and surrounding fluid temperature.

2. the second parameter, defined by the adimensional Nusselt number is linked to the flow dynamics in which the particle is immersed [42].

The knowledge of the motion field surrounding the particles is necessary in order to reproduce combustion and mass exchange. The fluid dynamic loads acting on the particle surface (represented by *Nu*) contribute indeed to remove the oxide layer continuously produced on the particle surface, which shields the particle from the surrounding oxidiser, slowing down the reaction. The oxide layer, in such a way, is accumulated towards an extremity of the particle (Fig. 91), while the remaining larger part of the particle surface can continue to efficiently react [33].

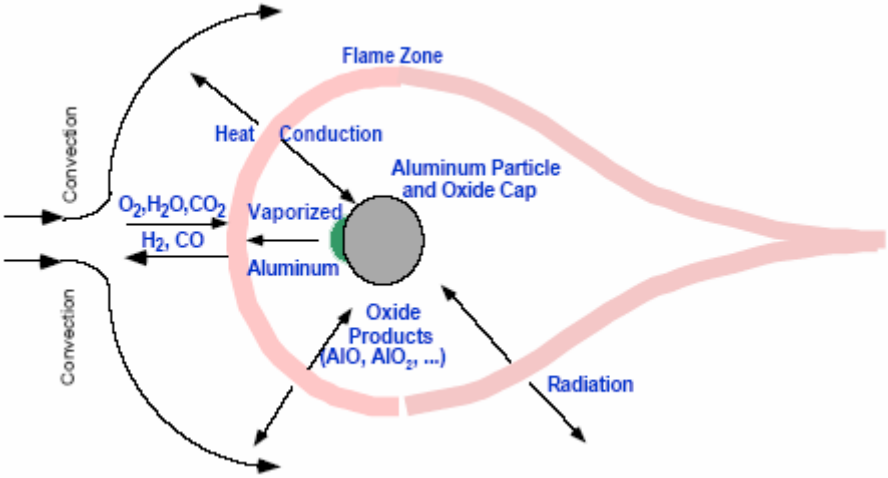

Fig. 91 – Chemical-physical phenomena occurring during combustion

However such accumulation is concentrated within a confined surface of the particle. The oxide covers this zone and inhibits contact between that particle surface and the surrounding fluid, which contains the oxidiser. Hence, due to this reduction of contact surface where the reactions occur, the combustion suffers a slowdown [34].

The last described phenomenon is very important because it leads to a strong dependence on the characteristic combustion time of the particle, as it can be observed in Fig. 92 [35].

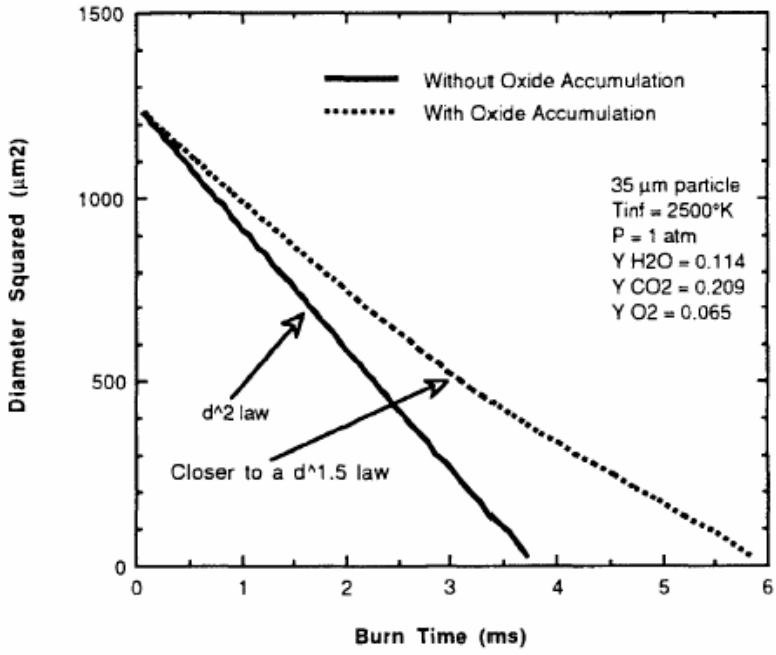

Fig. 92 – Effect of oxide accumulation on the combustion time

The modelling of mass evolution, hence, has been realised taking into account such effects. The law ruling the evaporation of a mass fraction from the particle is reported [36]:

$$\dot{m}_{P-F} = \frac{2\pi k_g Nu}{c_{pg}} r_p \cdot \ln\left[1 + B_{0,q}\right] \qquad \textbf{eq. 31}$$

where [36] [34]

$$B_{0,q} = \frac{\Delta h_{c\,prod} / \nu + c_{pg}\left(T_\infty - T_p\right)}{q_{i-l} + h_{fg}} \qquad \textbf{eq. 32}$$

is the term that takes into account the thermal properties and the intensity of reaction, while

$$Nu = 2 + \frac{0.555\,\mathrm{Re}^{1/2}\,\mathrm{Pr}^{1/3}}{\left[1 + 1.232/\left(\mathrm{Re}\,\mathrm{Pr}^{4/3}\right)\right]^{1/2}} \qquad \textbf{eq. 33}$$

is the Nusselt number [36] [34] [42] [46], which models the increase of reaction rate due to the removal of the alumina liquid layer from the surface of the particle.

The end of the combustion occurs only when either the Al has been totally consumed, or when the alumina accumulation has so deeply incorporated the remaining part of Al that the surface on which the reaction can still occur is negligible (Fig. 93).

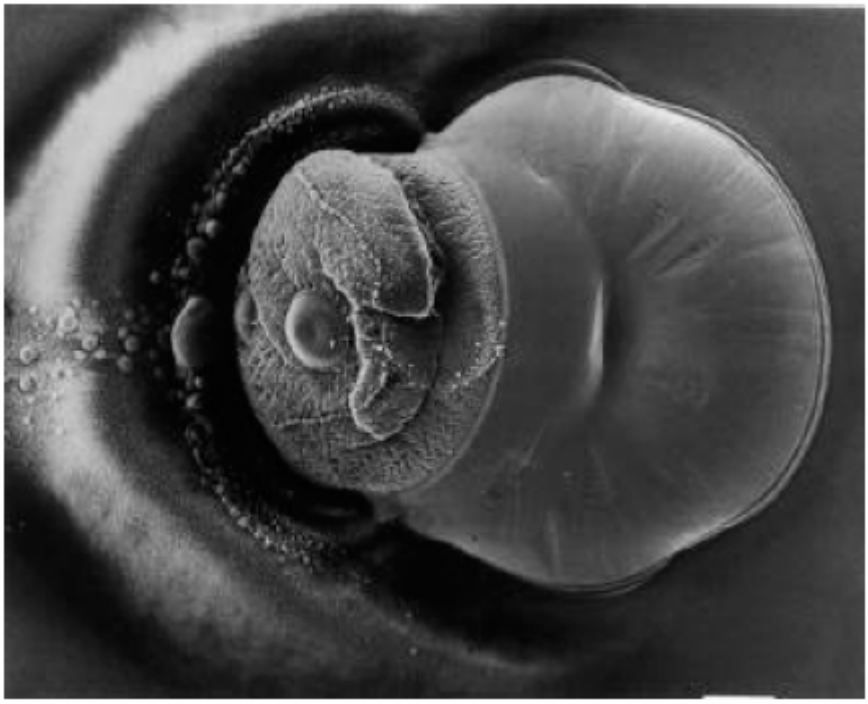

Fig. 93 – Example of Al particle partially incorporated in the oxide residual

I.III PARTICLE DIAMETER EVOLUTION

Isolating a generic instant during the early droplet combustion stages, has shown how such droplet is actually composed of the union of two drops: the first composed of Al and the second of alumina as shown in Fig. 89. The time evolution of the two droplets, which exchange mass, is quite different. Indeed, the Al drop decreases its size while the oxide increases its diameter.

Each phenomenon (size increasing for one drop and size reduction for the other), taken separately, has been used to define a proper modelisation of the effects of combustion.
Considering that:

1. the evolution of the Al particle size determines the amount of $\dot{m}$, which is a parameter tightly linked to the heat transfer;
2. the dimension of oxide drops are not negligible, especially during the final phase of combustion and then during the next transit phase of the particle towards the engine outlet;

both effects have been taken into account.

For what concerns the Al particle, considering the information related to the amount of mass removed from the particle, it is simple to obtain the variation law of its diameter in time.
Indeed, starting from the assumption that the particle density, during Al combustion, is almost constant (ρ_p=2700 Kg/m^3 [13]), it is possible to obtain its diameter from its mass, in any i-th instant in time:

$$\phi^i = \left(\frac{6m^i}{\rho_p \pi} \right)^{\frac{1}{3}} \qquad \textbf{eq. 34}$$

where the particle mass in a generic i-th time instant is equal to:

$$m^i = m^{i-1} - \dot{m}\Delta t \text{ e } \Delta t = t^i - t^{i-1} \qquad \textbf{eq. 35}$$

Such procedure allows to obtain the Al particle size at different i-th time instants.

As already mentioned, although this procedure is representative of both the evolution of the Al drop and the heat released to the external environment, it is not representative of the evolution of the size of the entire system.

The implementation of this formula within the numerical code must be done by restricting its use to the heat transfer evaluation, for which $\dot{m}$ represents an essential element.

For what concerns the global evolution of the entire particle composed by Al and oxide, it should be noticed that it presents a maximum size at the combustion beginning, where its diameter is exactly the diameter of the Al particle before reaction. On the other side, at the end of the reaction, the particle presents a size that is very similar to the one of the oxide drop (see Fig. 94).

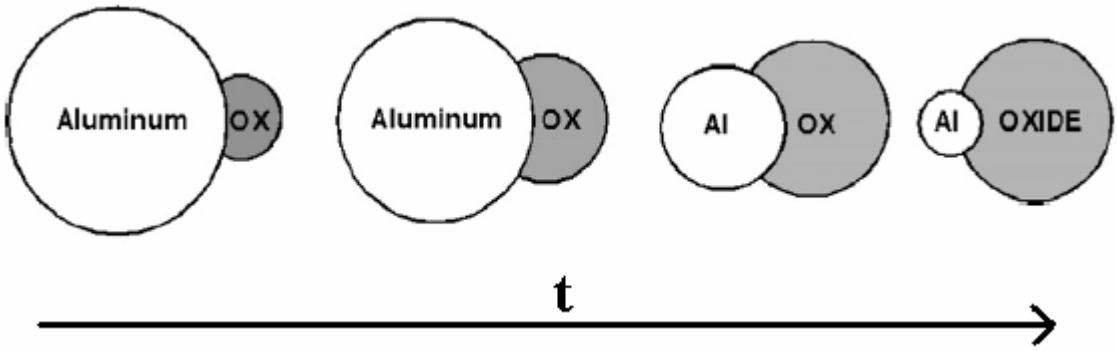

Fig. 94 – Particle shape evolution

In literature it is shown that the final dimension of the particles employed in solid rocket motors is typically equal to 70 [%] compared to the initial dimension of the Al particle [13].

In order to represent the diameter evolution of the particle during intermediate instants of time, some simplifying hypotheses have been introduced:

1. The system consisting of two bonded drops (Al and oxide) has been represented by a single particle;
2. The diameter of the particle evolves linearly in time starting from the initial dimension assumed by the Al drop, towards the final dimension adopted by the oxide drop, which is 70 [%] with respect the initial dimension.

The two hypotheses are validated by the next procedure:

Representing the combustion time in an adimensional abscissa [s], it is assumed that the volume of the drops evolves linearly, as shown in Fig. 95.

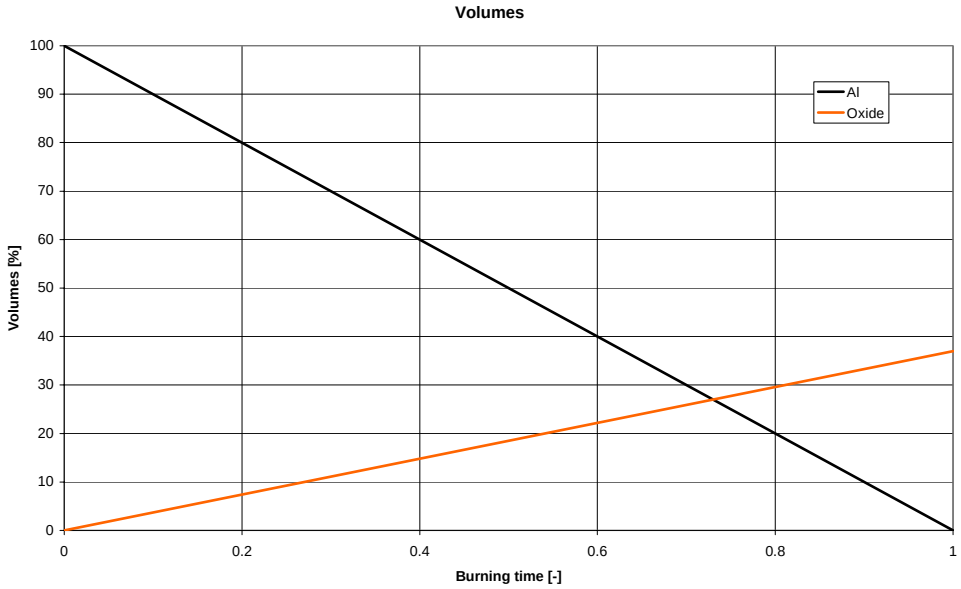

Fig. 95 – Al and alumina volume evolution

An important instant at which it is significant to evaluate the diameter of the droplets composing the particle is when the two drops show the same volume (and thus the same diameter).

In order to evaluate this instant of time, hypotheses of linear evolution have been adopted for the two drops.

$$V_{Al} = V_{Al_{in}} - \left(V_{Al_{in}} - V_{Al_{fin}}\right) \cdot s \qquad \textbf{eq. 36}$$

$$V_{Ox} = V_{Ox_{fin}} \cdot s = 0.7^3 \cdot V_{Al_{in}} \cdot s \qquad \textbf{eq. 37}$$

The two equations have been compared

$$0.7^3 \cdot V_{Al_{in}} \cdot s = V_{Al_{in}} - V_{Al_{in}} \cdot s \qquad \textbf{eq. 38}$$

and the value of *s*, for which the drops show the same diameter, has been obtained

$$s = \frac{V_{Al_{in}}}{1.343 \cdot V_{Al_{in}}} = 0.744 \qquad \textbf{eq. 39}$$

This value indicated that the two drops show the same dimension after about the 74 [%] of the total combustion time.

The volume of each single drop, at this instant is:

$$V = 0.343 \cdot V_{Al_{in}} \cdot 0.744 = 0.255 \cdot V_{Al_{in}} \qquad \textbf{eq. 40}$$

However, in this instant of time it should be recalled that two drops are present, each one characterised by its own mass. Considering the hypothesis to describe the particle evolution using only the larger

diameter presented by one of the two drops, would lead to an error. Indeed, in this manner the total mass, hence the inertia of the system composed of two particles would be underestimated.

A more correct representation should consider not only the diameter of the Al particle, but an equivalent diameter which takes into account the presence of the second drop.

Hence, considering as initial and final diameters the ones already mentioned, in order to follow the evolution of the particle, a third equivalent diameter has been computed next to the instant of time where the drops show the same diameter.

In this manner the diameter of the single drop has been evaluated

$$r^3 = 0.343 \cdot 0.744 \cdot r_{Al_{in}}^3 \qquad \textbf{eq. 41}$$

or

$$r = r_{Al_{in}} \sqrt[3]{0.343 \cdot 0.744} = r_{Al_{in}} \cdot 0.63 \qquad \textbf{eq. 42}$$

then, considering that the equivalent volume occupied by the two drops is double with respect to the one occupied by a single drop, the following equivalent dimension has been obtained:

$$r_{eq} = \sqrt[3]{2} \cdot 0.63 \cdot r_{Al_{in}} = 0.79 \cdot r_{Al_{in}} \qquad \textbf{eq. 43}$$

In the graph represented in Fig. 96 it is possible to estimate how the linear representation (red line) is similar to the one computed under such assumption (green line) showing a maximum error of about 2%.

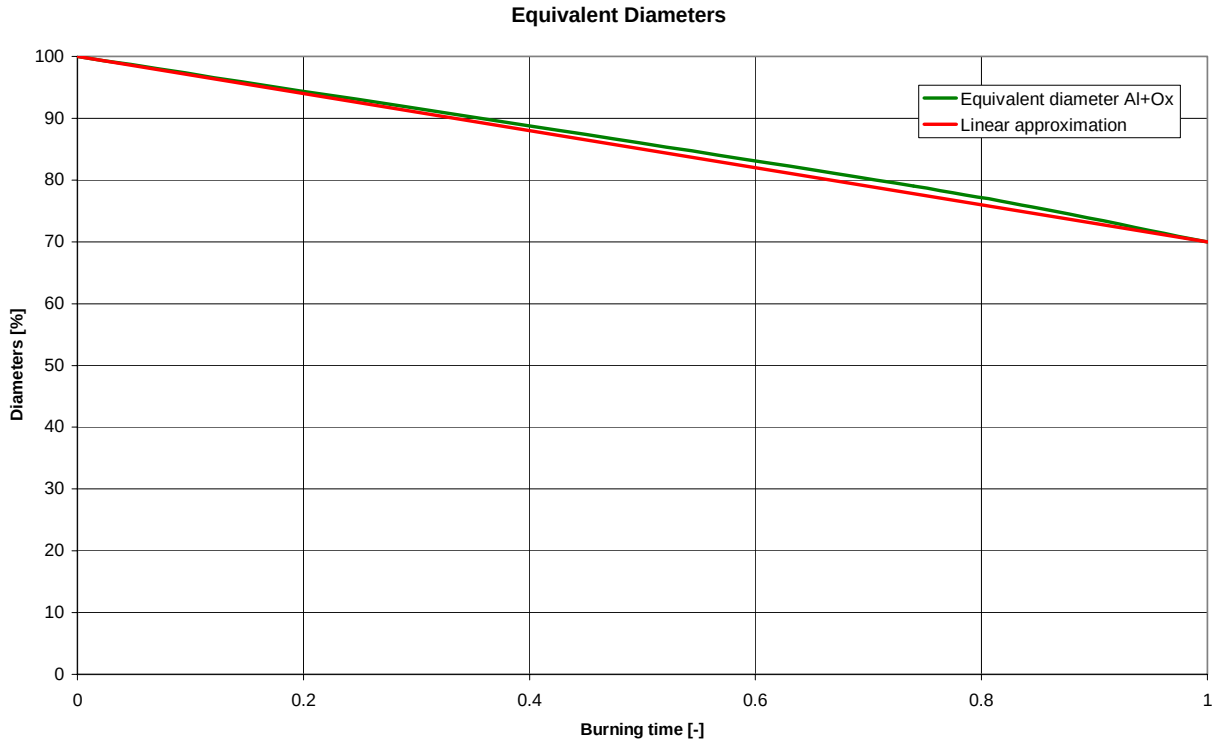

Fig. 96 – Diameter evolution of Al, oxide and equivalent particle

In the following graph it has been also reported the volume variation of the 2 single drops and the equivalent drop.

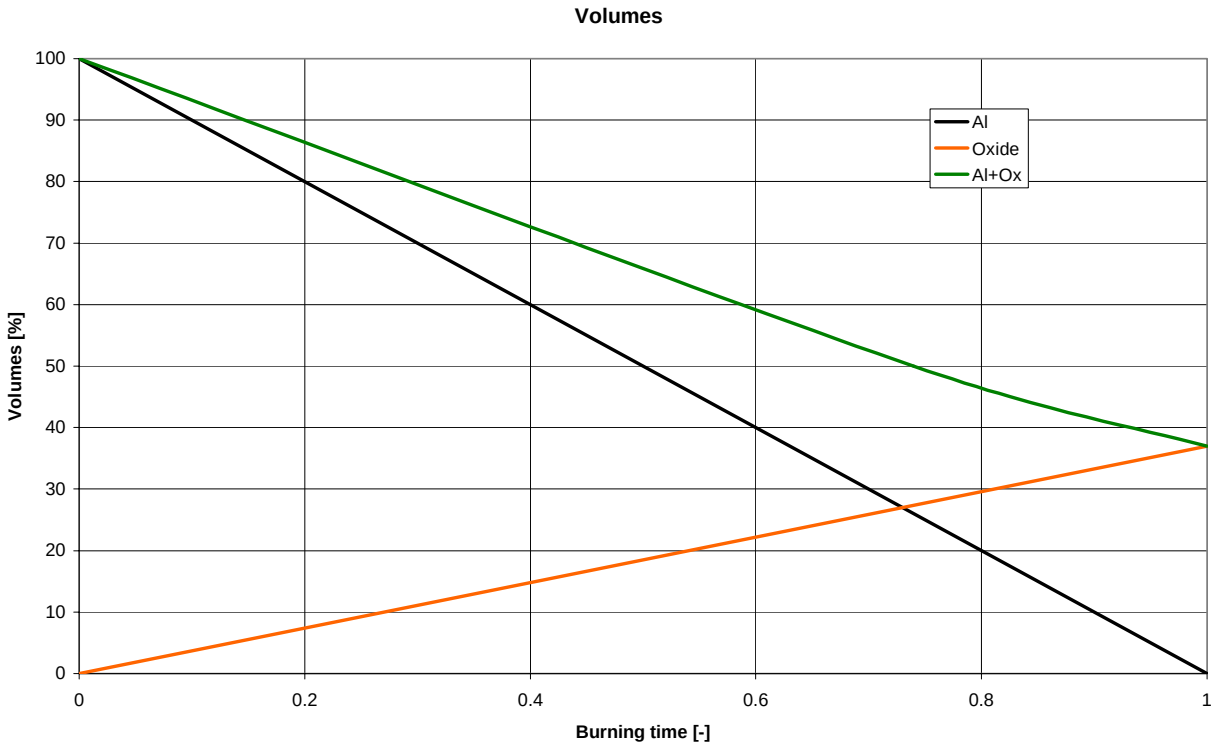

Fig. 97 – Volume evolution of Al, oxide and equivalent particle

I.IV CHARACTERISTIC TIMES

It has been shown that the particle combustion is a phenomenon which occurs along with the Al transformation in alumina. The dimension of Al particle then varies and decreases during combustion while simultaneously oxidation products accumulate, producing a second drop which increases its size during combustion (Fig. 89).

Adopting such simplification, in the previous chapter several laws have been introduced describing the fluid-dynamics and thermal effects on:

- combustion rate;
- particle mass evolution;

mainly modelling $B_{0,q}$ and Nu.

The effects, modelled in this work considering such numbers, would be otherwise extremely expensive in case a numerical approach would be followed.

In this section it is shown that these groups called $B_{0,q}$ and Nu, if introduced into engineering formulas widely used in literature to evaluate the characteristic times of combustion, allow to obtain reliable results.

I.IV.I CHARACTERISTIC TIMES COMPARISON

To assess the reliability of the model introduced, characteristic times of combustion obtained through the described model have been compared with those reported in the literature, which represent a wide casuistry.

To do this it was necessary to introduce the modelled terms ($B_{0,q}$ and Nu) within a law that represents the best fit of the experimental characteristic combustion times as a function of diameter variation obtained in a given period of time.

Such law is known as the D^2 law [36]

$$\phi^2(t) = \phi_0^2 - Kt \qquad \textbf{eq. 44}$$

Actually, the square law does not always correctly reproduce the evolution of the diameters because it fails to take into account the accumulation of oxide on the back of the particle [13], [37], [14]. The D^n law needs to be modified choosing a more adequate value for n. In literature several results are presented. They have been obtained through a wide range of experimental setups. Analysing such data, one can notice that the values of n reproducing the best fit for a remarkable sample of results, is 1.8 [-], [14], [33], [38].

Defining more clearly the variable K, the law takes the form:

$$\tau = \frac{\phi_0^{1.8} - \phi_{fin}^{1.8}}{\left(\frac{4}{\rho_p}\right)\left(\frac{k_g}{c_{pg}}\right) \cdot Nu \cdot \ln\left(1 + B_{0,q}\right)} \qquad \textbf{eq. 45}$$

Substituting the values of $B_{0,q}$ and Nu obtained in the previous paragraphs, in accordance with the modelling developed in this work, and taking as a representative samples five diameters in the range of abscissa shown in Fig. 98, the characteristic times have been obtained and reported in Tab. 13.

ϕ [μm]	30	60	180	300	600
Time [m-s]	9	21	96	200	538

Tab. 13 – Characteristic Al combustion times

By overlaying this result (red in Figure 98) with those reported in the literature, it can be noticed that the times, estimated only by modelling the effects, show a good agreement with consolidated and commonly accepted results.

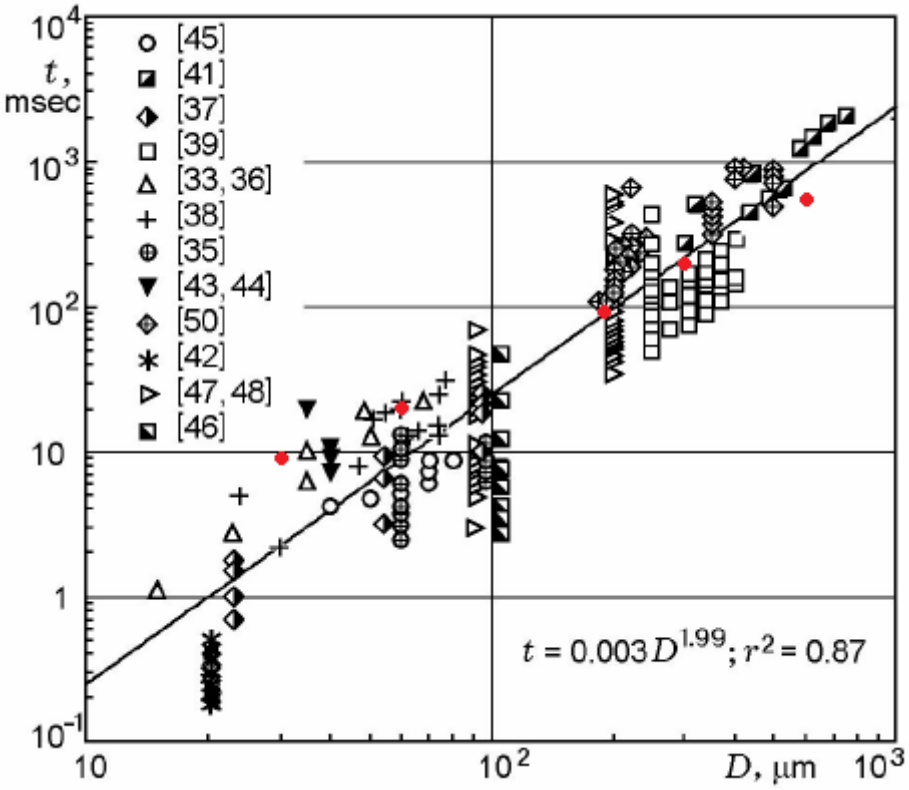

Fig. 98 – Characteristic Al combustion time from experimental tests

II AL→AL_2O_3 – CHEMICAL REACTION

The heat released by the combustion represented by the following reaction

$$2Al + 3/2\ O_2 \rightarrow Al_2O_3\ (\Delta H_C = -387.325\ Kcal/mol = -1619\ KJ/mol) \qquad \textbf{eq. 46}$$

is a function of the Al mass evaporated from the particle (i.e. $\dot{m}$).

As previously mentioned, during each instant of time, the heat globally released from the reaction is:

$$\dot{q} = \Delta H_C \cdot \dot{m} \qquad \textbf{eq. 47}$$

In the present work, since $\dot{m}$ is reported in [Kg/s] of aluminum, ΔH_C must be reported in an appropriate unit system, which is Kg instead of mole. In order to make such transformation it is necessary to calculate either the weight of a mole of product or reactant.

The weight of a mole of product (Al_2O_3) is equal to 102 [g], while the weight of an Al mole is equal to 27 [g].

From the reaction it can be noticed that for each mole of product, 2 Al moles are consumed (i.e. $2 \cdot 27$ [g]).

Hence in order to report the heat released from reaction in terms of reactant weight, it can be written:

$1619\ [KJ/mole_{prod}]/(2x0.027)[Kg_{Al}/mol_{prod}]=29981\ [KJ/Kg_{Al}]$.

While expressing the same amount in terms of product weight, it can be written as:

$1619\ [KJ/mole_{prod}]/(0.102)\ [Kg_{prod}/mol_{prod}]=15872\ [KJ/Kg_{prod}]$.

Each Kg of burned Al thus releases 29981 [KJ].

In literature [31] it is reported that typically the Al combustion occurring in SRM produce an energy release approximately equal to 7 [kcal/g], equivalent to 29.26 [KJ/g] = 29260 [kJ/Kg], which match with the value previously obtained.

III $B_{0,Q}$ AND NU EVALUATION

In order to obtain characteristic values for the mass transfer that occurs during combustion, the values to be introduced in the next law, also reported in Tab. 14, have been collected.

$$\dot{m}_{P-F} = \frac{2\pi k_g Nu}{c_{pg}} r_p \cdot \ln\left[1 + B_{0,q}\right] \qquad \textbf{eq. 48}$$

where

$$B_{0,q} = \frac{\Delta h_{c\,prod} / \nu + c_{pg}\left(T_\infty - T_p\right)}{q_{i-l} + h_{fg}} \qquad \textbf{eq. 49}$$

and

$$Nu = 2 + \frac{0.555\,\mathrm{Re}^{1/2}\,\mathrm{Pr}^{1/3}}{\left[1 + 1.232/\left(\mathrm{Re}\,\mathrm{Pr}^{4/3}\right)\right]^{1/2}} \qquad \textbf{eq. 50}$$

k_g	0.4267 [w/m-K];
c_{pg}	3660 [J/Kg-K]
μ_g	9.1e-5 [Kg/m-s];
$\mathrm{Pr} = {c_{pg}\mu_g}/{k_g}$	0.78 [-];
T_∞	3240 [K]
T_p	2750 [K]
$\nu = \frac{3/2 \cdot 32}{2 \cdot 27}$	0.89 [-]
$\Delta h_{c\,prod}$	15872 [KJ/Kg_{Al2O3}]
h_{fg}	10878 [KJ/Kg_{Al2O3}]

Tab. 14 – Parameters adopted for $B_{o,q}$ and *Nu* evaluation

For the ν evaluation, 32 and 27 indicate the molecular weight for O_2 and Al, while 3/2 and 2 are their stoichiometric coefficients.

h_{fg} = 293.7 [KJ/mol] is the energy needed to produce a single Al mole vaporisation. In terms of weight it can be written as: h_{fg} = 293.7 [KJ/mol] / 0.027 [Kg/mol] = 10878 [KJ/Kg].

q_{i-l} =0 is the heat necessary to transform Al from solid to liquid state. Actually such value is negligible (about 10 [KJ/mol]) if compared to the other heat transfer involved in the reaction.

The evaluation of the Reynolds number (*Re*) related to the particle dimensions is performed taking representative values for the fluid in which the particle is immersed.
In order to obtain such value, the definition of an order of magnitude for the particle diameter is needed.
These values are summarised in Tab. 15.

ρ	4 [Kg/m^3];
ΔU	40 [m/s]
D	120 [μm];
μ	9.1e-5 [Kg/(m s)];

Tab. 15 – Parameters used for the particle *Re* evaluation

In these conditions Re has been estimated to be about 200 [-].

Since the entire amount of data is now available, it is possible to evaluate the terms $B_{0,q}$ = 1.804 [-] and *Nu*=8.12 [-]

IV BALLISTICS FOR GRANULOMETRY VALIDATION

In order to conduct the validation of the method used to determine the most probable particle size inside the engine during its operation, it was necessary to trace the ballistics of the fluid in the combustion chamber. The baseline data, from which the mass flow rate introduced in the motor was derived, are presented by the following equation [23], which describes the regression rate of the grain as a function of the pressure inside the chamber during the test (Fig. 21)

$$r(cm/s) = 0.438 \cdot p^{0.37} \qquad \textbf{eq. 51}$$

where the pressure is referred in [MPa].
The availability of pressure behaviour in the time enables the integration of Eq. 51 in order to find the volume and then the mass instantly released by the propellant, for each generic instant of time during engine operation.

Since the propellant used in this validation is exactly the one employed onboard the Ariane 5, the composition and in particular the mass fraction taken up by Al are well known. This has allowed the differentiation of the amount of gas and particles released into the combustion chamber of the engine.

V UDF DEFINITION

As previously mentioned, the modelling of the most important phenomena occurring during aluminum combustion in the chamber is either not possible by the fluid dynamic code otherwise it is so computationally expensive to consider the numerical calculation not feasible. Among these phenomena, the most important for this study is the generation, during combustion, of a drop of alumina, which develops growing bonded behind the drop of Al (Fig. 89).
This phenomenon is not reproducible by the calculation code and therefore must be modelled.
Moreover, at the aim of avoiding the numerical code solution also for chemical reaction introducing further complications to the already complex two-phase flow, the heat release to the surrounding environment has been modelled.

The model should be implemented in a User Defined Function (UDF) written in C++ language as an externally readable subroutine. In this UDF the diameter variation laws of the particle and the heat release caused by the combustion must be included.

The problem is actually more complicated than expected because the particles, seen by the code as a single spherical entity, are indeed composed of the bounding of two spherical drops, which dimensions evolve over the time.
It becomes necessary, within the code, to differentiate the two particles that evolve over time.
At this aim, the Al particle is considered as if after a series of time steps it moves from the initial condition (the moment when the burning starts - diameter = 100 [%]) to the final condition (when the combustion ends and Al diameter is null).
The variation of mass occurring for the Al drop is expressed as:

$$\frac{4}{3}\frac{\pi}{8}\left(d_{In_{Al}}^3 - d_{Fin_{Al}}^3\right)\rho = \dot{m}\cdot dt\cdot N_{step} \qquad \textbf{eq. 52}$$

where the left term indicates the difference between the mass at the beginning and at the end of combustion, while the right side term expresses the change in mass that occurs after a certain number of time steps.
From this expression it is possible to derive the number of time steps needed to consume the particles of Al:

$$N_{step} = \frac{\rho\cdot\pi}{6\cdot\dot{m}\cdot dt}\left(d_{In_{Al}}^3 - d_{Fin_{Al}}^3\right) \qquad \textbf{eq. 53}$$

It is known that at the end of combustion (i.e. after N_{step} time steps) the particle presents a diameter that is equal to 70 [%] with respect the initial one.

Such behaviour can be expressed as:

$$d_{In} - N_{step} \cdot \Delta d_{step} = 0.7 \cdot d_{In} \qquad \textbf{eq. 54}$$

where Δd_{step} indicates the equivalent particle diameter variation occurring after each time step, and the equivalent d_{In} match with $d_{In_{Al}}$.

Substituting N_{step} in this equation, next law can be obtained:

$$\Delta d_{step} = \frac{0.3 \cdot d_{In} \cdot 6 \cdot \dot{m} \cdot dt}{\rho \cdot \pi \cdot \left(d_{In_{Al}}^3 - d_{Fin_{Al}}^3 \right)} \qquad \textbf{eq. 55}$$

In this manner a more explicit form could be written for the variation of the equivalent diameter (which is different from those of the Al particle) as a function of the mass ejected from the Al particle.

As represented in eq. 31, however, the $\dot{m}$ term depends on the particle size of Al. It is hence necessary to keep track of this dimension during the evolution of the entire particle otherwise it would be impossible to properly reproduce the process.

To do this, a correspondence has been defined between the equivalent particle diameter and the diameter of the Al drop.

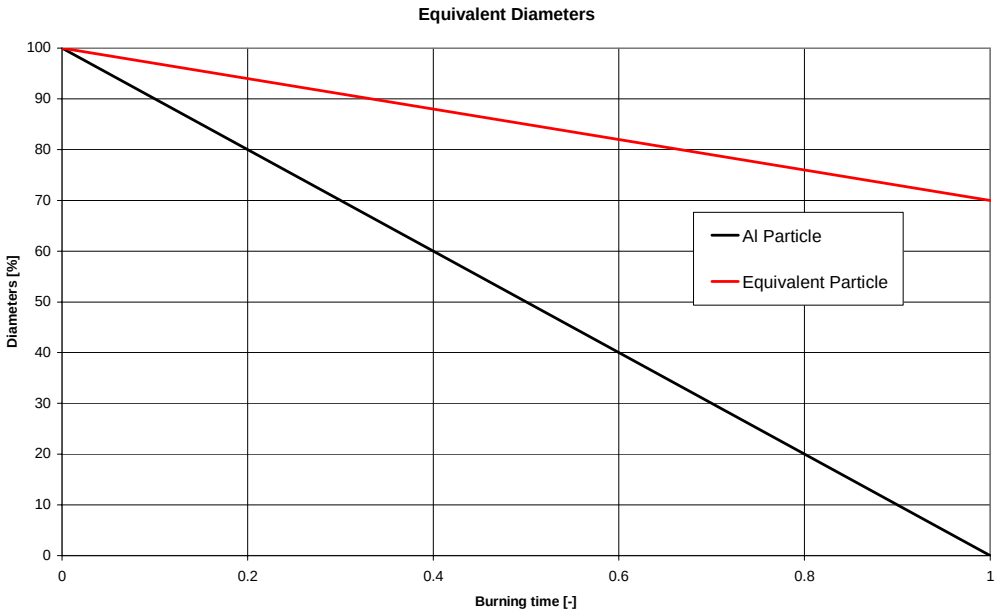

Fig. 99 – Evolution of Al and equivalent particle

Observing the trends of the particle sizes represented in Fig. 99 and representing both behaviours in the graph of Fig. 100,

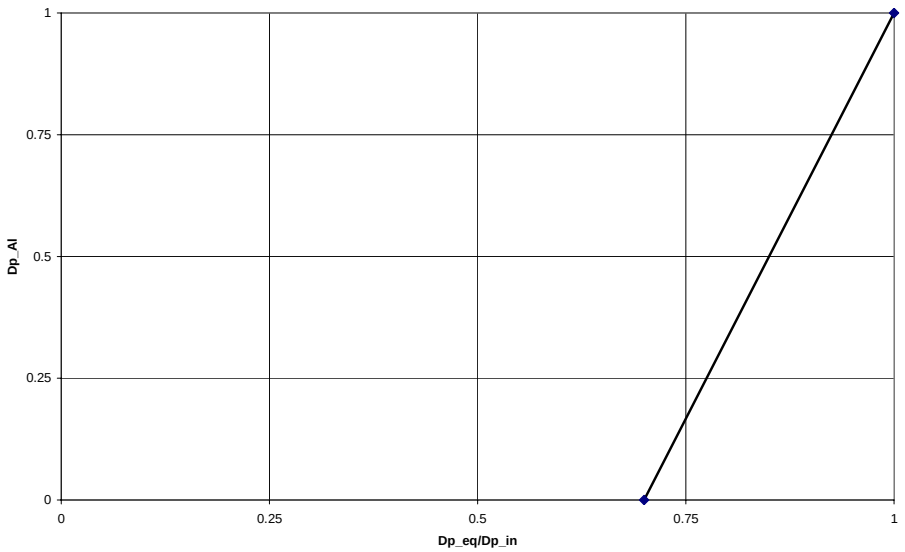

Fig. 100 – Graphic representation of eq. 56

it is possible to derive the following formula describing the particle size of Al depending on the size of the equivalent diameter:

$$d_{p\,Al} = \frac{d_{p\,In_{Al}}}{0.3}\left(\frac{d_{p\,eq}}{d_{p\,In_{Al}}} - 0.7\right) \qquad \textbf{eq. 56}$$

All the elements necessary to implement the UDF are now ready.

BIBLIOGRAPHY

[1] S. Scippa, P. Pascal, F. Zanier. Ariane5-MPS - Chamber Pressure Oscillations - Full Scale Firing Results Analysis and Further Studies. *AIAA* 94-3068

[2] N. Lupoglazoff, F. Vuillot. Comparison between firing tests and numerical simulation of vortex shedding in a 2-d test solid motor. *AIAA* 93-3066

[3] A. Kourta. Computation of vortex shedding in solid rocket motors using time.dependent turbulence model. Journal of Propulsion and Power. Vol. 15, No.3 (1999)

[4] Y. Fabignon et all. A Survey of French Research and Technology Program on the Internal Aerodynamics of Segmented Solid Motors. *Space Solid Propulsion Conference, Paper* 50, Rome 2000

[5] SNPE. Avancement des activités Demonstrateur OdP phase 1, Justification du choix d'echelle. *Reunion Europropulsion*, 16/03/07

[6] Y. Fabignon, O.Orlandi, J. F. Trubert, D. Lambert and J. Dupays. Combustion of Aluminum Particles in Solid Rocket Motors. *AIAA* 2003-4807

[7] N. Lupoglazoff, F. Vuillot, J. Dupays, Y. Fabignon. Numerical Simulations of the Unsteady Flow Inside Ariane 5 P230 SRM Booster with Burning Aluminum Particles. *Space Solid Propulsion Conference, Paper* 87 Rome 2000

[8] A. Annovazzi, A. Tamburini and F. Gori. An Integrated Approach to Predict the Ignition Transient and Steady State Phases in Solid Rocket Motors. *Fifth International Symposium on Special Topics in Chemical Propulsion Combustion of Energetic Materials*, 19- 22 June, 2000

[9] Y. Fabignon, J. Dupays, G. Avalon, F. Vuillot, N. Lupoglazoff, G. Casalis, M. Prévost. Instabilities and pressure oscillation in solid rocket motors. *Aerospace Science and Technology* 7 (2003) 191–200. 2002.

[10]J. Sun, R. Dobashi, T.Hirano. Structure of flames propagating through aluminum particles cloud and combustion process of particles. 2006

[11]R.A. Reed. Review of Aluminum Oxide Rocket Exhaust Particles. *AIAA*-93-2819, 1993

[12]T. Bazyn, H. Krier, N.Glumac. Evidence fort he transition from the diffusion-limit in aluminum particle combustion. *Proc. of the Comb. Institute* 31 (2007) 2021-2028.

[13]M. K. King. Aluminium combustion in a solid rocket motor environment. 2008

[14]M. W. Beckstead. Correlating Aluminum Burning Times. 2004

[15]V.A. Babuk, V.A. Vasilyev. Model of Aluminum Agglomerate Evolution in Combustion Products od Solid Rocket Propellant. *Jou. of Prop. and Pow.* Vol 18, No.4, 2002

[16] X. Wang, C. Zhu, R. Ahluwalia. Numerical simulation of evaporating spray jets in concurrent gas–solids pipe flows. *Powder Technology* 140 (2004) 56-67

[17]H. Tang, V.A.O. Anjorin, A.J. Morgan, L.C. Wrobel, I.E. Barton, Z. Fan. Numerical and experimental investigation of the morphology development of expansion clouds by a powder jet flow. *Fire Safety Journal* 39 (2004) 601–617

[18]C.T. Crowe , T.R. Troutt, J.N. Chung. Numerical Models for Two-Phase Turbulent Flows. *Annu. Rev. Fluid. Mech.* 1996. 28:11-43

[19]G. Gouesbet, A. Berlemont. Eulerian and Lagrangian approaches for predicting the behaviour of discrete particles in turbulent flows *Progress in Energy and Combustion Science,* 25 (1999) 133–159

[20]Dupays et all. Some Aspects of Two-Phase Flows in Solid Propellant Rocket Motors. Progress in Astronautics and Aeronautics, vol. 185. *AIAA* 2000

[21]Dupays et all. Combustion of aluminum particles in solid rocket motors. ODAS 2000 – *ONERA/DLR Aerospace Symposium*, 2000

[22]N. Cesco, G. Lavergne, J.L. Estivalezes. Simulation of the two phase flow in solid rocket motors. *AIAA*-96-2640

[23]Traineau et all. Particle Size Distribution Measurements in a Subscale Motor for the Ariane 5 Solid Rocket Booster. ONERA. *AIAA* 92 – 3049.

[24]G. Kokcamustafaogullari, S.R. Smits, J. Razi. Maximum and mean droplet sizes in annular two-phase flow. *Int. J. Heat Mass Transfer*, Vol.37. N.6, 1994

[25]R.W. Bartlett and L.J. Delaney. Effects of liquid surface tension on maximum particle size in two-phase nozzle flow. *Pyrodynamics*. 1966. Vol.4 pp.337-341

[26]R.A. Reed. Review of Aluminum Oxide Rocket Exhaust Particles. *AIAA*-93-2819. 1993

[27]J.O. Hinze. Fundamentals of the Hydrodynamic Mechanism of Splitting in Dispersion Processes. *A.I.Ch.E Journal*, Vol.1, No.3

[28]F. Risso. The Mechanisms of Deformation and Breakup of Drops and Bubbles. *Multiphase Science and Technology*, Vol.12, pp.1-50. 2000

[29]K. Jurski, E. Géhin. Splitting and coalescence criteria of droplets in a turbulent flow in a nozzle. *J. Aerosol Sci*. Vol.1, Suppl.1, 1998

[30]R.Duan, S. Koshizuka and Y. Oka. Numerical and Theoretical Investigation of Effect of Density Ratio n the Critical Weber Number of Droplet Breakup. *Journal of Nuclear Science and Technology*, Vol. 40, No. 7, p. 501–508 (July 2003)

[31]P. Politzer, P. Lane, M. E. Grice. Energetics of Aluminum Combustion. 2001

[32]W. Cai, P. Thakre, V. Yang. A Model of AP/HTPB Composite Propellant Combustion in Rocket-Motor Environments. *Combust.Sci. and Tech*., 180: 2143-2169, 2008.

[33]M.W. Beckstead. A Summary of Aluminum Combustion. *RTO/VKI Special Course*, RTO-EN-023, 2002

[34]E.L. Dreizin. On the Mechanism of Asymmetric Aluminum Particle Combustion. *Combustion and Flame* 117:841–850 1999

[35]M.W. Beckstead and K.P. Brooks. Distributed combustion in solid propellants. *Report for The US Air Force*, 1993

[36]S. R. Turns. An Introduction to Combustion. Concepts and Applications 2nd edition. 2000

[37]M. Jackson, M. L. Pantoya, W. Gill. Characterization of a gas burner to simulate a propellant flame and evaluate aluminium particle combustion. 2008

[38]Y. Huang, G. A. Risha, V. Yang, R. A. Yetter. Combustion of bimodal nano/micron-sized aluminum particle dust in air. *Proc. of the Combustion Institute* 31 (2007) 2001–2009

[39]Y. Fabignon et. all. Slag Accumulation in Large Segmented Solid Motors with a Submerged Nozzle. *Space Solid Propulsion Conference*, *Paper 43,* Rome, 2000.

[40]Fluent 6.3 Documentation

[41]Stella F., Paglia F., Giangi M., D'Ascenzi M.: Numerical simulation of pressure oscillation in SRM: definition and assessment of methodology. Technical report (2005).

[42]J. Lienhard IV, J. Lienhard V. A Heat Transfer Textbook, third Edition. 2004

[43]B. Eckhardt, T.M. Schneider, B. Hof, J. Westerweel. Turbulent Transition in Pipe Flow. *Annu. Rev. of Fluid Mech.* 2007. 39:447–68

[44]A. Guha. Transport and Deposition of Particles in Turbulent and Laminar Flow. *Annu. Rev. Fluid Mech.* 2008. 40:311–41

[45]H.D. Baehr, K. Stephan. Heat and Mass Transfer, Second Edition. Springer, 2006

[46]A. Bejan, A.D. Kraus. Heat Transfer Handbook. John Wiley & Sons, Inc. 2003

[47]R. Zevenhoven. Particle / turbulence interactions and CFD modelling of dilute suspensions. *Topical meeting on Modelling of Combustion and Combustion Processes. Turku, Finland*, November 15-16, 2000

[48]S. Apte, V. Yang. Unsteady Flow Evolution and Combustion Dynamics of Homogeneous Solid Propellant in a Rocket Motor. *Combustion and Flame* 131:110–131 (2002)

[49]J. Glimm, D. Saltz and D.H. Sharp. Two-Phase Modelling of a Fluid Mixing Layer. *J. Fluid Mech.* (1999), *vol.* 378*, pp.* 119-143.

[50]Y. Hardalupas, S. Horender. Fluctuations of Particle Concentration in a Turbulent Two-Phase Shear Layer. *International Journal of Multiphase Flow* 29 (2003) 1645–1667

[51]A.M. Tartakovsky, P. Meakin, T.D. Scheibe, R.M. Eichler West. Simulations of Reactive Transport and Precipitation with Smoothed Particle Hydrodynamics. *Journal of Computational Physics* 222 (2007) 654–672

[52]Z. Zeng, L. Zhou, Z. Liu. Second-Order Moment Model for Dense Two-Phase Turbulent Flow of Bingham Fluid with Particles. *Applied Mathematics and Mechanics (English Edition),* 2006, 27(10):1373–1381

[53]V.A.O. Anjorin, H. Tang, A.J. Morgan, I.E. Barton. An experimental and numerical investigation into the dispersion of powder from a pipe. *Experimental Thermal and Fluid Science* 28 (2003) 45–54.

[54]W. Kosiwczuk, A. Cessou, M. Trinite´, B. Lecordier. Simultaneous velocity field measurements in two-phase flows for turbulent mixing of sprays by means of two-phase PIV. *Experiments in Fluids* (2005) 39: 895–908

[55]J. Ouyang, J. Li. Particle-motion-resolved discrete model for simulating gas/solid fluidization. *Chemical Engineering Science* 54 (1999) 2077-2083

[56]D.J. Glaze, S.H. Frankel. E€ect of dispersion characteristics on particle temperature in an idealized nonpremixed reacting jet. *International Journal of Multiphase Flow* 26 (2000) 609-633

[57]H. Pokharna, M. Mori, V.H. Ransom. The Particle Fluid Model and Using Lagrangian Representation in Two-Phase Flow Modeling. *Nuclear Engineering and Design* 175 (1997) 59-69.

[58]O. Ayala, W.W. Grabowski, L. Wang. A hybrid approach for simulating turbulent collisions of hydrodynamically-interacting particles. *Journal of Computational Physics* 225 (2007) 51–73

[59]S.J.M. Cartaxo, S.C.S. Rocha. Object-oriented simulation of the fluid-dynamics of gas–solid flow. *Powder Technology* 117 2001 177–188

[60]M.F. Goz, S. Laìn, M. Sommerfeld. Study of the numerical instabilities in Lagrangian tracking of bubbles and particles in two-phase flow. *Computers and Chemical Engineering* 28 (2004) 2727–2733

[61]S. Venkateswaran, J.W. Lindau, R.F. Kunz and C.L. Merkle. Computation of Multiphase Mixture Flows with Compressibility Effects. *Journal of Computational Physics* 180, 54–77 (2002)

[62]H. S. Udaykumar, Heng-Chuan Kan, Wei Shyy, and Roger Tran-Son-Tay. Multiphase Dynamics in Arbitrary Geometries on Fixed Cartesian Grids. *Journal of Computational Physics* 137**,** 366–405 (1997)

[63]F. Frishman, M. Hussainov, A. Kartushinsky and U. Rudi. Distribution Characteristic of the Mass Concentration of Coarse Solid Particles in a Two-Phase Turbulent Jet. *J. Aerosol Sci.* Vol. 30, No. 1, pp. 51-69, 1999

[64]B. Wang, H.Q. Zhang, X.L. Wang. Large eddy simulation of particle response to turbulence along its trajectory in a backward-facing step turbulent flow. *International Journal of Heat and Mass Transfer* 49 (2006) 415–420.

[65]M.G. Andac, F.N. Egolfopoulos, C.S. Campbell. Hot-gas ignition of non-premixed methane flames in the presence of inert particles. *Proceedings of the Combustion Institute* 30 (2005) 431–437

[66]J. Ouyang, J. Li. Discrete simulations of heterogeneous structure and dynamic behaviour in gas-solid fluidization. *Chemical Engineering Science* 54 (1999) 5427-5440

[67]M. Chiesa, V. Mathiesen, J.A. Melheim, B. Halvorsen. Numerical simulation of particulate flow by the Eulerian–Lagrangian and the Eulerian–Eulerian approach with application to a fluidized bed. *Computers and Chemical Engineering* 29 (2005) 291–304.

[68]A. Kitagawa, Y. Murai, F. Yamamoto. Two-way coupling of Eulerian-Lagrangian model for dispersed multiphase flows using filtering functions. *International Hournal of Multiphase Flow* 27 (2001) 2129-2153

[69]V.G. Levich. Physicochemical Hydrodynamics. *Prentice Hall, Englewood Cliffs, NJ (1962)*

[70]F.F. Grinstein. Recent Progress on Monotone Integrated Large Eddy Simulation of Free Jets. *JSME International Journal, Series B, Vol.49, No.1, 2006*